

TRIPLET EXCITON PHENOMENA
IN BENZENE CRYSTALS

Thesis by
George Carroll Nieman

In Partial Fulfillment of the Requirements
For the Degree of
Doctor of Philosophy

California Institute of Technology
Pasadena, California

1965

(Submitted August 7, 1964)

ACKNOWLEDGMENTS

I would like to express my thanks to my research adviser, Dr. G. Wilse Robinson, for his assistance with the work herein reported. Dr. Robinson has contributed greatly to the development of my scientific understanding.

I would also like to acknowledge the financial assistance of the National Science Foundation, whose fellowships for the past three years have made possible my research.

ABSTRACT

Various aspects of the triplet exciton problem are investigated. By studying three-component isotopic mixed crystals of benzene it is shown that trap-to-trap triplet excitation migration is very rapid compared to singlet excitation migration. The closely related phenomenon of triplet-triplet annihilation is also discussed. Triplet-triplet annihilation accounts for the production of delayed fluorescence in molecular crystals and for the quenching of all phosphorescence from pure crystals of π -electron molecules.

By studying the small quasiresonance shifts introduced in the C_6H_6 phosphorescence by changing the degree of deuteration of the benzene host crystal, the nearest neighbor "pairwise" triplet exciton matrix element (β) for benzene is determined to be $12 \pm 1 \text{ cm}^{-1}$. This compares very well with the rough value of 9 cm^{-1} determined from excitation transfer studies and is only slightly less than that (18 cm^{-1}) found for the singlet exciton interaction. These investigations also imply a new interpretation of the factor group splitting of the first singlet-singlet transition in crystalline benzene.

Optical evidence is presented which shows that benzene in its lowest triplet state is not a regular hexagon. Rather detailed phosphorescence spectra of various deuterated benzenes are also presented.

TABLE OF CONTENTS

ACKNOWLEDGMENTS	ii
ABSTRACT	iii
I. INTRODUCTION	1
II. EXPERIMENTAL PROCEDURES	8
1. Equipment and Procedures	8
2. Photographic Plates	11
3. Chemicals	13
4. An Experimental Apparatus for the study of the Decay of Moderately Short-lived Delayed Fluorescence	15
5. Photomultiplier Switching	22
III. TRIPLET EXCITATION MIGRATION	36
1. Description of the Experiments	36
2. Mechanism for Excitation Migration	38
3. Calculation of the Exciton Matrix Element	44
IV. TRIPLET-TRIPLET ANNIHILATION AND DELAYED FLUORESCENCE	56
1. Introduction and Some Preliminary Experiments	56
2. Description of the Mechanism and Calculation of the Annihilation Rate	59
3. Kinetics	68
4. Experiments by Other Workers	76
5. Conclusions	78

TABLE OF CONTENTS (Continued)

V. METHOD OF VARIATION OF ENERGY DENOMINATORS . . .	83
1. Description of the Technique	83
2. Vibrational Exciton Effects	85
3. Observed Shifts	86
4. Analysis of the Data	94
VI. THE EXCITON BAND STRUCTURE OF BENZENE . . .	101
1. General Theory	101
2. Computer Calculations	114
3. The Singlet Exciton Band	134
VII. NONHEXAGONAL BENZENE IN THE TRIPLET STATE .	142
1. Introduction	142
2. Experimental Evidence	143
3. Explanation of These Observations . . .	144
4. Other Experiments	155
APPENDIX	158
A. Phosphorescence Spectrum of C_6H_6 . . .	159
B. Phosphorescence Spectrum of C_6H_5D . . .	163
C. Phosphorescence Spectrum of 1,4- $C_6H_4D_2$.	169
D. Phosphorescence Spectrum of 1,3,5- $C_6H_3D_3$	173
E. Intensity Distribution for Benzene Phosphorescence	175
F. Fermi Resonance Splittings	176
G. Assignment of the 1004 cm^{-1} Line . . .	177
H. Frequency Correlations	178
PROPOSITIONS	179

TRIPLET EXCITON PHENOMENA IN BENZENE CRYSTALS

I. INTRODUCTION

The solid state physics of aromatic molecular crystals has been a very active field in recent years. Only recently has it been realized that the triplet states of these molecules in the crystal are very important in determining the observed optical properties. My interest has been primarily to study the nature of the interaction of a benzene molecule excited to its lowest triplet state with its environment.

Earlier work by El-Sayed, Wauk, and Robinson (1) using naphthalene had implied that, contrary to the accepted view (2), this exciton interaction for the lowest triplet state of aromatic molecules was nearly as large as that for the first excited singlet state. This was implied by the ability of triplet excitation to migrate from one molecule to another. It was my objective to obtain more quantitative information concerning the magnitude of the matrix elements of these excitation transfer (exciton) interactions in crystalline benzene. In other words, I hoped experimentally to

(1) M. A. El-Sayed, M. T. Wauk, and G. W. Robinson, Mol. Phys., 5, 205 (1962).

(2) Since in first order the exciton interaction for triplet states is an intermolecular exchange interaction, it was thought to be vanishingly small. See Sect. VI for a further discussion of this point.

evaluate matrix elements of the type $\langle \Psi_A^* \Psi_B^0 | V_{AB} | \Psi_A^0 \Psi_B^* \rangle$, where Ψ_1^0 is the ground state wavefunction and Ψ_1^* is the lowest excited triplet state wavefunction for the molecules A and B, and V_{AB} is the intermolecular interaction potential. It should be noted that the net effect of this intermolecular interaction is to transfer the excitation from molecule A to molecule B. Thus the name "excitation transfer" interaction.

The direct observation of triplet factor group splittings in π -electron organic crystals presents a very difficult experimental problem because of the extremely low oscillator strength (3) of the first singlet-triplet transitions in these molecules. The spectrum at liquid helium temperature of a transparent crystal of high chemical purity, and of the order of a few tenths of a meter long, would have to be obtained to observe the splittings directly in absorption. Furthermore, the triplet-singlet emission (phosphorescence) spectra of these crystals are virtually impossible to obtain just because of the large intermolecular exchange interactions. Such interactions are responsible not only for triplet factor group splittings and for triplet excitation migration through the crystal but also for rapid triplet-triplet annihilation processes (4) which strongly quench

(3) G. W. Robinson, Methods of Experimental Physics, edited by D. Williams (Academic Press Inc., New York, 1962), Vol. 3, p. 217.

(4) See Sect. III.

phosphorescence in the pure crystal. Retardation of both excitation migration and annihilation by isotopic dilution methods, however, provides a good way by which the phosphorescence can be observed and the triplet exciton interaction studied.

The greatest portion of my work was performed with isotopic mixed crystals of benzene. As this technique is of universal importance to this research I should like briefly to describe this experimental technique. Mixed crystals are not only convenient but they are necessary for this work. In addition they are what one commonly deals with in nature.

Consider a mixed crystal of host plus a small concentration of guest molecules. Assume, as is most often the case, that the triplet (singlet) excitation energy of the guest lies below that of the host. The triplet state of the guest thus act as a trap of depth ΔE into which host excitation may rapidly flow providing $kT \ll \Delta E$. Such a system would be an "isotopic mixed crystal" of 1% perprotonated benzene (C_6H_6) dissolved in perdeuterated benzene (C_6D_6) or a "chemically substituted mixed crystal" such as β -methylnaphthalene dissolved in naphthalene. The guest molecules may be added on purpose, as in my experiments, or they may occur accidentally as chemical or isotopic impurities which are difficult to detect, identify, and/or remove by standard techniques.

Because of the extremely long radiative lifetime of the lowest benzene triplet state, one must isolate it rather

completely to observe any emission. The use of mixed crystals allows one effectively to isolate the triplet excitation and thus to study the phosphorescence. By the judicious choice of guest, host, and temperature it is possible to study movements and interactions of the quasi-mobile triplet excitations. The best impurity to choose is one which is very similar, both chemically and physically, to the host material so that it does not tend to segregate upon freezing and so that it distorts the crystal structure very slightly. Thus the most ideal impurities are isotopically substituted host molecules since they are from most every point of view very nearly identical to the host molecules.

Consider an isotopic mixed crystal of C_6H_6 dissolved in C_6D_6 . Electronically the excitation energies of these two molecules are to a very high degree of approximation the same. However, the zero-point vibrational energies do not undergo the same change in going from the ground to the excited electronic state. Thus both the lowest singlet and triplet excitation energies of C_6H_6 lie approximately 200 cm^{-1} below (to lower energy than) those of C_6D_6 (5). As a

-
- (5) This shift can be determined to sufficient accuracy from the phosphorescence spectra of benzene in solid argon (6). It is essentially the same as the value for the first singlet-singlet transitions in the gas phase (7).
- (6) G. W. Robinson, J. Mol. Spectry., 6, 58 (1961).
- (7) F. M. Garforth, C. K. Ingold, and H. G. Poole, J. Chem. Soc., 1948, 513.

consequence of the "sum rule" (8) for vibrational frequencies of isotopically substituted species, the difference in excitation energy is approximately 33 cm^{-1} per deuterium atom substituted for a hydrogen atom of benzene (9). Conveniently at liquid helium temperature this magnitude of trap depth is ideal for studying exciton effects.

Benzene was chosen for this study not only because it is a prototype aromatic molecule but also because it is readily available in a high degree of chemical purity. It is also quite stable in storage (10), easy to purify, and does not require heating, with the associated chance of oxidation and decomposition, to form crystals suitable for optical studies. For benzene there are also available a large number of deuterated species many of which have been rather extensively studied.

In the following sections of this thesis I shall

-
- (8) E. B. Wilson, Jr., J. C. Decius, and P.C. Cross, Molecular Vibrations (McGraw-Hill Book Co., Inc., New York, 1955), p. 186. See also Ref. (7).
- (9) This has been confirmed for the triplet state by the phosphorescence spectra of the various deuterated benzenes in isotopic mixed crystals and in solid argon. The experiments in solid argon were performed by the author and Dino S. Tinti. Here the shifts are 0, 33, 60, 101, and 201 cm^{-1} , respectively, for 0, 1, 2, 3, and 6 substituted deuterium atoms. The values in the crystal are $1-2 \text{ cm}^{-1}$ less.
- (10) V. L. Broude, Usp. Fiz. Nauk, 74, 577 (1961) [English Transl. Soviet Phys.-Usp., 4, 585 (1962)]. See also the discussion of Ref. (15).

phosphorescence spectra of various deuterated benzenes. These are presented because the presently accepted phosphorescence spectrum of benzene (11) is very much less detailed than those spectra available from these mixed crystal studies.

The work discussed in the following pages, I believe, shows that the triplet exciton interaction between nearest neighbor pairs of molecules is of the order of 10 cm^{-1} for benzene crystals and for aromatic molecular crystals in general. The long lifetime of the triplet state provides a ready means of energy storage, and triplet-triplet annihilation reactions provide a ready means of energy multiplication. Therefore one must always be aware of the importance of the triplet states of these crystals, and especially of the triplet states of impurities, when one considers problems involving energy storage, transport, and/or multiplication.

(11) H. Shull, J. Chem. Phys., 17, 295 (1949).

II. EXPERIMENTAL PROCEDURES

1. Equipment and Procedures. Most of the experiments described herein were performed on essentially the same optical set-up (Fig. II-1). This consisted of a lamp, filters to remove background light, a quartz-tipped pyrex double dewar to contain the sample in liquid helium, the sample benzene crystal between quartz plates, and a spectrograph to record the spectra.

The lamp was either a high pressure xenon arc lamp (Hanovia, 800 w) or for the more recent experiments a high pressure mercury arc lamp (PEK 200) housed in a Bausch and Lomb monochromator (model 33-86-01). The filters used with the xenon arc lamp were an interference filter with peak transmission at 2630 \AA (200 \AA wide) and one 5 cm cell each of chlorine and bromine gas at about atmospheric pressure. When the monochromator was used it was set to pass a region about 100 \AA wide around the 2536 \AA line of mercury. The chlorine and bromine filters were also used to remove stray scattered light of the fluorescence and phosphorescence wavelengths.

In some experiments a phosphoroscope was used which consisted of two slotted disks, one on each side of the dewar, set so as to alternately expose the sample to unfiltered exciting light or to the spectrograph. The minimum time delay between the interruption of excitation and the recording of long-lived emission was about 0.1 sec. The quartz dewar

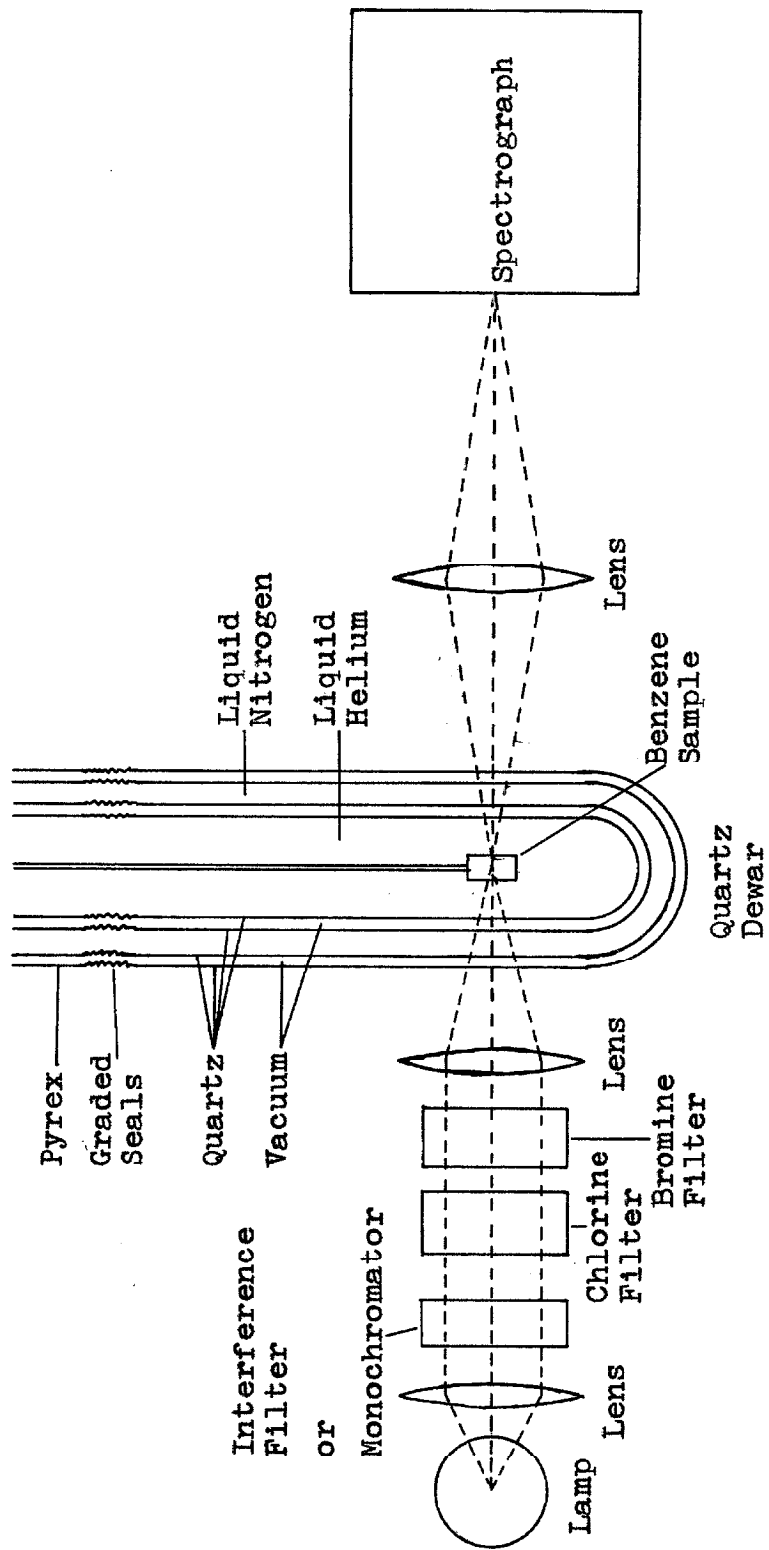


Fig. II-1. Schematic diagram of the optical set-up.

consisted of an outer liquid nitrogen dewar (outside diameter 2") and an inner liquid helium dewar (inside diameter 1") containing the sample suspended from the top of the dewar. The pressure within the inner dewar could be reduced to perform experiments at superfluid helium temperatures ($\sim 2^{\circ}$ K). However the greatest portion of these experiments was performed at 4.2° K (the boiling point of liquid helium at standard atmospheric pressure).

The benzene crystals were prepared by slowly (30 minutes from room temperature to liquid nitrogen temperature) freezing the liquid benzene mixtures between quartz windows ($5/8$ " diameter) in a brass holder suspended in cold nitrogen gas above liquid nitrogen. The liquid benzene mixtures were degassed (deoxygenated) by repeated saturation with nitrogen or helium gas followed by freezing and by repeated freeze-thaw cycles. The benzene was placed then upon one of the quartz windows in a nitrogen atmosphere of a dry box. The windows were then pressed together and the brass holders fastened together. Experience showed that in order to form satisfactory crystals, the crystals needed to be quite thin. Recent work by Al Kalantar (12) has shown that such crystals are 1-10 μ thick and, while polycrystalline, may contain areas as large as several square millimeters which are of a single orientation.

(12) Using an optical wedge and counting interference fringes.

The spectrograph most often used was an f/12 instrument with a 600 lines/mm grating in a 2-meter mount. In second order where the phosphorescence spectra were recorded the dispersion is about $4.16 \text{ \AA}^{\circ}/\text{mm}$ and in third order where the fluorescence spectra were recorded the dispersion is about $2.77 \text{ \AA}^{\circ}/\text{mm}$. The slit width used was usually 50μ . While this may seem rather wide, the line widths observed for the phosphorescence lines were approximately three times those observed for the iron standard lines which came through the same entrance slits. Thus the observed line widths ($\sim 3 \text{ cm}^{-1}$) were natural and not a function of the instrumental slit width. An iron-neon arc was used as a wavelength standard.

2. Photographic Plates. The photographic plates used were Kodak 103a-0 spectrographic plates. Some quantitative intensity measurements were made by means of microdensitometer tracings of the photographic negatives. To do this a characteristic curve for these plates was constructed from the tracings of a photograph of the iron-neon standard source taken at several different exposures times (at 4150 \AA°). This curve which relates optical density of a line to its intensity is shown in Fig. II-2. The accuracy available from this curve is about 10%. The largest error seems to be due to inhomogeneities in the plates and in their development (13).

(13) The developing conditions were: develop, $4-4\frac{1}{2}$ min.; water rinse, 30 sec.; fix, 15-20 min.; water rinse, 12-18 hrs. The temperature was not constant.

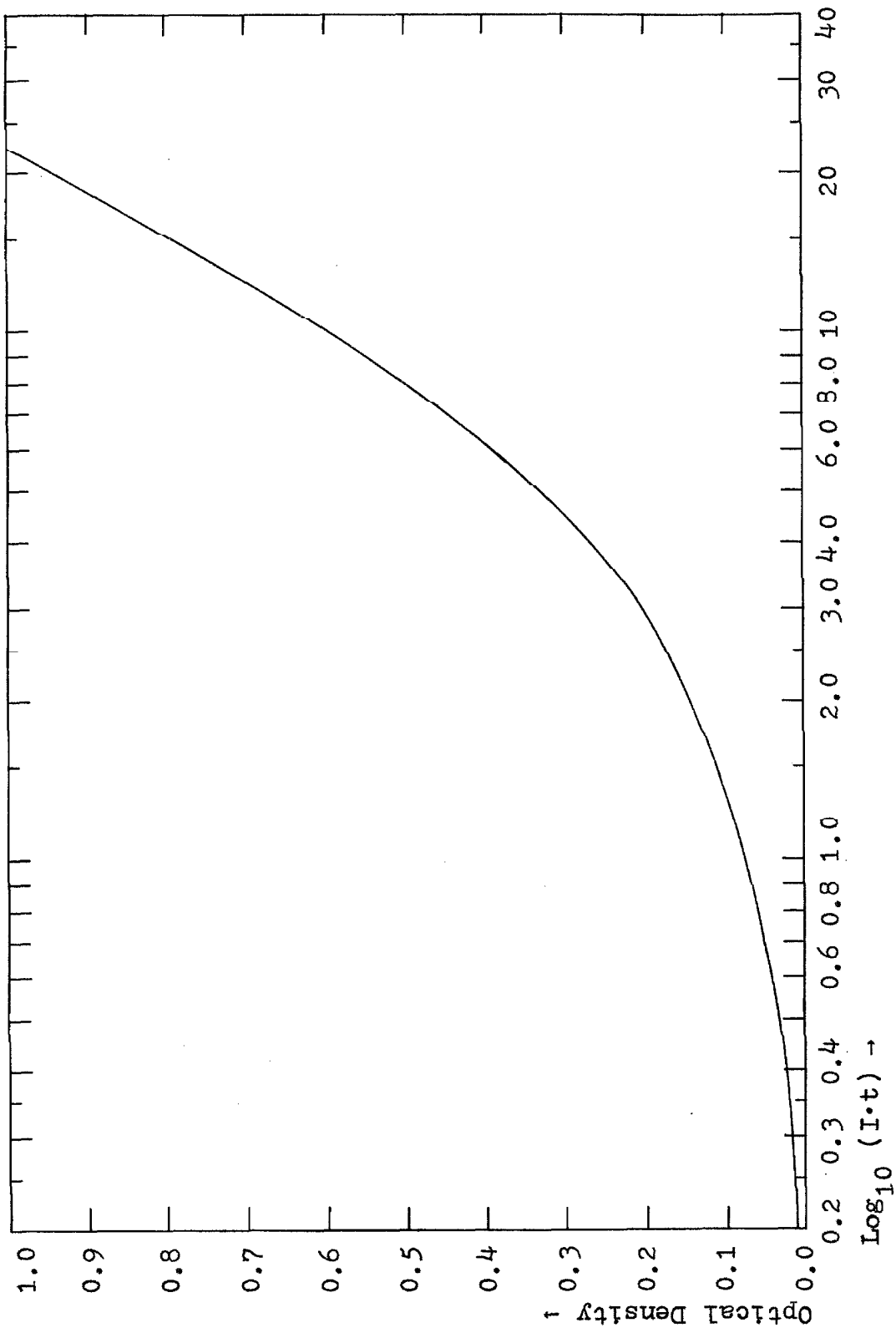


Fig. II-2. Characteristic Curve for Kodak 103a-0 photographic plates.

3. Chemicals. All of the deuterated benzenes used in these experiments were obtained from Merck, Sharp, and Dohme, Montreal, Canada. Table II-1 lists the deuterated benzenes used along with their supposed isotopic purity. The perprotonated benzene was Phillips Petroleum research grade. Fortunately the chemical purity of these materials was sufficient for our use after a single vacuum distillation (14). The presence of phenol resulting from air oxidation in these benzenes has been confirmed by absorption studies of large crystals (15) and by emission studies of the "pure" crystals. Vapor phase chromatography has shown the presence of some volatile components (16). Emission studies at liquid nitrogen temperature (actually anything above about 15° K) show a blue-green, long-lived ($\tau > 10$ sec.) impurity phosphorescence only. None of these impurities were of consequence to the present studies since the benzene phosphorescence was much sharper than the impurity emission and seemed to dominate at liquid helium temperatures. The isotopic purity did leave something to be desired. However, as each isotopic species has its own distinct, resolvable spectrum, lines due to the

(14) A large amount of stopcock grease was found in one of the samples, but was easily removed by distillation.

(15) From these absorption studies by Mrs. Lelia Coyne there appeared to be 1-10 ppm phenol depending upon the length of exposure to air. Fortunately the deuterated benzenes were relatively phenol free as they came from the manufacturer in evacuated ampules. See also Ref. (9).

(16) A. Lamola, private discussion.

Table II-1.

Available deuterated benzenes.

Deuterated Benzene	Isotopic Purity (Atom %)*
C_6D_6	99.5%
1,3,5- $C_6H_3D_3$	97.
1,4- $C_6H_4D_2$	97.
C_6H_5D	99.

* Manufacturer's literature.
Merck, Sharp, and Dohme,
Montreal, Canada.

various less deuterated impurities could be easily identified. More highly deuterated impurities did not appear because, lying at higher energy, they transferred their energy to the more plentiful lower lying guests.

4. An Experimental Apparatus for the Study of the Decay of Moderately Short-Lived Delayed Fluorescence. Much time and effort was devoted to an attempt to study the short-lived ($\tau \sim 10^{-4}$ sec.) delayed fluorescence from spinach leaves. It was hoped to study the temperature and light intensity dependence of this non-exponentially decaying emission. This emission is thought to arise from triplet-triplet annihilation in the chlorophyll molecules (17). This study might provide some evidence for the role, if any, played by the lowest triplet state of chlorophyll in photosynthesis. Also this being a bimolecular reaction, it would provide valuable evidence concerning the mechanisms of photosynthesis, such as establishing the size of the photosynthetic unit, the smallest grouping of chlorophyll molecules capable of performing the reactions of photosynthesis.

While this work was not directly related to my benzene research, the apparatus constructed and tested has other applications and represents a system worthy of discussion. There were many experimental problems encountered, not the

(17) G. W. Robinson, Proc. Natl. Acad. Sci. U. S., 49, 521 (1963); G. W. Robinson, Annual Reviews of Physical Chemistry, 15 (Annual Reviews, Inc., Palo Alto, California, 1964), to be published.

least of which was the fact that the spinach chosen for these experiments did not seem to show a strong delayed fluorescence. Experiments performed set an upper limit to the delayed fluorescence intensity at room temperature of 10^{-4} times the intensity of the normal fluorescence. This implied a quantum yield of the order of 10^{-6} . Previous experiments by Calvin (18) and by Arnold (19) indicated this order or higher intensity for the delayed fluorescence. The use of algae or other plant materials may be the answer to this problem.

Fig. II-3 shows schematically the apparatus constructed to perform these experiments. Basically it consists of a light source to excite the chlorophyll, a shutter mechanism to quickly turn off this excitation, a dewar to hold the sample at a variable temperature, a mirror to collect the front surface fluorescence, and a photomultiplier which could be gated on and off to detect the emission.

The lamp used was a Sylvania "Sun Gun" photographer's lamp. This is a high wattage (600 w) tungsten filament lamp and was operated on 60 cycle A.C. from a Variac. There was only a very small amount of 60 cycle ripple in the light

(18) G. Tollin, E. Fujimori, and M. Calvin, Proc. Natl. Acad. Sci. U. S., 44, 1035 (1958).

(19) B. L. Strehler and W. Arnold, J. Gen. Physiol., 34, 809 (1951). More recent data is given in W. Arnold and J. B. Davidson, in Photosynthetic Mechanisms of Green Plants (NAS-NRC Publ. 1145, Washington, D.C., 1963), 698.

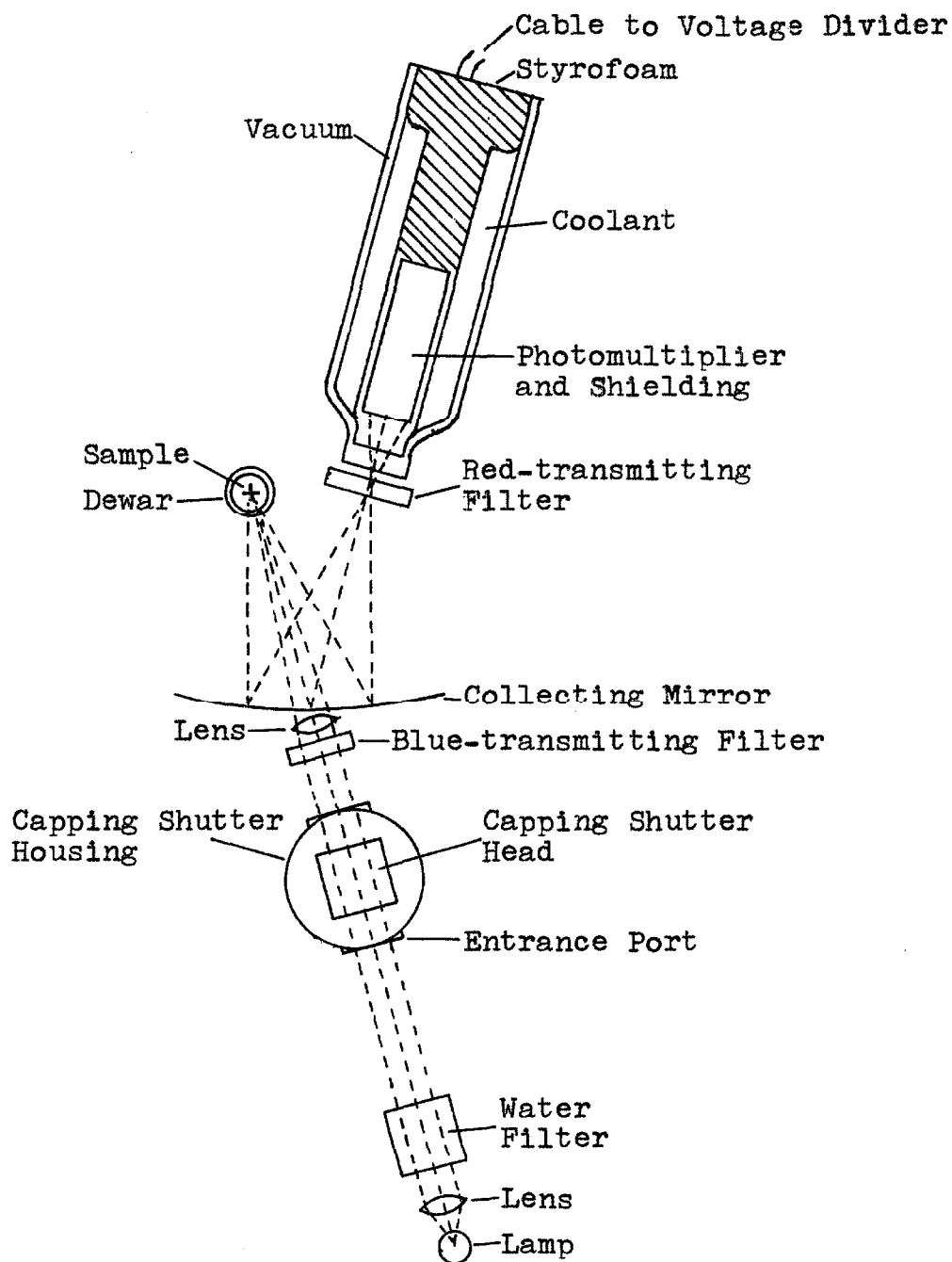


Fig. II-3. Schematic diagram of the apparatus built to study short-lived delayed fluorescence.
 Scale: $1/8'' \sim 1''$.

output of this lamp. Hindsight reveals that a D.C. operated compact xenon arc lamp (PEK X200) would probably be a much better choice for a light source, especially if it were used in connection with a monochromator.

The shutter mechanism was a capping shutter (model MCS-125) made by Electro-Optical Instruments, Inc., Monrovia, California. This device is essentially a high speed electro-mechanical shutter which serves to interrupt the exciting light beam. The working end of this apparatus is a coil of wire embedded in epoxy resin into which an aluminum foil (0.002") cylinder ($1\frac{1}{4}$ " diameter, 2" long) is inserted. When a current pulse is sent through the coil, eddy currents in the aluminum foil cylinder cause it to collapse. The sharpness of the closure was improved by placing small ($\frac{1}{4}$ ") baffling disks along the centerline of the capping shutter head. Thus effectively the excitation is turned off when the cylinder is about 90 per cent closed. This removes the long tail of light associated with the slowness of the final closing of the foil cylinder. An evacuable enclosure was built to house the capping shutter head with the hopes that removal of the air would increase the speed of collapse of the aluminum foil. This it did, but it also reduced the electrical breakdown potential to the point that an electrical failure destroyed the capping shutter head. After getting another head it was discovered that helium gas was nearly as effective as a vacuum in increasing the closure speed (a

factor of 2) with none of the hazardous side effects. There is, however, some arcing across the seam of the cylinder upon closure which does produce a light pulse of short (20 μ sec.) duration. Under normal operating conditions (14 KV) a complete closure time of 50 microseconds was regularly achieved. The use of a Kerr Cell would greatly reduce this closure time, but presents problems in that closure is not complete. There is also a tendency for a Kerr Cell to reopen after a short time period.

The filters in the light input side were originally arranged to provide 6800 \AA excitation of the chlorophyll. However, filtering problems with the fluorescence made it desirable to excite into the Soret bands of chlorophyll (4360 \AA). The use of a monochromator, instead of Corning glass filters and interference filters, should allow direct 6800 \AA excitation, or even better, a variable excitation energy.

The sample dewar was a double dewar system made of pyrex and similar to that used for liquid helium experiments. This arrangement was used to provide a variable temperature. The leaf to be studied was held between glass plates with an indium metal gasket within a brass holder. This sample holder was then suspended in a bath of isopentane within the inner dewar. Also in this bath were a nichrome wire heater and a nitrogen gas bubbler to stir the isopentane. The outer dewar was filled with liquid nitrogen. A balance between heater heat input and radiation from the inner to the outer dewar,

then allowed the maintenance of a constant temperature (less than 1° change in 15 min.).

The fluorescence collecting mirror was a surplus spherical aluminized mirror of 11.5" focal length with an $1\frac{1}{4}$ " diameter hole drilled in the center. The use of a mirror allowed observation of the front surface emission. This is very important in studies of broad fluorescence since it greatly reduces the amount of self-absorption of the fluorescence by the sample.

The detector was originally an RCA 7102 photomultiplier. However, this tube did not prove to be sensitive enough and the photomultiplier was changed to an RCA 7265 tube. This phototube, if anything, proved to be too sensitive as its very fast time response and high current amplifying characteristics gave it the capability of single photon detection. This gave a very noisy appearance to the signal output. The photomultiplier was housed in a three-walled dewar system. This system was a dewar whose coolant storage volume contained a chamber into which the phototube was placed. The walls of this chamber were in direct contact with the coolant except for the windows. This chamber and the phototube were thermally insulated at the open end with Styrofoam. This system allowed the operation of the phototube at any temperature from liquid nitrogen to room temperature in an atmosphere of dry, cold nitrogen gas at atmospheric pressure. Because of the rather high electrical potentials (-2500 v)

involved, the use of an atmospheric pressure system was advantageous. The use of helium gas instead of nitrogen gas caused arcing. Electrostatic and magnetic shields were placed concentrically around the photomultiplier. The electrostatic shield was a ground potential and the magnetic shield was at nearly cathode potential with a sheet of polystyrene between them. The front windows (in front of the photocathode) of the phototube dewar had attached Corning sharp-cutoff glass filters to admit only fluorescence radiation to the phototube. Great pains had to be taken to minimize stray light. The output signal was transmitted by coaxial cable to the input of a Tektronix oscilloscope (Type 585 with a Type 82 plug-in unit).

The integrated systems worked basically as follows. The light source excited the spinach leaf to a steady state photosynthesis. During this time the photomultiplier was switched into a non-operating condition electronically in order to protect it from the strong exciting light and normal fluorescence. Then three trigger pulses of +10, +50, and +150 v were simultaneously produced by discharging a capacitor through a series of resistors. These pulses went respectively to the trigger inputs of the oscilloscope (Tektronix, Type 585), the variable time delay generator (Rutherford, Model A2), and the capping shutter (Electro-Optical Instruments, Model MCS 125). The capping shutter then closed in approximately 50 microseconds. This closure

could be monitored simultaneously with the delayed fluorescence using an RCA 1P28 photomultiplier whose output was fed to the second trace input of the dual beam oscilloscope. Experience showed that this monitoring was not necessary, and that it only interfered with the desired signal because of the chopped mode of operation. Thus this monitoring was discontinued. The time delay generator was set to produce a trigger pulse (+50 v) at a variable time after the capping shutter had closed. This pulse activated a switching circuit which then turned the photomultiplier on. The phototube output signal was then fed to the oscilloscope whose horizontal sweep had been earlier initiated by the original pulse. The resulting trace was then photographed in the normal manner.

5. Photomultiplier Switching. Of the many electronics problems encountered the most difficult involved switching the photomultiplier "on" and "off". There are several means of accomplishing this. One is to switch the entire high voltage supply (-2500 v) with a hydrogen thyratron switching circuit. However the fairly low current flowing and the large dynode chain resistance involved (10 ma, 250K) make this not too desirable a method. Perhaps the major criticism of this approach is that the photocathode is a semiconducting material and especially at low temperatures it responds rather slowly (~30 μ sec.) to a voltage change. This means that there is a rather long period before the phototube is

operating at equilibrium (20).

The photomultiplier switching can also be accomplished by pulsing the entire dynode chain with a high voltage, short time pulse. This method gives only a single point of the decay curve. The entire decay curve is gotten from repeated experiments with successively longer delay times between excitation and measurement. For flash techniques where fast repetitive cycling is possible this method works very well even though the phototube is not operating at equilibrium. In the present case where the capping shutter head must be disassembled and reloaded for each cycle, this method is not practical.

The first approach to be tried involved switching only the dynode-1 potential. Dynode-1 is the dynode whose potential is closest to that of the photocathode. In this scheme, tried on the RCA 7102 photomultiplier, the dynode-1 potential was at its normal operating potential (+200 v relative to the photocathode) when the phototube was "on", and at -50 v relative to the photocathode when the phototube was "off". By only switching the dynode-1 potential the voltage switched was small and most important, the potential change of the photocathode was very small.

The first attempt to use this approach was to use a vacuum tube flip-flop circuit using a 6SN7 duel triode. The

(20) U. Farinelli and R. Malvano, Rev. Sci. Instr., 29, 699 (1958).

flip-flop is a bistable circuit in which the potential at several points can be changed between one of two values by the application of a trigger pulse to an appropriate point in the circuit. The major problem with this design is that the photocathode is at a high negative potential (-1250 v) and thus the internal ground for the flip-flop is also at about this potential. Aside from electrical shielding of these floating circuit components, there is the problem of the filament supply to the tube or tubes. This involves having rather bulky batteries at a high negative potential.

It was then suggested (21) that we use a transistorized flip-flop to eliminate the need for a filament supply. Since ordinary transistors operate in the 10-25 volt range, it was necessary to use the new flip-flop as a control device to regulate some other device which switched the required 250 v. In the last couple of years a solid state device, called a field effect transistor, has become available which can accomplish this task.

The final configuration of the switching circuit is shown schematically in Fig. II-4. This circuit is mounted on an ordinary 8-prong socket for ease of use with different photomultipliers. The voltage supply to the transistorized flip-flop comes from a Zener diode (a constant voltage solid

(21) I would like to gratefully acknowledge the assistance of Dr. Peter Hauk of our group for his help in the design and construction of many of these electrical components.

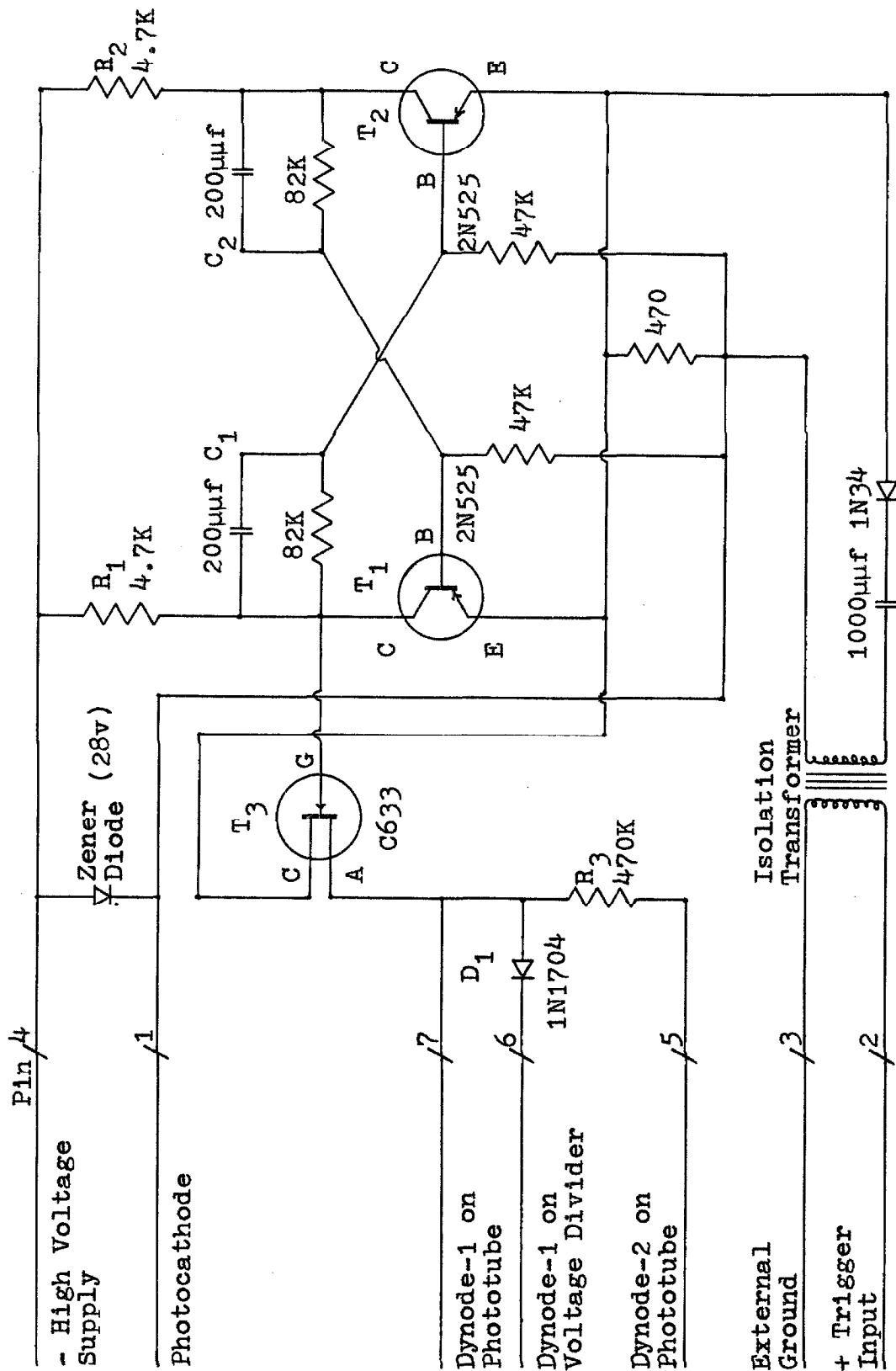


Fig. II-4. Photomultiplier Switching Circuit (Flip-Flop).

state device) in series with the dynode chain. In this way the same switch can be used on a variety of photomultipliers with dynode currents ranging from 5 to 15 milliamperes, thus making it quite versatile.

This switching circuit (Fig. II-4) operates as follows. As mentioned earlier, a flip-flop is a bistable multivibrator consisting of two identical halves arranged so that when one transistor is conducting current the other is non-conducting and vice versa. Depending upon which transistor (T_1 or T_2) is conducting there is or is not a large voltage drop across the resistor R_1 . This voltage drop in turn controls the conductive properties of the field effect transistor (T_3). When the voltage drop across R_1 is small (1.3 v) the field effect transistor is biased "off". When the field effect does not conduct, leakage through the diode D_1 shorts dynode-1 to its normal supply point. Consequently the photomultiplier is functioning normally.

A positive voltage pulse (+50 v, 5 μ sec.) from the time delay generator (blocking oscillator) is then feed through the isolation transformer and its associated circuitry. This sharpens the pulse which is now of the order of two volts high and one microsecond wide. This pulse applied to the emitters (E) of both transistors (T_1 and T_2) renders the flip-flop unstable and the discharge of the capacitor C_1 reverses the roles played by the two transistors. The previously conducting one (T_2) now becomes non-conducting, and

vice versa in about two microseconds. Thus the voltage drop across the resistor R_1 becomes large (25 v) and this in turn allows a current of about 0.8 milliamperes to flow through the field effect transistor (T_3). Because of the resulting voltage drop across the resistor R_3 , dynode-1 is now at nearly the cathode potential of the field effect transistor (C of T_3). This potential can be adjusted (by placing a resistor between pin-1 and the photocathode) to a negative value relative to the photocathode of the photomultiplier. Therefore the photomultiplier is in the "off" position.

The next trigger pulse applied to the flip-flop transistors (T_1 and T_2) reverses the above processes and turns the photomultiplier "on" again. Thus the length of time in the "on" or "off" position is completely arbitrary. The switching time "off to on" is approximately 20 microseconds and "on to off" is approximately 50 microseconds. This switching time is much longer than hoped for and is a function of the parasitic capacitance and low current carrying capability of the field effect transistor used (Crystalonics, C633). A different switching circuit was designed to overcome this difficulty by using a silicon control rectifier as the switching element, but this circuit was not tested.

Fig. II-5 shows the complete circuit schematic for the switch and photomultiplier. By adjusting the values of the resistors R_3 and R_4 this switching circuit can be made generally applicable to many phototubes. For the RCA 7102 tube

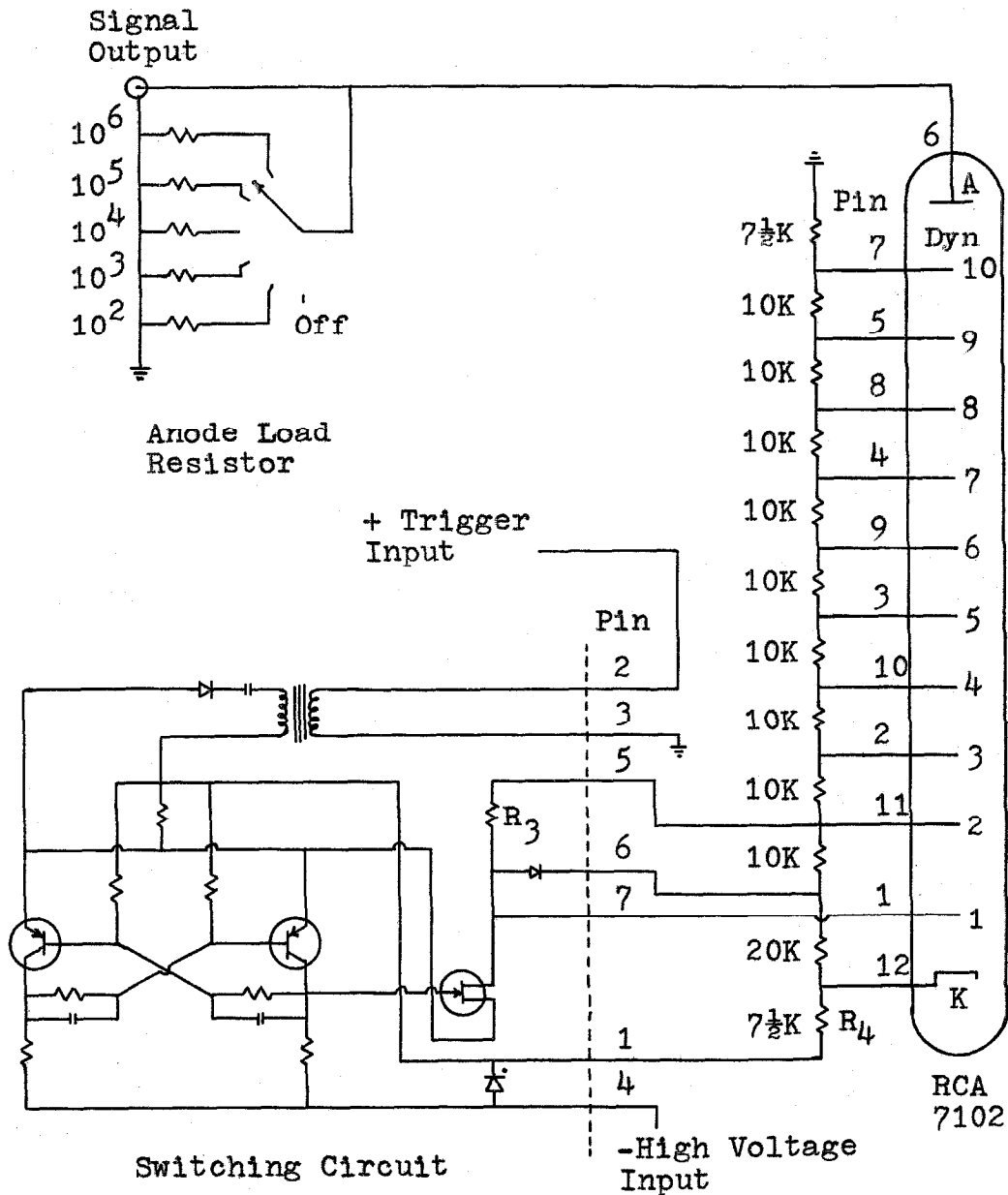


Fig. II-5. Electrical schematic for the RCA 7102 photomultiplier as used with the flip-flop switching circuit. The details of the switching circuit are given in Fig. II-4. The interdynode potential is normally 100 v., i.e., the voltage divider current is 10 ma. By the proper choice of R_3 and R_4 this same basic circuit will allow the switching of most photomultipliers. A: Anode; K: Photocathode.

the ratio of the "on" sensitivity to the "off" sensitivity is about 200. When not needed this switching circuit can be unplugged and a shorting plug inserted in its place to operate the photomultiplier normally.

Unfortunately this switching scheme did not prove to be useful on the RCA 7265 phototube, presumably because of the sophisticated nature of this tube. Fig. II-6 shows a measured curve of this tube's light sensitivity as a function of the dynode-1 potential, all other potentials remaining constant. The rather odd behavior, especially at voltages negative relative to the photocathode, is not understood. Fortunately, a few modifications of the dynode chain wiring allowed the use of the above transistorized switching circuit in a new application.

In this new application the dynode-1 potential is kept constant and the dynode-3 potential is changed. Fig. II-7 shows the measured light sensitivity of the RCA 7265 tube as a function of the relative dynode-3 potential. From this curve it is seen that shorting dynode-3 and dynode-1 is a very effective means of destroying the light sensitivity of this phototube. Now the voltage drop across the field effect transistor's load resistor R_3 can be used to change the dynode-3 potential just as easily as the dynode-1 potential. By switching the dynode-3 potential from its normal value to one very close to that of dynode-1, the photomultiplier can be turned "off" and "on".

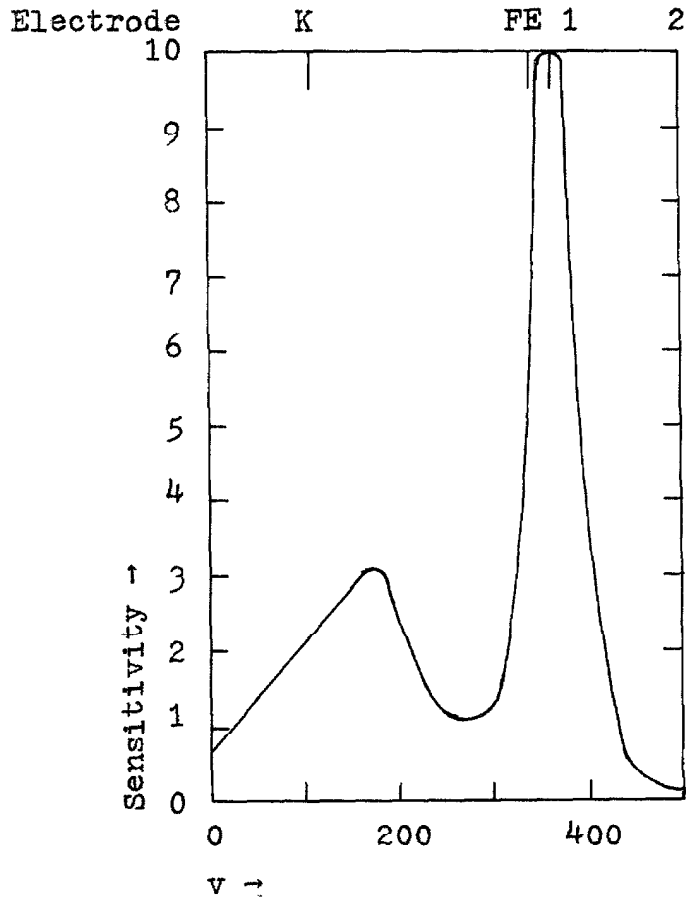


Fig. II-6. Photosensitivity of the RCA 7265 photomultiplier as a function of the relative dynode-1 potential. The interdynode potential is about 130 v. All dynode potentials, except that on dynode-1, are kept constant. The electrodes labelled K, FE, 1, and 2 are, respectively, the photocathode, the focusing electrode, dynode-1, and dynode-2. The lines indicate their nominal potentials

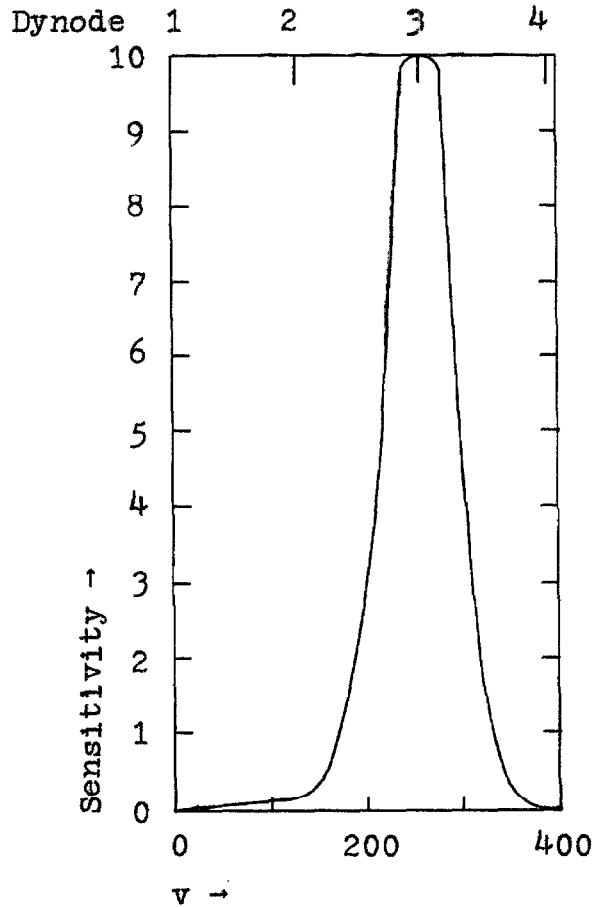


Fig. II-7. Photosensitivity of the RCA 7265 photomultiplier as a function of the relative dynode-3 potential. The interdynode potential is about 130 v. The relative light sensitivities at dynode-1, -2, -3, and -4 potentials are, respectively, 0.005, 0.10, 10, and 0.05. All dynode potentials, except that on dynode-3, are kept constant.

Fig. II-8 shows the schematic for the complete RCA 7265 photomultiplier using the plug-in switching circuit. Here the ratio of "on" to "off" sensitivity is about 2000 to 1. This ratio can be increased somewhat by simultaneously shorting dynodes-1, -2, and -3, but this complicates the electronics and would mean the use of a new and less versatile switching circuit.

Because of the use of a cooled phototube and its associated dewar system, the dynode supply and switching circuits were housed in a separate box with about two feet of cable connecting them to the phototube. The parasitic capacitance thus introduced lengthened the switching time, but not in an adverse manner. A typical switch-on response as a function of time to a constant light input is shown in Fig. II-9. The point to note is that while the time from trigger input to full response is 50 microseconds, the time from zero response to full response is 10 microseconds. Changing the delay time between the capping shutter closure and the triggering of the phototube switch can compensate for this. The turn-on time is slightly light intensity dependent, being longer for lower light intensities. The nature of the initial negative response is not understood, but its magnitude and duration seem to be light intensity independent.

The use of a cathode (emitter) follower for impedance matching to prevent cable ringing was abandoned because of the difficulties involved in designing a wide bandpass

Signal Output

33.

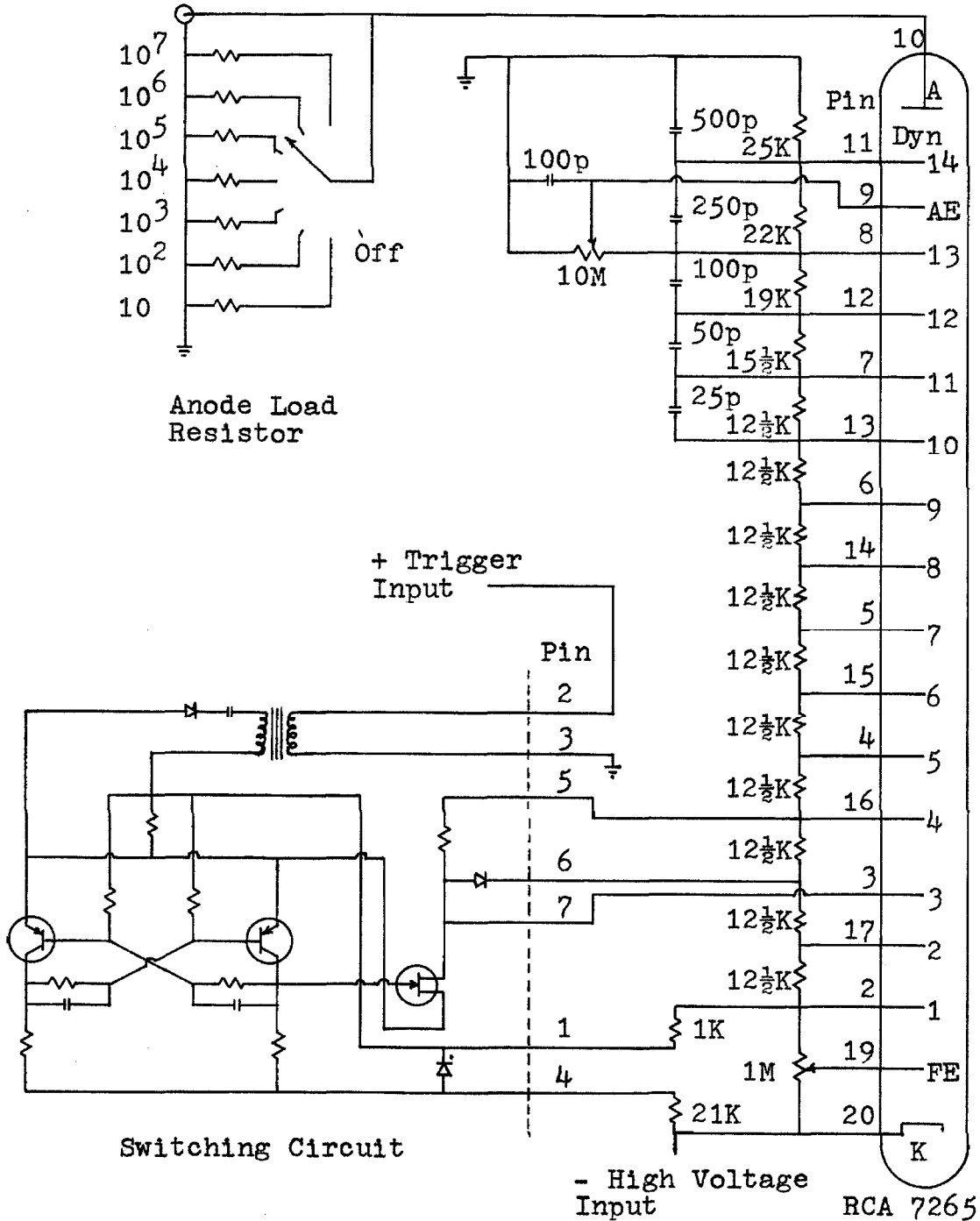


Fig. II-8. Electrical schematic for the RCA 7265 photomultiplier as used with the flip-flop switching circuit. The details of the switching circuit are given in Fig. II-4. The voltage divider current is normally 10 ma. A: Anode; AE: Accelerating Electrode; FE: Focusing Electrode; K: Photocathode.

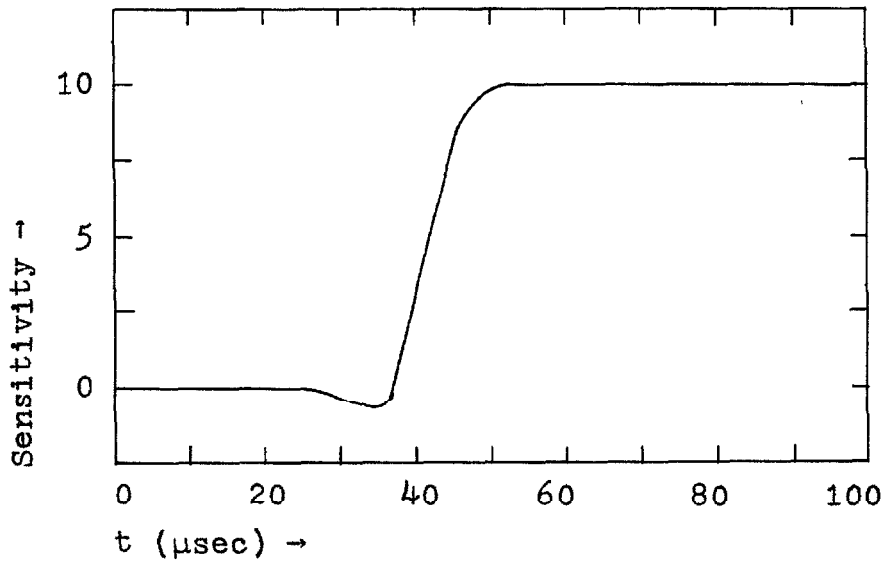


Fig. II-9. Typical "turn-on" characteristics of the RCA 7265 photomultiplier using the switching circuit shown in Fig. II-8. The long initial delay is due to parasitic capacitance in the cable connecting the phototube to the voltage divider.

cathode follower. Also the high frequency of the cable ringing (>10 mc) made it unimportant for the chlorophyll work.

One final point which I should like to make concerns radio frequency noise. For proper shielding of the output leads from the phototube one must use a continuous, unbroken, concentric shield around the cable and phototube. Thus, since the ordinary oscilloscope probe tips do not have a continuously concentric ground, they cannot be used. One must use BNC type connectors throughout to keep unshielded wires from acting as radio antennae. A connection made up of a coaxial cable, followed by a wire without a concentric ground (i.e., with a parallel ground wire), and then another coaxial cable is as bad as having no ground at all. The same applies to the electrostatic shield on the photomultiplier, i.e., it must be continuously connected around its periphery to the ground shield surrounding the cable input to the base of the phototube. Contrary to the manufacturer's suggestion I found that operation of the electrostatic shield at the cathode potential instead of at ground potential connected to the other shields, was ineffective in reducing radio frequency noise introduced into the phototube output. Experience would seem to indicate that the continuity of the concentric ground shield is of paramount importance in reducing electrical noise.

III. TRIPLET EXCITATION MIGRATION

1. Description of the Experiments (22). The exciton interaction which we wish to measure is directly responsible for two effects which might be experimentally studied. These are: 1) the factor group (Davydov) splitting observed in the absorption spectrum of the crystal, and 2) the migration of excitation from one lattice site to another. Because of the very small oscillator strength ($f \sim 8 \cdot 10^{-11}$) (23) of the ground state to the lowest triplet state ($^1A_{1g} - ^3B_{1u}$) transition of benzene, it is presently impractical to attempt the first method with benzene. Therefore it was decided to study the migration of triplet excitation in crystalline benzene. Earlier work (24) had shown that the triplet state is quite mobile in solid naphthalene and the same was found to apply to benzene in which impurities are not so great a problem. A recent review article by Ermolaev (25) gives a summary of much of the foreign work on triplet excitation migration in the solid phase, especially in low temperature glasses.

-
- (22) A brief report of some of Section III appears in G. C. Nieman and G. W. Robinson, J. Chem. Phys., 37, 2150 (1962).
- (23) G. W. Robinson, J. Mol. Spectr., 6, 58 (1961).
- (24) M. A. El-Sayed, M. T. Wauk, and G. W. Robinson, Mol. Phys., 5, 205 (1962).
- (25) V. L. Ermolaev, Usp. Fiz. Nauk, 80, 3 (1963) [English Trans. Soviet Phys.-Uspekhi, 6, 333 (1963)].

To study triplet excitation migration it is necessary to have a way of identifying where the excitation started and where it ended. This can be accomplished by the use of a three-component isotopic mixed crystal. Such a crystal might contain $\frac{1}{3}\%$ C_6H_6 and $\frac{1}{3}\%$ C_6H_5D dissolved in C_6D_6 . In such a crystal the C_6D_6 serves as the host and the C_6H_6 and C_6H_5D serve as energy traps of slightly different trap depths. In zero order these depths are respectively 200 and 167 cm^{-1} . At liquid helium temperature ($4.2^\circ\text{K} \sim 3\text{ cm}^{-1}$) energy migration will tend to enhance the population, and thus the phosphorescence of the lower lying of the two traps (C_6H_6) compared to that originally present. Because of the similarity of the trapping species it is reasonable to assume that the two traps are initially populated (following host excitation) in the same ratio as their concentrations. It is also necessary to assume that the two traps have the same intersystem crossing rates since the energy mostly enters the traps as singlet excitation. They must also have the same lifetimes in the crystal. For the two traps, C_6H_6 and C_6H_5D , these assumptions would appear to be valid. Thus the singlet state, which is essentially non-migrating, shows emission (fluorescence) from the traps in the same ratio as their concentration. Also the low concentration limit of the phosphorescence ratio appears to be the trap concentration ratio. However, these assumptions break down if one further changes the degree of deuteration of the trap species. For the traps

C_6H_6 and $C_6H_3D_3$ it appears that the $C_6H_3D_3$ is preferentially populated by a factor as large as two (26).

Fig. III-1 shows a portion of the densitometer tracings resulting from two of these excitation migration experiments. As an example of the degree of this migration of the triplet state note the upper trace of Fig. III-1. This represents the phosphorescence of a reference solution containing 0.8% C_6H_5D dissolved in C_6D_6 , but shows that one quarter of the total phosphorescence originated from C_6H_6 impurity even though its concentration was only about 0.01%. Also note that in the lower trace of Fig. III-1 almost 95 per cent of the phosphorescence was from the lower trap even though the traps were present in equal concentrations (0.4%). Table III-1 summarizes the findings of some of these triplet excitation transfer studies. Because of differences in the Franck-Condon factors for the two traps, the figures given in this table are for the total intensity of the measurable lines (about 90% of the total intensity).

2. Mechanism for Excitation Migration. In order to calculate the excitation migration matrix element from the results of excitation migration experiments one needs to know the mechanism and statistics of the transfer process. Because of the extremely long lifetime of the triplet state a

(26) Further triplet excitation transfer studies by Steve Colson using various deuterated benzene traps have shown some rather strange results.

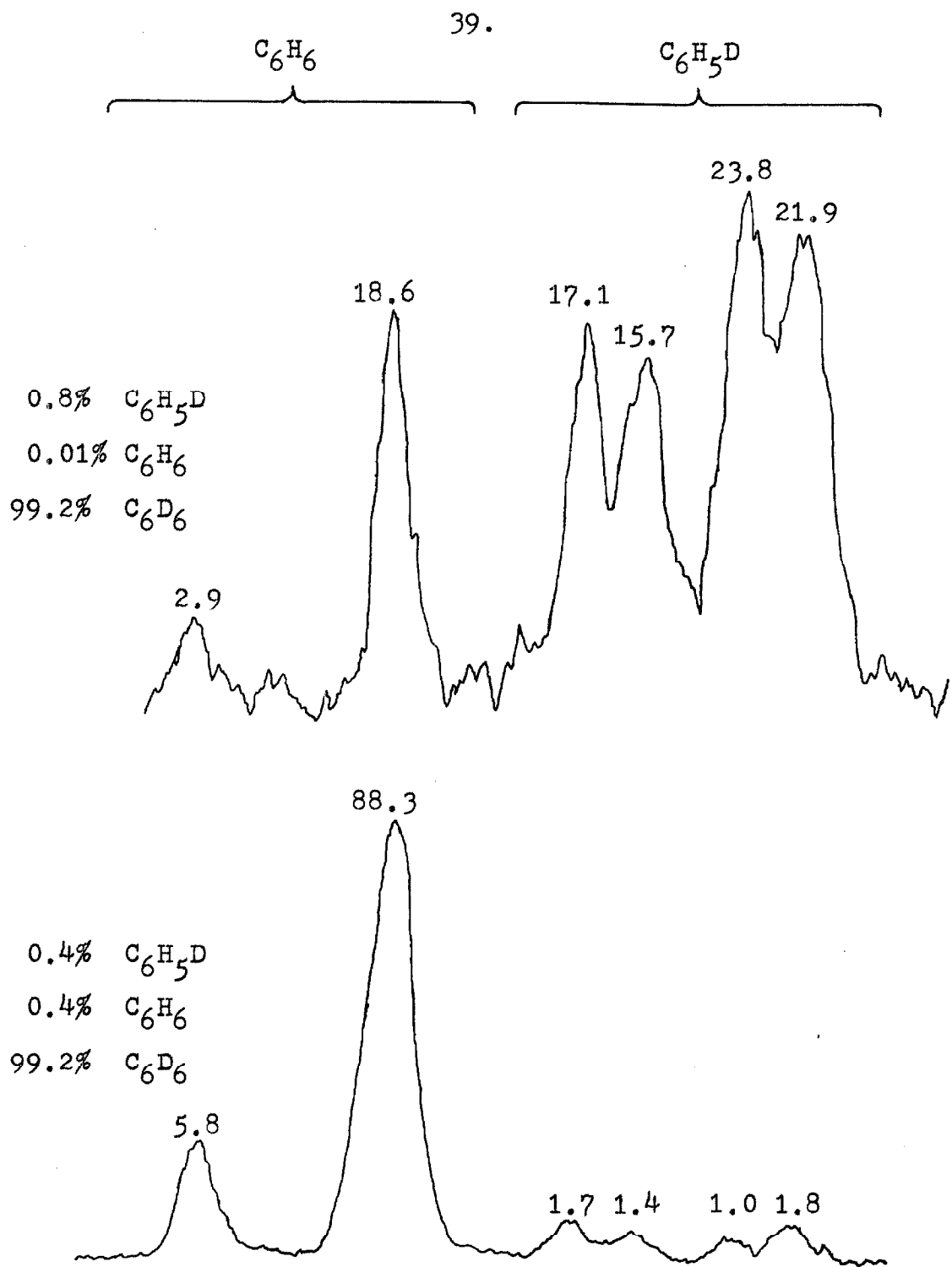


Fig. III-1. Densitometer tracing of a portion of the phosphorescence spectrum of a three-component benzene crystal. Note the enhancement of the C_6H_6 emission due to triplet energy transfer from the high energy trap, C_6H_5D , to the low energy trap, C_6H_6 . These lines are the Fermi resonance components at approximately $(0,0)-1600\text{ cm}^{-1}$. The numbers above each line are the normalized intensities (%).

Table III-1.

Results of triplet excitation migration studies.*

f_T [C ₆ H ₅ D]	f_S [C ₆ H ₆]	f_S/f_T	$\frac{I(C_6H_6)}{I(C_6H_5D)}$	γ
Phosphorescence				
0.008	0.0001	0.01	0.33	0.76
0.004	0.004	1.0	20.	0.095
0.0009	0.0001	0.1	0.19	0.93
0.0004	0.0004	1.0	3.0	0.50
Fluorescence				
0.008	0.0001	0.01	0.07**	0.94
0.004	0.004	1.0	1.7	0.74
0.0009	0.0001	0.1	0.1**	1.0
0.0004	0.0004	1.0	1.0**	1.0

* f_T and f_S are, respectively, the fraction of traps (C₆H₅D) and the fraction of supertraps (C₆H₆); $I(C_6H_6)/I(C_6H_5D)$ is the ratio of intensities for phosphorescence or for fluorescence; and γ is the fraction of traps (T) excited which in turn emit. The host lattice is always C₆D₆.

** Visual estimate, since high background intensity makes densitometer results unreliable.

very small intermolecular interaction energy can account for a considerable amount of trap-to-trap excitation migration. Still, the direct interaction between guest molecules, such as that calculated on the basis of the formulae of Förster (27), may be many orders of magnitude too small. The mechanism proposed here to explain the observed energy migration does not depend upon this direct coupling, but instead depends upon the indirect trap-to-trap interaction through the close lying virtual excited states of the host lattice.

The average time (τ_N) for a trap-to-trap energy transfer between two traps separated by N intermediate host molecules is given by the uncertainty relation:

$$\tau_N \sim \hbar \beta_N^{-1}. \quad (1)$$

Here \hbar is Planck's constant over 2π and β_N is the matrix element for the exciton interaction through N host molecules.

A rough estimate of β_N may be gained by consideration of the one-dimensional problem which can be solved exactly for nearest neighbor interactions in the limit of perturbation theory where $\Delta E \gg f_\beta \beta_0, f'_\beta \beta'_0$ (28,29). For a linear chain

(27) T. Förster, Disc. Faraday Soc., 27, 7 (1959). Because of the dependence upon the oscillator strength of the transition and upon the overlap of the absorption and emission spectra in Förster's formulae, they can not be successfully applied to the present problem.

(28) K. Herzfeld, J. Chem. Phys., 10, 508 (1942).

(29) H. M. McConnell, J. Chem. Phys., 35, 508 (1961).

of N intermediate hosts having a guest at each end the matrix element for transfer of triplet excitation from one guest to the other is:

$$\beta_N = g(f_\beta \beta_0)^2 (f'_\beta \beta'_0)^{N-1} (\Delta E)^{-N}, \quad N \geq 1. \quad (2)$$

Here ΔE is the zero-order energy difference, roughly equal to the difference between the excitation energy of the free guest molecule and that of the free host. The matrix elements β_0 and β'_0 represent the nearest neighbor purely electronic interaction between respectively the guest and host and the host and host. The quantities f_β and f'_β are vibrational factors equal to the square of vibrational overlap integrals between the appropriate pair of initial, final, or virtual states. The quantity g is a degeneracy factor which is unity for the linear case.

For strong coupling in the host crystal relative to molecular vibrational binding (30), $f'_\beta = 1$, while in the weak coupling limit $f_\beta \sim f'_\beta < 1$. These vibrational factors are identical to the ones which govern the shape of the Franck-Condon envelope in radiative transitions (31). In many cases, f_β for vibrationally unexcited initial and final states is of the order of 0.1. Coupling may, of course, take place

(30) See, for example, W. T. Simpson and D. L. Peterson, J. Chem. Phys., 26, 588 (1957).

(31) G. W. Robinson and R. P. Frosch, J. Chem. Phys., 38, 1187 (1963).

through certain vibrationally excited virtual states of the host and in general a sum over all such states must be included in the evaluation of β_N . However, in the present case ΔE is small compared with vibrational excitation energies, and the greatly increased energy denominators for the vibrationally excited virtual states cause their neglect to be usually justifiable. Also since the vibrational overlap factors are uninteresting for the present discussion, it is convenient to absorb them into an interaction matrix element $\beta = f_\beta \beta_0$ (likewise $\beta' = f_{\beta'} \beta'_0$). We thus arrive at a new form for Eq. 2:

$$\beta_N = g(\beta)^2 (\beta')^{N-1} (\Delta E)^{-N}. \quad (3)$$

In a two- or three-dimensional crystal to correctly calculate the transition probability between two guests, the right side of Eq. 3 must be multiplied by a factor ($g \neq 1$) which represents the increased degeneracy of virtual states, i.e., the increased number of transition pathways. For a two-dimensional isotropic crystal this factor is the binomial coefficient $\binom{x+y}{x}$ where (x,y) is the coordinate of the second trap relative to the first trap located at the origin (32). In this case the number of intermediate host molecules (N) is $x+y-1$. A product of such factors should apply in other cases.

(32) I am indebted to Mike Green who did much theoretical work on this degeneracy factor. This portion of the discussion follows closely his unpublished results.

In one-dimension there is only one direct path between two traps, i.e., a path with no "missteps". However, in two- or three-dimensions there are many of these non-direct paths between two traps. Since "missteps" must occur in pairs, each such path has a much lower transition probability (by a factor of about 1/200 for the case of benzene). This is somewhat offset by the greatly increased number of paths, so that in many cases this factor may be of the same magnitude as the factor for the degeneracy of the direct paths. For the two-dimensional isotropic crystal the "misstep" factor (33) is the product of binomial coefficients $\binom{2k}{k+\frac{x-y}{2}} \cdot \binom{2k}{k-\frac{x+y}{2}}$, where $2k-1$ is the actual number of sites in the path, including missteps. Thus for the case of a pair of missteps $2k-1=x+y+1$. It should be pointed out that the above product is too large by a factor of about two because it includes "re-steps", i.e., paths which simply reverse the previously taken step.

3. Calculation of the Exciton Matrix Element. To relate the above transition probabilities between individual trap sites to experimental observables, we need to ask the question, "How many different traps will an excitation visit during its lifetime?" The problem of the migration of excitation through a lattice is similar to a diffusion problem,

(33) C. Jordan, Calculus of Finite Differences (Chelsea Publishing Co., New York, 1960), 2nd edition, pp. 633-638.

but it cannot be approached as an ordinary random walk. The traps are spaced randomly rather than uniformly in the lattice and the transition probabilities are very strongly distance dependent. Thus any attempt to calculate an average jump frequency and an average jump distance would give an answer strongly distorted by the relatively large number of jumps between a few near neighbor traps. These jumps do not occur in random directions, but are such that the excitation simply remains in its original neighborhood, despite an apparently high diffusion coefficient (34).

To properly answer the above question we need to know how many lattice sites are "seen" by a particular guest molecule. That is to say, over what volume can a transfer occur during the lifetime of the excited state? For this calculation we note that an excitation in one trap will transfer to another trap at some given distance in a time either short, or long, compared to its radiative lifetime with very few intermediate cases. Thus, because of the exponential nature of Eq. 3, this volume "seen" by a trap has a well defined boundary.

For an isotropic two-dimensional crystal the true shape of this volume (area) "seen" can be calculated by using Eq. 3 modified to account for the increased degeneracy of the virtual transfer paths to each lattice site (molecule). In this

(34) See also the "scavenger effect" in Sect. IV.

case one finds that this area "seen" is roughly circular for $\beta/\Delta E \sim 0.1$ and shrinks towards a diamond shape as $\beta/\Delta E \rightarrow 0$ (35). For the benzene energies the radius (half-diagonal) of this area is between 1 and $1\frac{1}{4}$ times that $(N+1)$ which corresponds to the neglect of the degeneracy of the direct paths and missteps. Having chosen a model for the crystal of interest one can, thus, calculate the number of molecules "seen" by a particular trap molecule.

We now need to relate this number to the experimentally observed ratio of the phosphorescence from the two different types of traps. For this purpose it is convenient to introduce a new measure (γ) of the degree of the excitation migration. We shall define γ as the ratio of the number of higher lying traps (C_6H_5D) emitting phosphorescence (i.e., not transferring) to the number which were initially excited. Thus γ , which is a sort of quantum yield, can never exceed unity at low temperatures; and γ conveniently relates experiments using different concentration ratios of the upper and lower traps.

Let us now relate γ to the experimentally observed ratio of phosphorescence intensities. We shall also consider briefly the effect of a third even lower lying impurity trap. For simplicity we shall call the higher lying trap, the trap (T), and the lower lying trap, the supertrap (S).

(35) M. Green, unpublished results.

Now by definition,

$$\gamma = \frac{[T]_e - [T]_t}{[T]_e}, \quad (4)$$

where $[T]_e$ is the concentration of traps (T) excited and $[T]_t$ is the concentration of traps transferring their excitation to a supertrap (S).

The observed phosphorescence ratio is given by,

$$\left(\frac{S}{T}\right)_0 = \frac{[S]_e + [T]_t - [S]_d}{[T]_e - [T]_t - [T]_d}. \quad (5)$$

Here $[S]_e$ is the concentration of supertraps excited and $[T]_d$ and $[S]_d$ are respectively the concentrations of traps and of supertraps which transfer their excitation to a third, deeper trap. From Eq. 5 it is apparent that a third, deeper trap can appreciably distort the observations. For the common case where $[T]_e = [S]_e$, it is reasonable to expect that $[T]_d \sim [S]_d$ for a chemical trap lying much lower than both trap and supertrap. In this case it is seen that the observed ratio, $\left(\frac{S}{T}\right)_0$, is larger than the true ratio, i.e., the presence of an impurity tends to indicate more excitation transfer than there actually is.

Solving Eq. 5 for $[T]_t$ and substitution into Eq. 4 gives,

$$\gamma = \frac{1 + [S]_e/[T]_e}{1 + (S/T)_0} - \frac{[S]_d - [T]_d \cdot (S/T)_0}{[T]_e \cdot [1 + (S/T)_0]}. \quad (6)$$

The last term represents the effect of impurities and is zero if energy transfer to impurities can be neglected. Because of a lack of adequate information concerning the

quantitative effects of impurities, we shall henceforth neglect the last term of Eq. 6, (36). Eq. 6 assumes that the non-radiative decay probabilities from trap and supertrap are the same and that there is only energy transfer from the trap to the supertrap and not from the supertrap to the trap at liquid helium temperatures [$E(T)-E(S)\sim 33\text{ cm}^{-1}$ while $4.2^\circ\text{K}\sim 3\text{ cm}^{-1}$]. For the analysis of the experimental data it is convenient to assume that $[S]_e/[T]_e$ is the ratio of the concentrations of supertrap and trap originally put into the mixture. Experimentally this number is the low trap concentration limit of the phosphorescence ratio. It is also approximately the observed ratio of the fluorescence from the supertrap to that from the trap, since the singlet state is essentially non-migrating. Both of these checks imply that for $\text{C}_6\text{H}_5\text{D}$ and C_6H_6 the ratio of triplet states excited is the same as the concentration ratio.

It still remains to relate γ to the number of sites "seen" by a trap and to the concentrations of trap and supertrap. This problem is complicated by the presence of multiple jumps among the traps (T) before the excitation is transferred to a supertrap. Excitation transfer between the supertraps does not affect the experimental results, because it cannot be observed.

(36) Weak visual impurity phosphorescence can sometimes be seen, but attempts to photograph this emission have failed. The crystals studied showed little of this emission.

Now the probability that neither a trap nor a supertrap will be in the volume "seen" by a trap site is,

$$\gamma' = (1 - f_S - f_T)^{\zeta_N}. \quad (7)$$

Here f_S and f_T are respectively the fraction of the molecules (including host molecules) which are supertraps and the fraction which are traps; ζ_N is the total number of molecules (lattice sites) "seen" by the original trap. Remember that γ is the fraction of excited traps (T) which do not transfer their excitation to a supertrap.

Now at low concentrations the probability that one trap, but not a supertrap will be "seen" is,

$$[(1 - f_S)^{\zeta_N} - (1 - f_S - f_T)^{\zeta_N}]. \quad (8)$$

In other words it is the probability of finding no supertraps minus the probability of finding no supertraps or traps. This probability times the probability of no transfer (γ') gives the probability of no transfer to a supertrap by means of an intermediate transfer to a trap (T). By similar reasoning for multiple transfers among the traps (T) one finds,

$$\gamma = (1 - f_S - f_T)^{\zeta_N} \cdot \left(1 + \sum_{m=1}^{\infty} [(1 - f_S)^{\zeta_N} - (1 - f_S - f_T)^{\zeta_N}]^m \right), \quad (9)$$

or,

$$\gamma = \frac{(1 - f_S - f_T)^{\zeta_N}}{1 - [(1 - f_S)^{\zeta_N} - (1 - f_S - f_T)^{\zeta_N}]}. \quad (10)$$

The exponent ζ_N is the total number of molecules, both host and guest, in the volume "seen" by a trap. This can be related to N of Eq. 3 according to the model used for the crystal. Examination of the crystal structure of benzene indicates that an isotropic two-dimensional model might be a good representation of the true structure (37). For an isotropic two-dimensional crystal this relationship is,

$$\zeta_{N=4} \sum_{N_1=0}^N (N_1+1) = 2N^2 + 6N + 4, \quad (11)$$

if one neglects the effect of the multiplicity of paths. Including this effect increases ζ_N by perhaps as much as 50%. For the present let us assume that Eq. 11 holds.

Analysis of the available excitation transfer data (Table III-1) by means of Eq. 10 implies that for the mixed crystals investigated $\zeta_N=250$ to 350. Fig. III-2 shows a plot of γ as a function of f_T and f_S/f_T for $\zeta_N=300$, along with the experimentally measured values. Inserting $\zeta_N=250$ to 350 into Eq. 11 gives $N=10$ to 12 ($\zeta_N=264$ to 364). Let us choose the former value to make some allowance for the path multiplicity effect.

The approximately 7-second lifetime of the triplet state in these systems implies (Eq. 1) that $\beta_N \sim 1.2 \cdot 10^{-12} \text{ cm}^{-1}$. Letting $\Delta E = 170 \text{ cm}^{-1}$ and substituting into Eq. 3, then gives $\beta \sim (1/g)^{1/11}$. Here it has been assumed that $\beta = \beta'$, i.e., the

(37) See the discussion of Sect. VI.

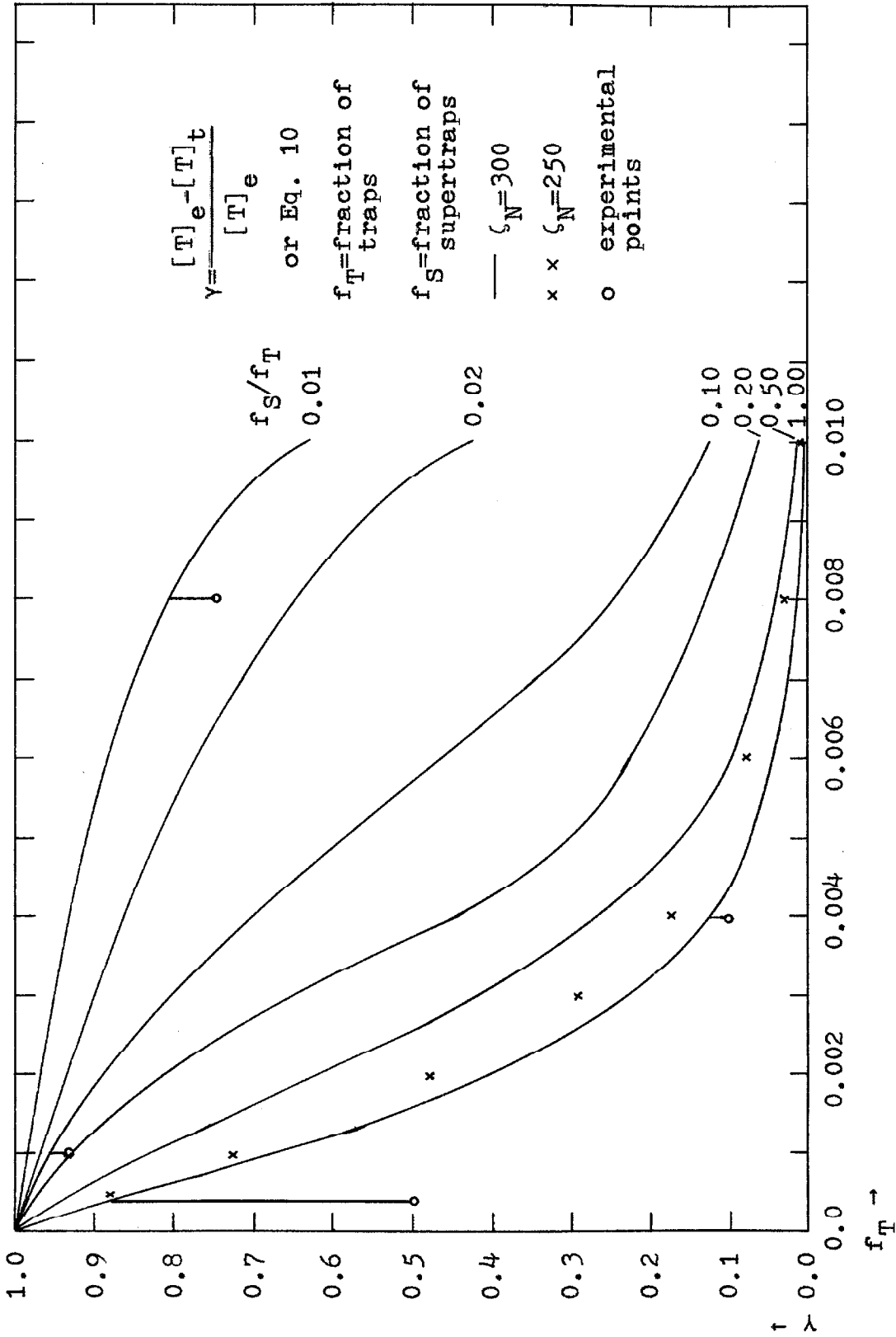


Fig. III-2. Nontransfer quantum yield (γ) versus fraction of traps for $\zeta_N=300$.

host-guest and the host-host interactions are equal. This should be a good approximation for these closely related isotopically substituted species, since the electronic portions of the intermolecular interactions are identical and the vibrational factors are very nearly identical. One should note that even for $g=1000$, $(1/g)^{1/11}=0.53$. Thus the degeneracy factor, which may average 10 to 100 for this size N , does not appreciably effect the magnitude of the calculated value of β , the exciton matrix element, which is $\sim 9 \text{ cm}^{-1}$.

In the above treatment the effect of non-resonance between initial and final states and the effect of vibrational relaxation have been neglected. Thus in the excitation transfer from a $\text{C}_6\text{H}_5\text{D}$ guest to a C_6H_6 guest approximately 33 cm^{-1} of excess energy must be given to the lattice. These effects may be important factors in determining the rate of excitation transfer, especially when large amounts of excess energy are involved. The non-resonance effect may well completely compensate for the path multiplicity effect. An interesting set of experiments have just been undertaken (38) which involve the study of energy transfer between $\text{C}_6\text{H}_4\text{D}_2$ and C_6H_6 where the energy difference is approximately 67 cm^{-1} . This value is very nearly equal to that ($\sim 70 \text{ cm}^{-1}$) (39) of a

(38) This study is being undertaken by Steve Colson.

(39) A. Fröhling, J. Chem. Phys., **18**, 1119 (1950); A. Fröhling, J. Phys. Radium, Series VIII, **2**, 88 (1948).

very prominent benzene lattice vibration which appears in the phosphorescence, fluorescence, and absorption spectra benzene crystals.

For the first excited π, π^* triplet state in aromatic hydrocarbons we may take 10 cm^{-1} to be a rough universal value of β . By assuming weak coupling in the crystal where $\beta \sim \beta'$, it is easy to see that trap-to-trap transfers having a mean life of about one second may take place through $N=12$ intermediate host molecules for $\Delta E=100 \text{ cm}^{-1}$, through $N=6$ intermediates for $\Delta E=1000 \text{ cm}^{-1}$, and through $N=4$ intermediates for $\Delta E=10\,000 \text{ cm}^{-1}$. These three energy differences between guest and host correspond respectively to ranges where the guest and host are related by isotopic substitution, where the guest and host are related by chemical substitution (40), and where the guest is immersed in an "inert" π -electron host (41). In the case where the host is a low temperature glass, such as EPA, ΔE may be somewhat larger than $10\,000 \text{ cm}^{-1}$ but, more important, the host-host matrix elements associated with the more localized electronic transitions

(40) β -methylnaphthalene in naphthalene yields $\Delta E \sim 497 \text{ cm}^{-1}$.

(41) A probable low- ΔE example is naphthalene and phenanthrene in biphenyl as host. Here, $E(\text{biphenyl})-E(\text{phenanthrene}) \sim 1500 \text{ cm}^{-1}$. See R. W. Brandon, R. E. Gerkin, and C. A. Hutchison, Jr., J. Chem. Phys., 37, 447 (1962), where long-range transfer of triplet excitation among phenanthrene molecules (mole fraction $\sim 9 \cdot 10^{-3}$) is apparently occurring with the subsequent trapping of part of the triplet excitation on naphthalene molecules (mole fraction $\sim 5 \cdot 10^{-4}$).

in such solvents may be quite small. Nevertheless, triplet excitation transfer through one or two of these kinds of host molecules during the one second triplet state lifetime would not be surprising (42).

The preceding holds only for 0°K. Raising the temperature populates states where ΔE is smaller causing still more rapid transfer to occur (43). One sees then that fairly long-range, trap-to-trap triplet excitation migration in π -electron systems can take place through rather high-lying virtual states of the host during the long lifetime of the triplet state. It is seen that the mechanism predicts a large temperature effect (44), a large concentration effect, and a large solvent effect on the rate of long-range triplet energy migration in these crystals, since it is the nearness of solvent (host) states, as well as the number of intermediate host molecules through which the transition must occur, which determine the trap-to-trap excitation transfer (exciton) matrix elements and therefore the transition probabilities.

(42) A possible example is the work of A. N. Terenin and V. L. Ermolaev, Dokl. Akad. Nauk, USSR, 85, 547 (1952).

(43) The "activation energy" for such a process does not correspond to the trap depth since excitation tunneling occurs even at 0°K.

(44) Above about 15°K no benzene phosphorescence can be detected from these isotopic mixed crystals because rapid triplet energy transfer and subsequent quenching by impurities and by triplet-triplet annihilation quench the benzene triplet states. See also M. A. El-Sayed, M. T. Wauk, and G. W. Robinson, Mol. Phys., 5, 205 (1962).

The large triplet excitation migration matrix element coupled with the long triplet state lifetime implies some important consequences: 1) the possibility of approximately 10^{12} triplet excitation transfers per radiative lifetime in pure organic crystals compared with only about 10^4 - 10^6 for the lowest singlet; 2) trap-to-trap migration of triplet excitation in chemically impure organic crystals, the rate depending upon the depth of the impurity trap, the temperature, and the impurity concentration; 3) possible biological importance where it appears no longer reasonable to ignore energy transfer via the triplet state; and 4) rapid triplet excitation migration and the closely related process of triplet-triplet annihilation leads to the quenching of phosphorescence from pure organic crystals and the production of delayed fluorescence from chemically impure organic crystals.

In Sect. V we shall return to a more accurate determination of β and to a correlation of this "pairwise" interaction for the model crystal with the true crystal interactions.

IV. TRIPLET-TRIPLET ANNIHILATION AND DELAYED FLUORESCENCE

1. Introduction and Some Preliminary Experiments (45).

During the course of the preliminary experiments designed to test the feasibility of using isotopic mixed crystals of benzene to study the triplet state, it was decided to look for the phenomenon of delayed fluorescence. Delayed fluorescence had been observed from crystals of naphthalene and other aromatics by Blake and McClure (46) and by Sponer, Kanda, and Blackwell (47). Recent studies by Azumi and McGlynn (48) concerning the delayed fluorescence of aromatic molecules in low temperature glasses closely parallel the present work. Delayed fluorescence from anthracene crystals excited by ruby laser light has also been observed by Kepler and co-workers (49). Other workers (50) have observed delayed fluorescence

-
- (45) Most of Sect. IV is also discussed in H. Sternlicht, G. C. Nieman, and G. W. Robinson, J. Chem. Phys., 38, 1326 (1963).
- (46) N. W. Blake and D. S. McClure, J. Chem. Phys., 29, 722 (1958).
- (47) H. Sponer, Y. Kanda, and L. A. Blackwell, J. Chem. Phys., 29, 721 (1958).
- (48) T. Azumi and S. P. McGlynn, J. Chem. Phys., 39, 1186 (1963).
- (49) R. G. Kepler, J. C. Caris, P. Avakian, and E. Abramson, Phys. Rev. Letters, 10, 400 (1963).
- (50) See, for example, C. A. Parker and C. G. Hatchard, J. Phys. Chem., 66, 2506 (1962); B. Stevens, E. Hutton, and G. Porter, Nature, 185, 917 (1960); and Ref. (48).

in the liquid and the gaseous phases.

For the purposes of this discussion delayed fluorescence shall be defined as that singlet-singlet emission having all the characteristics of the normal fluorescence except that it has a much longer lifetime. We shall be primarily interested in this phenomenon in the crystalline phase. The original explanation of Sponer (47) involved ionization with emission upon recombination of electron and hole. It seems to be more reasonable to assign this emission to the end product of triplet-triplet annihilation.

It has been shown in Section III that triplet excitation is very mobile in molecular crystals, and thus there is ample opportunity for the interaction of two triplet states. The mutual annihilation of a pair of triplet states can produce a single molecule excited to a singlet, triplet, or quintet state at approximately twice the lowest triplet state energy. A portion of these highly excited states can then degrade by very fast radiationless processes to the lowest excited singlet state which can then fluoresce in the ordinary manner. The lifetime of this fluorescence, however, is determined by the relatively slow migration and annihilation of triplet excitations and not by the lifetime of the radiative transition.

Since this proposed mechanism of delayed fluorescence production requires two quanta of incident light to produce one quantum of emission, a square dependence upon source

light intensity was sought. Experimentally this involved the simultaneous recording on a spectrographic plate of the phosphorescence and the delayed fluorescence using a phosphoscope having approximately a 0.1 second time delay between excitation and observation of the sample. On the same plate a second exposure was made using a neutral density screen (36% transmission) in the exciting light beam and a longer exposure time designed to give a nearly constant energy input (51). The non-linear response of the delayed fluorescence compared to the nearly linear response of the phosphorescence to the light intensity change was clearly evident. A densitometer tracing of this plate (52) showed the following:

$$\frac{I(DF,1)}{I(DF,2)}=3.3$$

$$\frac{I(P,1)}{I(P,2)}=1.3.$$

This result seems to indicate a greater than square-law dependence of delayed fluorescence intensity upon excitation intensity but this may well be due to errors in the measurement of the weak delayed fluorescence intensities.

Very crude measurements were also made of the phosphor-

(51) Because of an error in a previous calibration of the screen's transmission, instead of equal energy inputs the true ratio was, $(I,1)/(I,2)=1.6$. Note that the less than linear phosphorescence response is what one expects as one approaches a large trap concentration. See the later discussion of the reaction kinetics.

(52) This experiment was performed at 4.2°K with a crystal containing 2% C_6H_6 dissolved in C_6D_6 .

escence decay using a photomultiplier (EMI 9514S) as the light detector. In this case the phosphoroscope was turned manually and the oscilloscope trace of the photomultiplier output was triggered by the signal itself. Unfortunately at this early time my electronics abilities left much to be desired and the techniques used were very unsophisticated. These decay curves showed increasing non-exponential character the higher the concentration of traps. Fig. IV-1 shows the decay curve for the phosphorescence of a crystal containing 5% C_6H_6 dissolved in C_6D_6 . More about this curve will be said later. Unfortunately no decay curves were obtained for the delayed fluorescence because of its weakness and related problems of filtering out the strong phosphorescence and of the presence of much noise in the phototube output. Future experiments by myself at the University of Rochester and/or by Steve Colson here at the California Institute of Technology should provide a much better experimental basis for the discussion to follow.

2. Description of the Mechanism and Calculation of the Annihilation Rate. The problem of the production of delayed fluorescence involves two closely related processes: 1) long-range triplet excitation migration, and 2) long-range triplet-triplet annihilation. Again let us consider a mixed crystal containing a small amount of impurities (chemical or isotopic). This is the physically important case, since in the pure crystal, or in the very dirty crystal, the rates of

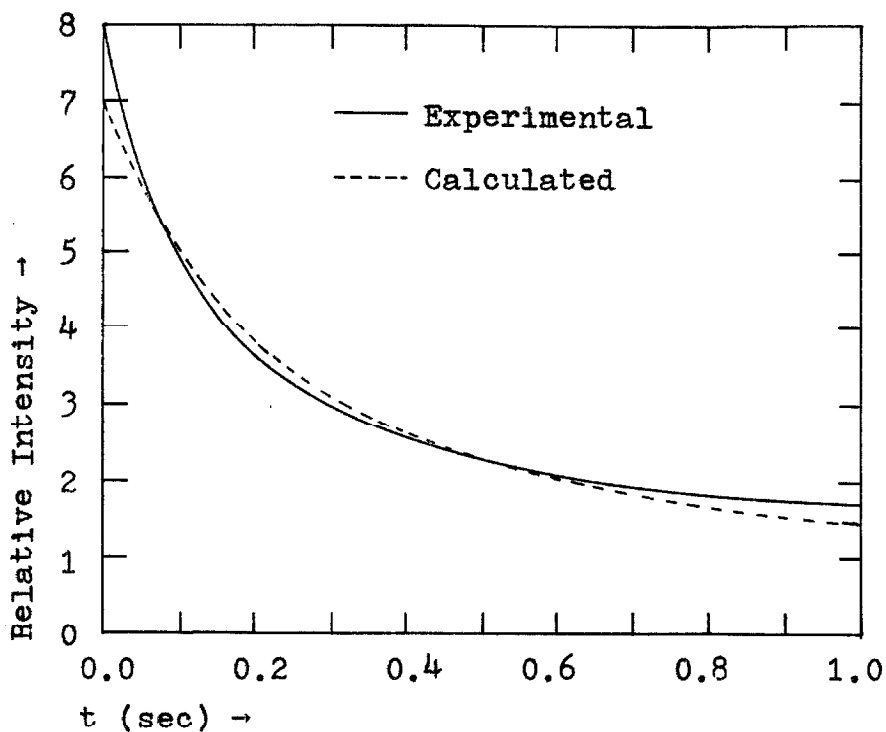


Fig. IV-1. Experimental and calculated phosphorescence decay curves for a 5% C_6H_6 -95% C_6D_6 crystal. The calculated curve assumes $A=0.98$, i.e., $(I/I_0)_T=1/(1+4t)$. Note that the calculated curve predicts too slow a decay at the beginning and too fast a decay at the end due to the "scavenger" effect, i.e., the nonuniform distribution of traps.

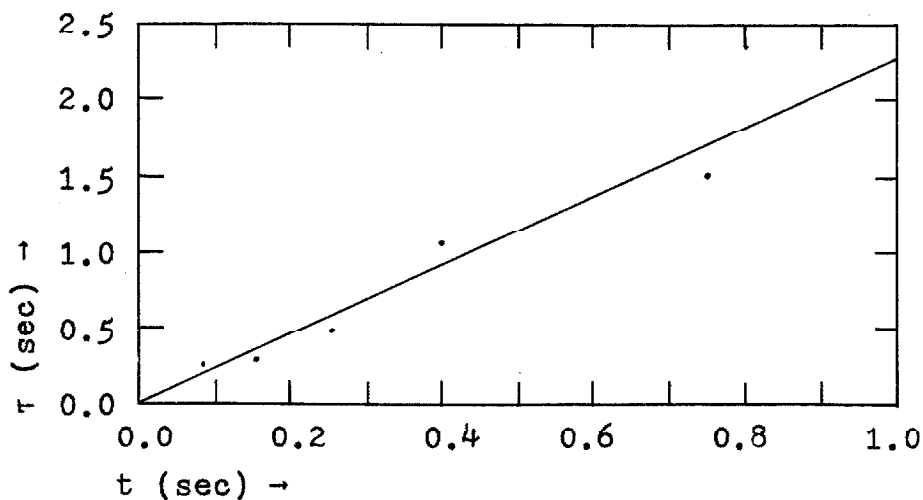


Fig. IV-2. Initial phosphorescence lifetime as a function of time after excitation cutoff for a C_6D_6 crystal containing 5% C_6H_6 .

triplet migration and annihilation become so rapid that the delayed fluorescence produced has a lifetime approaching the natural fluorescence lifetime. Triplet excitation migration can and does bring triplet states together, but it is not necessary to have two triplet excitations on nearest neighbor sites to produce annihilation. The annihilation interaction matrix element (γ_N) is thought of as proceeding through virtual host states just as in the excitation migration problem. Again the most important set of virtual states of the host crystal are those through which the trap-to-trap interaction can take place in lowest order.

Consider, as in the excitation migration problem, a linear chain of N solvent molecules with a trap at each end (a and b) and denote the solvent states by a prime. Let the initial state with both traps excited to their lowest triplet states (T_1) be $|GT_{1a} S'_{01} S'_{02} \dots S'_{0N} T_{1b}\rangle$. One final state with one trap in the ground state (S_0) and the other in a high singlet state (S_1) is $|GS_{1a} S'_{01} S'_{02} \dots S'_{0N} S_{0b}\rangle$. A set of virtual states which connects these initial and final states by an N^{th} order process is $|GT_{1a} S'_{01} S'_{02} \dots T'_{1N} S_{0b}\rangle$, $|GT_{1a} S'_{01} T'_{12} \dots S'_{0N} S_{0b}\rangle$, and $|GT_{1a} T'_{11} S'_{02} \dots S'_{0N} S_{0b}\rangle$. The first state of the set interacts with the initial state by way of a host-guest triplet excitation transfer interaction having matrix element $f_{\beta} \beta_0$. This matrix element is probably about 10 cm^{-1} as in the case of pure benzene. The intermediate states are associated with T_1 states of the solvent chain,

and the interaction between these states is by way of a host-host triplet excitation transfer interaction with matrix element $f'_\beta \beta'_0$. The N^{th} state, $|GT_{1a} T'_{11} S'_{02} \dots S'_{0N} S_{0b}\rangle$, interacts with the final state by way of a matrix element representing a nearest neighbor triplet annihilation interaction between host and guest.

Use of the above set of virtual states allows one to find easily by methods similar to those used (53, 54) for the triplet transfer problem that

$$\gamma_N = (f_\beta \beta_0) (f'_\gamma \gamma_0) (f'_\beta \beta'_0)^{N-1} (\Delta E)^{-N}, \quad N \geq 1. \quad (12)$$

Here f_β , f'_β , and f'_γ are products of vibrational overlap integrals and β_0 , β'_0 , and γ_0 are purely electronic interaction matrix elements between initial, final, and virtual states for the guest-host and host-host triplet excitation transfer processes, and for the nearest neighbor triplet-triplet annihilation process respectively. Thus, as in the trap-to-trap triplet excitation migration problem, the indirect interaction through the virtual states of the host falls off exponentially with the number of intervening host molecules.

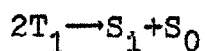
We now consider the problem of calculating the nearest neighbor annihilation probability (γ_0). Addition of the spin angular momenta of two molecules, each in its lowest triplet

(53) K. Herzfeld, J. Chem. Phys., 10, 508 (1942).

(54) H. M. McConnell, J. Chem. Phys., 35, 508 (1961).

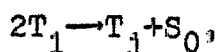
state (T_1) yields states of spin 0, 1, and 2 (singlet, triplet, and quintet).

We shall examine the two reactions,



and

(13)



where T_1 is the lowest lying triplet state, S_0 is the ground state, and S_1 and T_j are more highly excited singlet and triplet states whose electronic energies lie lower than twice the energy of T_1 , i.e., $2E(T_1) > E(S_1), E(T_j)$. Any excess energy between $2T_1$ and S_1 , the lowest excited singlet state, is then donated to the lattice as heat. Thus delayed fluorescence depends upon the existence of processes like those of Eq. 13 in addition to rapid ($\tau < 10^{-6}$ sec.) intramolecular radiationless transitions from S_1 or T_j to S_1 .

The relevant matrix elements for these two cases have been investigated (55) by using two-electron functions instead of the actual many electron eigenfunctions. Examination of these matrix elements leads to the conclusion that most of the 32 possible integrals for each case essentially vanish because of orbital orthogonality or because two-center integrals are further modified by small intermolecular

(55) H. Sternlicht, Dissertation (California Institute of Technology, Pasadena, 1963); H. Sternlicht, G. C. Nieman, and G. W. Robinson, J. Chem. Phys., **38**, 1326 (1963).

electronic overlap factors. There is however one purely exchange term which has an overlap coefficient of unity. Such an intermolecular exchange integral is of the same type as that which we shall see is responsible for triplet excitation migration. Consideration (in Section VI) of similar intermolecular exchange integrals associated with two carbon atoms whose distance and orbital orientations approximate those for the largest intermolecular π -orbital interaction in the benzene crystal, has indicated a value between 100 and 1000 cm^{-1} . Since the present exchange integral involves a higher lying orbital than that above its value is expected to be at least this large. We believe therefore that this term dominates all others and gives the major contribution to γ_0 . For the interaction in the actual molecular crystal, the integrals would have to be modified by the aromatic LCAO coefficients (56), summed over all carbon atoms, and multiplied by the appropriate vibrational factor.

Intermolecular exchange integrals, because they depend upon electronic coordinates of two molecules, are not so dependent upon molecular symmetry properties as are intermolecular Coulomb integrals which can be factored by use of the multipole expansion into products of integrals depending only upon the electronic coordinates associated with a single molecule. Since most of the aromatic crystals have little

(56) E. Hückel, Z. Physik, 76, 628 (1932).

symmetry except a center of inversion, the only important "selection rule" for triplet-triplet annihilation is that the excited states labeled S_1 or T_j must be g vibronic states.

The calculation of the transition probability from the interaction matrix element γ_0 is not as straightforward as it is for the excitation transfer problem since here the initial and final electronic states are not in resonance. The resonance criterion is met by the superposition of molecular and lattice vibrational states on the final electronic state of the system. Thus, at sufficiently low temperatures, the initial state corresponds to the zeroth vibrational level of $|GT_{1a}T_{1b}\rangle$, while the final state of the transition corresponds to vibrational excitation distributed over S_{1a} and S_{0b} of $|GS_{1a}S_{0b}\rangle$ or over T_{ja} and S_{0b} of $|GT_{ja}S_{0b}\rangle$. For such a case of electronic nonresonance it has been shown (57) that the transition probability has the form,

$$\frac{W(t)}{t} = \frac{2\gamma_N^2}{\alpha\hbar}, \quad (\gamma_N \ll \alpha \ll \Delta E). \quad (14)$$

Here $\hbar\alpha^{-1}$ is of the order of the molecular vibrational relaxation time in the vibrationally excited final electronic state, and γ_N is the matrix element for the annihilation interaction through the virtual states of N intervening solvent molecules. In the adiabatic approximation, γ_N^2 contains

(57) G. W. Robinson and R. P. Frosch, J. Chem. Phys., **32**, 1962 (1962).

vibrational factors f_γ which depend upon the product of vibrational overlap integrals between initial, final, and virtual states. For example, in the case of the nearest neighbor interaction at sufficiently low temperatures, the exact form of f_γ when the final state is $|GS_{1a}S_{0b}\rangle$ would be

$$f_\gamma = \sum_m \sum_n \langle \varphi_0(T_1) | \varphi_m(S_0) \rangle^2 \langle \varphi_0(T_1) | \varphi_n(S_1) \rangle^2, \quad (15)$$

where the vibrational eigenfunctions φ are those for the entire system and therefore include not only molecular modes but also lattice modes (57). The summation arises from the fact that the total transition probability is a sum of probabilities for transitions to each of the accessible final states. It runs over all vibrational states m and n of S_0 and S_1 , respectively, which meet the energy conservation requirement,

$$2E(T_1) - E(S_1) - \alpha \lesssim E_m^{\text{vib}} + E_n^{\text{vib}} \lesssim 2E(T_1) - E(S_1) + \alpha. \quad (16)$$

Similar arguments can be applied if $|GT_{ja}S_{0b}\rangle$ is the final electronic state. Because of the expected increased density of electronic states at high electronic excitation energies, in all likelihood there exists one or a number of molecular electronic g states S_1 or T_j meeting the criterion $2E(T_1) \gtrsim E(S_1)$ or $E(T_j)$, but having energies not too far removed from $2E(T_1)$. In benzene, for example, the states ${}^1E_{2g}^+$ and ${}^3E_{2g}^+$ might serve nicely as final states for the primary step in the triplet-triplet annihilation process. The

quintet state (${}^5A_{1g}$) of benzene is also a possible final state (58).

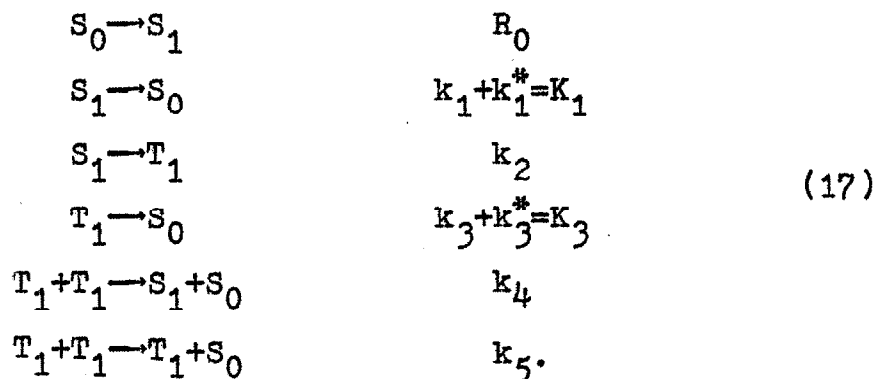
In a nonradiative process involving final states whose electronic energies differ little from the energy of the initial electronic state, the transition needs to convert only a small amount of electronic energy into vibrational energy. In this case vibrational overlap integrals may not be much less than unity. Therefore, the fourth-power dependence of f_γ on vibrational overlap integrals in Eq. 15 need not imply that f_γ is extremely small. In general the vibrational factor is extremely difficult to calculate rigorously, but a good guess would set $f_\gamma \sim 0.01$. We shall furthermore take γ_0 , the purely electronic annihilation interaction matrix element for nearest neighbors, to be about 100 cm^{-1} because of its similarity to the triplet excitation transfer matrix element β_0 . A rough estimate of $\hbar\alpha^{-1}$ would be 10^{-11} sec. It can be seen, therefore, that the time $\hbar(f_\gamma^{1/2}\gamma_0)^{-1}$ for a nearest-neighbor triplet-triplet annihilation process might easily be of the same order as the vibrational relaxation time. In this limit, Eq. 14 is not valid since vibrational relaxation may itself be the rate-determining step in the over-all process.

When $N \geq 1$, the important case for dilute mixed crystals, one expects γ_N to be much less than α , in which case Eq. 14

(58) F. A. Gray, I. G. Ross, and J. Yates, Austr. J. Chem., 12, 347 (1959); R. G. Parr, D. P. Craig, and I. G. Ross, J. Chem. Phys., 18, 1561 (1950).

can be applied. Combining Eq. 12 and Eq. 14 allows one to calculate the transition probability $W(t)/t$ for the process. The transition probabilities for nearest neighbor triplet excitation transfer and for triplet-triplet annihilation are of similar magnitudes. However, since annihilation falls off as the square of the long range matrix element γ_N , it is expected that in dilute systems excitation transfer is faster than annihilation. A temperature dependence, a concentration dependence, and a solvent dependence are expected in both cases because of the forms of Eqs. 2 and 12, (59).

3. Kinetics. The kinetics of the triplet annihilation problem in a mixed crystal cannot be easily treated rigorously since the traps are in fixed, inequivalent positions randomly distributed in the crystal lattice. For a uniform distribution of traps where the second-order rate constants do not vary throughout the crystal, one can obtain relationships among the excited state populations and their time dependencies by assuming the following mechanistic scheme:



(59) See Sect. III.

Here S_0 , S_1 , and T_1 refer to the ground state and the first excited singlet and triplet states of the traps, respectively. In the above equations energy is conserved by radiation of light or by conversion of electronic energy into heat or both. Unstarred constants represent nonradiative processes while the starred constants k_1^* and k_3^* refer to the radiative transition probabilities for fluorescence and phosphorescence, respectively. The rate at which traps in their ground state are excited to S_1 depends upon the light intensity, and the absorption coefficient and thickness of the whole crystal, since excitation is transferred from the host to the guest in a time which is short compared with the processes of interest here. We shall let the over-all rate associated with the production of S_1 states be designated R_0 , a quantity which depends linearly upon light intensity. The constants K_1 , k_2 , and K_3 have units sec.^{-1} ; k_4 and k_5 have units $\text{sec.}^{-1}\text{conc.}^{-1}$; while R_0 has units conc. sec.^{-1} . The processes with rate constants k_4 and k_5 proceed through higher states (i.e., S_1 and T_j) by fast radiationless transitions. The details are unimportant providing such radiationless transitions are not rate determining. Therefore, for simplicity we have written these reactions as if S_1+S_0 and T_1+S_0 are produced directly. The constant k_4+k_5 associated with the over-all triplet-triplet annihilation process is related to the theoretical transition probability $W(t)/t$ through the statistical probability that two excited triplets are separated by N hosts.

Straightforward manipulation yields for the stationary concentration of excited triplet states of the traps,

$$[T_1]_0 = \frac{K_3}{2k_6} \left(\left[1 + \frac{4k_2 k_6 R_0}{(K_1 + k_2) K_3^2} \right]^{\frac{1}{2}} - 1 \right), \quad (18)$$

which, when multiplied by the radiative transition probability k_3^* and the energy per quantum, is equal to the phosphorescence intensity $[I_0]_T$ under steady-state conditions. In Eq. 18 the constant k_6 is defined as,

$$k_6 = [(2K_1 + k_2)/(K_1 + k_2)]k_4 + k_5.$$

The rate equation for the disappearance of T_1 (i.e., the phosphorescence decay curve) can be expressed as an equation for the first- and second-order decays occurring simultaneously. This simplification is possible since the production of S_1 from two triplets rapidly produces T_1 or S_0 states. Therefore, for times after the irradiation cutoff which are long compared with $(K_1 + k_2)^{-1}$, S_1 can be considered to be a short-lived intermediate whose concentration is negligibly small compared with that of T_1 and S_0 . Application of the stationary-state approximation leads to the relationship,

$$[S_1] = [k_4/(K_1 + k_2)][T_1]^2. \quad (19)$$

Using this expression, the equation representing the decay of T_1 emission with time then becomes,

$$(I/I_0)_T = (1-A)/[\exp(K_3 t) - A], \quad (20)$$

where

$$A = k_6 [T_1]_0 / (K_3 + k_6 [T_1]_0).$$

The intensity of delayed fluorescence is dependent upon the square of the instantaneous T_1 concentration. According to Eq. 20 one has for the ratio of the intensity of delayed fluorescence at times t and $t=0$,

$$(I/I_0)_D = (1-A)^2 / [\exp(K_3 t) - A]^2. \quad (21)$$

The general expressions given in Eqs. 18, 20, and 21, are not usually as useful as limiting laws for the limits of high and low concentrations. Such laws follow easily from the general equations if one defines a new dimensionless constant,

$$K = k_2 k_6 R_0 / (K_1 + k_2) K_3^2,$$

proportional to the exciting light intensity and notices that in dilute mixed crystals, where the annihilation rate is slow, one has $K \ll 1$. On the other hand, in concentrated mixed crystals, where the annihilation rate is fast, one observes that $K \gg 1$. Table IV-1 lists the limiting laws in terms of the parameter K .

A number of important conclusions can be drawn from an examination of Table IV-1, and these will now be emphasized. In the low concentration limit the intensity of phosphores-

Table IV-1.

Limiting laws in terms of the parameter K.*

	Dilute mixed crystal, $K \ll 1$	Conc. mixed crystal, $K \gg 1$
A	K	$1 - K^{-\frac{1}{2}}$
$[I_0]_T$	$k_3^* k_3 k_6^{-1} K$	$k_3^* k_3 k_6^{-1} K^{\frac{1}{2}}$
$[I_0]_D$	$\frac{k_1^* k_4 K_3^2 k_6^{-2} K^2}{(k_1 + k_2)}$	$\frac{k_1^* k_4 K_3^2 k_6^{-2} K}{(k_1 + k_2)}$
$(I/I_0)_T$	$[1 - K + K e^{-K_3 t}] e^{-K_3 t}$	$[1 + K^{\frac{1}{2}} K_3 t]^{-1}$
$(I/I_0)_D$	$[1 - 2K + 2K e^{-K_3 t}] e^{-K_3 t}$	$[1 + K^{\frac{1}{2}} K_3 t]^{-2}$

* $K = k_2 k_6 R_0 / (K_1 + k_2) K_3^2$; $A = k_6 [T_1]_0 / (K_3 + k_6 [T_1]_0)$; $[I_0]_T$ and $[I_0]_D$ when multiplied by the energy per quantum of emitted light are the phosphorescence intensity and the delayed fluorescence intensity, respectively under steady-state conditions; and $(I/I_0)_T$ and $(I/I_0)_D$ give the decay curves for phosphorescence and delayed fluorescence.

cence under excitation from a light source of constant intensity depends linearly on the source intensity; but in the high concentration limit there is a saturation effect, and the steady state phosphorescence intensity varies as the square root of the intensity of the exciting source. It has been found that on the basis of this criterion a C_6D_6 crystal containing 1% C_6H_6 is an experimental example of the first limit, while a 5% C_6H_6 crystal is an experimental example of the second limit.

The dependence of the steady-state delayed fluorescence intensity on the square of the excitation intensity in the dilute crystal limit should be noted in Table IV-1. This dependence has been approximately verified experimentally, as mentioned earlier, for a 2% solid solution of C_6H_6 in C_6D_6 using neutral density screen filters. The linear dependence on source intensity expected in the high concentration limit has not yet been verified.

Approximately exponential decay laws are seen to hold in the dilute mixed-crystal limit for phosphorescence and delayed fluorescence emission, the rate constant for the latter process being twice that for the former. With increasing concentration of traps, however, both processes become strongly nonexponential, finally approaching the time variation shown for the high concentration limit. A plot, for example, of $-\log I/I_0$ vs t would show a slope whose magnitude decreases with time.

It can be seen from Table IV-1 that the phosphorescence lifetime is also a good experimental criterion for distinguishing between the two limits. In the case where K is small, the triplet lifetime approaches K_3^{-1} , the lifetime of the triplet state in the absence of annihilation. When K is much larger than unity, the triplet state disappears in a time which is much shorter than the normal phosphorescence lifetime. In C_6H_6 , K_3^{-1} is about 16 seconds (60). For a 1% crystal, $\tau(T_1) \sim 7$ seconds, while for a 5% crystal most of the phosphorescence has decayed in 1 second (61). Therefore the 1% crystal at 4.2°K seems like a fair approximation to the dilute mixed-crystal limit, while the 5% crystal is approaching the concentrated mixed-crystal limit. The limits based on the lifetime criteria are therefore consistent with those based on intensity measurements for isotopic mixed crystals of benzene.

It is important to remember at this point that all the above formulas are based upon a uniform distribution of traps throughout the host. In a real mixed crystal such a distribution cannot, of course, be obtained. Instead, the traps are distributed randomly, some being bunched more closely together and some being more dispersed than the average

(60) G. W. Robinson, J. Mol. Spectry., 6, 58 (1961); M. R. Wright, R. P. Frosch, and G. W. Robinson, J. Chem. Phys., 33, 934 (1960).

(61) See Fig. IV-1.

distribution. Since A is concentration dependent, a different A is associated with each such region of the crystal. The decay laws given by Eqs. 20 and 21 and those in Table IV-1 must therefore be modified accordingly. Because of the difficulty of estimating these A's and the clumsiness of summing over-all statistical distributions, no attempt is made here to improve upon these equations. Rather, it should be noted that interactions in the high concentration regions are stronger than those in the low concentration regions. Thus phosphorescence and delayed fluorescence decay faster in some regions of the crystal than in others. In a given time interval, use of an average A in Eqs. 20 and 21 would predict too slow a decay at the beginning and too fast a decay at later times than that which is experimentally observed. At very long times in a relatively concentrated mixed crystal, for example, excitations in the statistically improbable highly dilute regions are all that remain, and the characteristics of the crystal emission, though weak, should behave like that of a dilute crystal. Thus decay curves for mixed-crystal phosphorescence and delayed fluorescence may be highly nonexponential, not only because of the forms of Eqs. 20 and 21, but also because of this "scavenger" effect.

For a 5% C_6H_6 -95% C_6D_6 isotopic mixed crystal, rough quantitative agreement between experiment and the high concentration ($K \gg 1$) limiting law of Table IV-1 is obtained for the phosphorescence decay in the $t < 1$ sec. range if A is

chosen to be about 0.98. Fig. IV-1 shows the experimentally observed phosphorescence decay curve and that calculated on the basis of $K_3^{\frac{1}{2}}K_3=4 \text{ sec.}^{-1}$ (62). Note, as mentioned above, that the calculated phosphorescence decay is too slow at the beginning and too fast at the end compared with the measured decay because of the "scavenger" effect. The extreme weakness of the phosphorescence intensity is also explained by this value which, according to the definition of A, shows that $K_3 \sim 0.02k_6[T_1]_0$, corresponding to a phosphorescence quantum efficiency of roughly 0.02.

4. Experiments by Other Workers. Other investigators have made studies which concerned delayed fluorescence in the solid phase. Two of the early investigations on aromatic crystals were by McClure and co-worker (63) and by Sponer and co-workers (64). In both cases some of the crystals were naphthalene containing, the then undiscovered impurity, β -methylnaphthalene (65) which has a trap depth of about 500 cm^{-1} . Sponer invoked hole-electron recombination to explain the delayed fluorescence observed. The above kinetics

(62) If $K_3^{-1}=16 \text{ sec.}$, then $K_3^{\frac{1}{2}}=64$, which implies that $A \sim 0.98$.

(63) N. W. Blake and D. S. McClure, J. Chem. Phys., 29, 722 (1958).

(64) H. Sponer, Y. Kanda, and L. A. Blackwell, J. Chem. Phys., 29, 721 (1958).

(65) This impurity with origin at $31\,062 \text{ cm}^{-1}$ was identified by M. T. Shpak and E. F. Sheka, Opt. i Spektroskopiya, 8, 66 (1960) [Opt. Spectry. (USSR), 8, 32 (1960)].

equations for the high trap concentration limit have been applied (66) successfully to the more complete experimental data of Blake and McClure (63). Here a small change in the constant A (from 0.99965 to 0.99925) with time to account for the "scavenger" effect brings about rough agreement between the calculated and the experimental decay curves at 80°K.

The delayed fluorescence of aromatic molecules dissolved in low temperature "glasses" (EPA) has been studied by Azumi and McGlynn (67). Their results seem to confirm the picture presented here for the case of molecular crystals. Delayed fluorescence has also been produced by the direct ruby laser excitation of the lowest triplet state of anthracene in the crystalline phase by Kepler (68). These experiments show definitely that the triplet state is involved in the production of delayed fluorescence since it is the only state directly excited by red light. Similar experiments by Lipsett (69) studying the temperature dependence of the red light excited fluorescence of anthracene crystals using a xenon lamp

-
- (66) H. Sternlicht, G. C. Nieman, and G. W. Robinson, J. Chem. Phys., 38, 1326 (1963).
- (67) T. Azumi and S. P. McGlynn, J. Chem. Phys., 39, 1186 (1963). This paper contains a good bibliography of other work in this field.
- (68) R. G. Kepler, J. C. Caris, P. Avakian, and E. Abramson, Phys. Rev. Letters, 10, 400 (1963); P. Avakian, E. Abramson, R. G. Kepler, and J. C. Caris, J. Chem. Phys., 39, 1127 (1963).
- (69) S. Singh and F. R. Lipsett, to be published.

and a monochromator as a light source indicate the role played by various impurities.

5. Conclusions. The lack of detectable phosphorescence from many systems is often taken as an indication of a low population of the triplet state, whereas, in actuality, it may indicate that just the exact opposite is true. Triplet excitation migration and triplet-triplet annihilation may so rapidly quench triplet excitations that no phosphorescence can be detected because of the long radiative lifetime of the triplet state. Thus if the lifetime of the triplet state in a system is about 10^{-3} times the radiative lifetime, no phosphorescence might be detected. Yet the lifetime of the triplet state in this system could still be approximately 10^3 times the lifetime of the lowest excited singlet state, implying a consequently higher triplet state population. Therefore the triplet state can still be an important chemical and physical intermediate even though no phosphorescence can be detected.

Because of the rapid migration and mutual annihilation of triplet states in pure π -electron molecular crystals, it is very doubtful that phosphorescence from pure crystals of this type can be detected. Thus experiments which report the phosphorescence spectra of pure aromatic crystals, such as those by Sponer and co-workers (70) are very suspect. From

(70) H. Sponer and Y. Kanda, J. Chem. Phys., 40, 778 (1964).

the experience gained by studying mixed crystals of various isotopic benzenes it would appear that the phosphorescence detected from "pure" aromatic crystals is due entirely to small amounts of residual chemical impurities. These are often so closely related to the bulk material (as 8-methylnaphthalene in naphthalene) that their removal is impossible by ordinary separation techniques. Also the impurity spectrum may so closely resemble that of the host that at the relatively low resolution used the emission can roughly be interpreted on the basis of the host frequencies.

For isotopic benzene crystals, unless special precautions are taken, phosphorescence is from a species containing at least three more hydrogens than the host, i.e., 100 cm^{-1} traps. At superfluid helium temperatures ($\sim 2^\circ\text{K}$) weak phosphorescence can be detected from a 67 cm^{-1} trap, but only if no other close lying traps are present, i.e., only from C_6H_6 dissolved in $\text{C}_6\text{H}_4\text{D}_2$. Several attempts to detect benzene (C_6H_6) phosphorescence from $\text{C}_6\text{H}_5\text{D}$ (1% C_6H_6) or from pure C_6H_6 have ended in failure (71). In these cases all of the weak phosphorescence observed is from unidentified chemical impurities even though the level of these impurities does not exceed several parts per million. Thus, by analogy, the reported observations of phosphorescence from aromatic crystals,

(71) These experiments at 2°K could easily detect a phosphorescence intensity 10^{-4} times that of 1% C_6H_6 in C_6D_6 , or about 10^{-5} times that of 1% C_6H_6 in $\text{C}_6\text{H}_4\text{D}_2$.

such as toluene (72), are open to question.

Even though the above results do indicate that detectable phosphorescence is not expected to occur from pure crystals of π -electron molecules, not all organic crystals necessarily show low phosphorescence quantum yields. Factors which are favorable for organic crystal phosphorescence are 1) short triplet state radiative lifetimes, and 2) small triplet resonance interactions. An example of an organic crystal which fulfills these conditions is benzophenone. The (n, π^*) triplet radiative lifetime is short, and the excitation is roughly localized near the carbonyl group. The fact that the excitation is localized and the fact that the carbonyl groups on different molecules are relatively far apart combine to help lower the magnitude of the excitation transfer interaction in this case. The relatively short-lived emission process can then favorably compete with the annihilation mechanism which itself is slowed because of its square dependence upon smaller steady-state triplet concentrations. Presumably, therefore, detectable $T_1 \rightarrow S_0$ emission in a crystal like benzophenone can occur.

In passing it should also be mentioned that the C_6H_6 fluorescence quantum efficiencies of C_6H_5D (1% C_6H_6 natural impurity) and of pure C_6H_6 are respectively 20 and 50 times less than the C_6H_6 fluorescence quantum efficiency of a 1%

(72) Y. Kanda and H. Sponer, J. Chem. Phys., 28, 798 (1958).

solid solution of C_6H_6 in $C_6H_4D_2$. Furthermore, benzene fluorescence is observed only from 67 cm^{-1} , or lower, traps, if they are present. In the case of C_6H_5D or C_6H_6 nearly half of the observed fluorescence originates from the phenol impurity. It would thus appear that not only is triplet-triplet annihilation important in π -electron molecular crystals, but also singlet-singlet annihilation is very important in very pure crystals or in crystals containing very shallow traps. The exact end product, or products, of this latter annihilation are unknown, but this reaction accounts for the degradation of a considerable portion ($>95\%$) of the energy put into a pure crystal of benzene. Studies of the disappearance of this energy may well have some bearing upon photoconductivity measurements of molecular crystals as ionization may result from this singlet-singlet annihilation (73).

The mutual annihilation of singlet excitations in dilute mixed crystals is expected to be much less important than that of triplet excitations because the singlet lifetime is much shorter. The necessary high concentration of excited states is therefore much harder to maintain. In the case of benzene and naphthalene, for example, lowest singlet resonance interactions and singlet-singlet annihilation inter-

(73) S. Choi and S. A. Rice, J. Chem. Phys., 38, 366 (1963).
See also D. R. Kearns, J. Chem. Phys., 39, 2697 (1963).

actions are probably no more than ten times greater than those for the triplets. In addition, the lifetime, and thus the concentration of excited states, is about 10^7 times less. The rate of singlet-singlet annihilation is therefore expected to be only about $10^2 \cdot (10^{-7})^2$ as fast as that of triplet-triplet annihilation under the same excitation intensity for the case of the dilute mixed crystal. On the other hand, the singlet-singlet annihilation process may approach the efficiency of triplet-triplet annihilation in the limit where the annihilation rate is comparable with or faster than the reciprocal of the unperturbed fluorescence lifetime. This limit is expected to exist in concentrated mixed crystals or in pure organic crystals.

In summary then, some of the important consequences of triplet-triplet annihilation are: 1) fast triplet-triplet annihilation in pure aromatic crystals strongly quenching phosphorescence; 2) triplet-triplet annihilation in chemically impure organic crystals giving rise to delayed fluorescence; 3) the production of high energy excited states from low energy quanta, especially forbidden states such as triplets and quintets; 4) possible biological importance as an energy escalation mechanism; and 5) triplet-triplet annihilation, along with singlet-singlet annihilation, may give rise to some intrinsic photoconductivity in molecular crystals.

V. METHOD OF VARIATION OF ENERGY DENOMINATORS

1. Description of the Technique (74). The observed long range trap-to-trap migration of triplet excitation in crystalline benzene has been attributed to relatively large intermolecular exchange interactions in this crystal. On the basis of excitation transfer experiments with three-component isotopic mixed crystals, a rough estimate of the pairwise (75) benzene (0,0) interaction was 9 cm^{-1} (Sect. III). Because of the assumptions necessary in the analysis of these energy transfer experiments, the resulting calculated value for β is not very well defined. Therefore a new approach to this problem was attempted. This section deals with this approach which was used to better define the value of β , the triplet excitation transfer matrix element.

The technique, which I shall now briefly describe, to measure these interactions directly may be called the method of variation of energy denominators. The method consists simply of the study of perturbations of the energy levels of a guest molecule by nearby crystal states of the host. Use of different hosts allows a variation of the energy denominator ΔE in the perturbation problem. The matrix elements of

(74) Most of Section V is reported in G. C. Nieman and G. W. Robinson, J. Chem. Phys., 39, 1298 (1963).

(75) See the discussion in Section VI for the validity of characterizing this as simply a pair interaction.

interest here are the ones which are off-diagonal in the zero-order states of a tight binding approximation (76). When the energy difference between the zero-order states is zero ($\Delta E=0$), as in the pure crystal, such matrix elements are responsible for resonance interactions. When the energy difference is nonzero, as in isotopic mixed crystals, the zero-order states may be considered to be in quasiresonance.

The point of this approach is to use the method of variation of energy denominators to induce energy shifts of the lowest triplet state of benzene, experimental observation of the shifts being made through a study of the phosphorescence spectrum. Analysis of the shifts as a function of energy denominator allows a direct determination of the magnitude of the triplet exciton interaction.

The detection and measurement of small quasiresonance shifts require sharp spectral lines, the absence of extraneous shifts, and the ability to make a series of changes in the energy denominators over a range comparable to the magnitude of the interaction energy of interest. Since the matrix elements for this kind of interaction are not expected to exceed more than a few cm^{-1} , only subtle shifts can be hoped for even in the range of small energy denominators. Because the expected effects are small, various isotopically

(76) F. Bloch, Z. Physik, 52, 555 (1928); C. Kittel, Introduction to Solid State Physics (John Wiley & Sons, Inc., New York, 1956), 2nd ed., pp. 586-587.

substituted benzenes are the only suitable host molecules for these experiments. It is known from earlier work and it is illustrated in Fig. V-1 that C_6H_6 phosphorescence lines are quite sharp (77) in these kinds of mixed crystals. In addition, the energy denominators are small and can be changed by different isotopic substitution without appreciably distorting the crystal structure. Furthermore, it is expected, and is assumed here, that the off-diagonal matrix elements as well as the diagonal terms in the quasiresonance interaction and the higher-order dispersion terms are all invariant with respect to isotopic substitution in the host (78).

2. Vibrational Exciton Effects. It should be remembered that a perturbation shift may also arise because of the presence of vibrational exciton interactions both in the ground and excited states of the crystal. Quasiresonance vibrational shifts will not, of course, exist in the zeroth vibrational level in either electronic state. Therefore, the (0,0) band of the electronic transition experiences only the

(77) These lines are approximately kT wide ($\sim 3 \text{ cm}^{-1}$).

(78) When the electronic interaction becomes comparable to molecular vibrational energies, the purely electronic matrix element, even though invariant with respect to isotopic substitution, contains vibrational factors which depend on the degree of localization of the electronic excitation. Since the degree of localization depends on the electronic energy difference between host and isotopically substituted guest, the method of variation of energy denominators must be used with caution for interactions in the realm of intermediate coupling.

electronic shift while other vibronic transitions are subjected to both electronic and vibrational quasiresonance shifts. In the case of the benzene phosphorescence spectrum where the (0,0) band is extremely weak and not easily observed, both electronic and vibrational interactions must be considered in analyzing the energy shifts. At sufficiently low temperatures all of the emission comes from the zeroth vibrational level in the upper electronic state. Vibrational shifts in the low-temperature spectrum therefore are caused by ground-state perturbations only. The electronic excitation energy of C_6H_6 lies lower, but the vibrational frequencies lie higher, than those of any of its deuterium substituted derivatives. Thus, both electronic and vibrational quasiresonance interactions are expected to lead to increasing "red" shifts, i.e., shifts towards longer wavelength, of the C_6H_6 phosphorescence spectrum with decreasing degree of deuteration in the host crystal.

3. Observed Shifts. We now examine experimentally the phosphorescence spectrum at liquid helium temperatures of C_6H_6 dissolved in host crystals of C_6D_6 , 1,3,5- $C_6H_3D_3$, and 1,4- $C_6H_4D_2$. The energy denominators (ΔE) are approximately 200, 100, and 67 cm^{-1} , respectively (79). A small portion of the spectrum in each of the three host crystals is shown in Fig. V-1. The small shifts can be seen most clearly by

(79) Caused by zero-point energy effects. See Refs. (5,6,7).

A PORTION OF THE C_6H_6 PHOSPHORESCENCE SPECTRUM
IN ISOTOPIC MIXED CRYSTALS SHOWING THE
PERTURBATION SHIFT

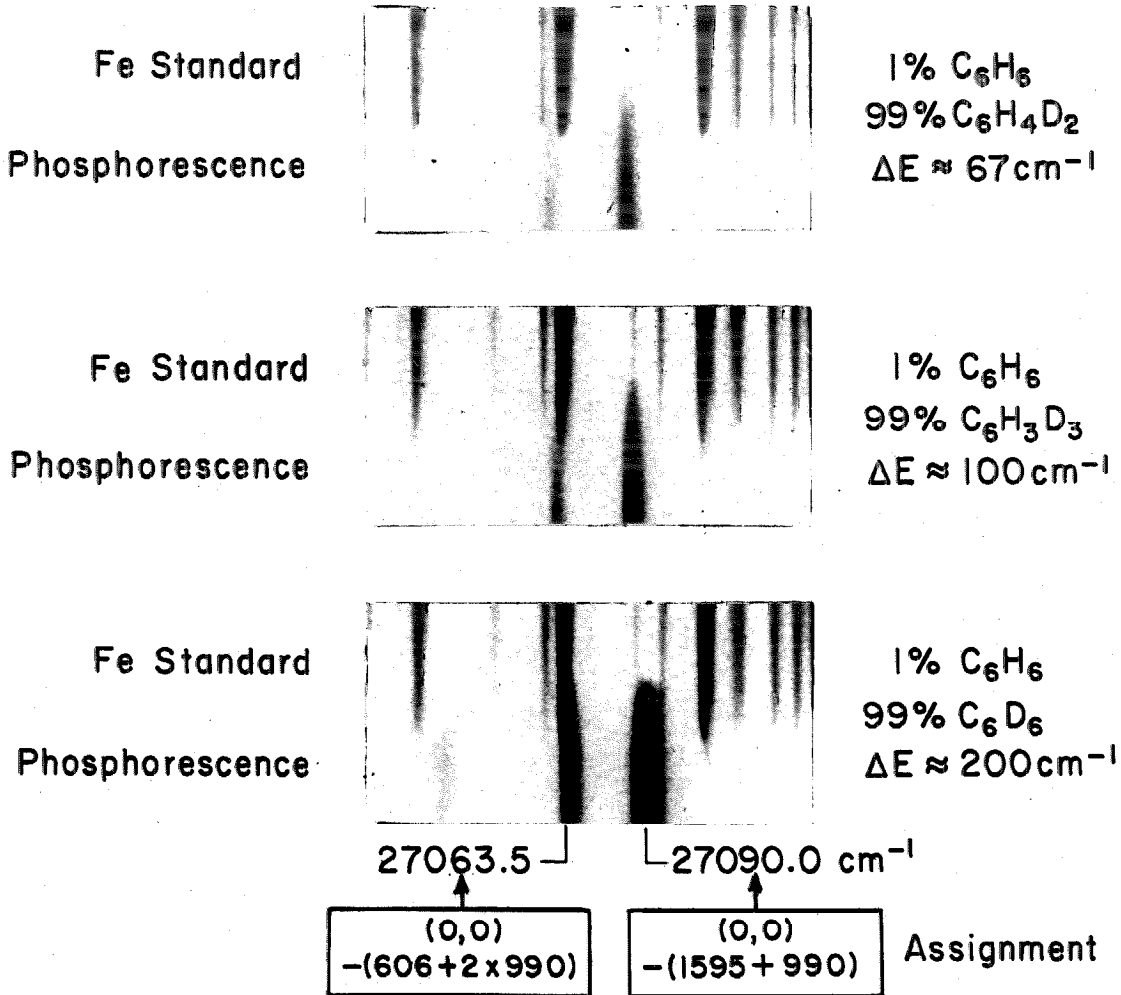


Fig. V-1. The small quasiresonance shifts can be seen most clearly by comparing the phosphorescence line positions in the three photographs with nearly coincident iron standard lines above each.

comparing the phosphorescence line positions in the three photographs with nearly coincident iron standard lines above each. The extreme sharpness and moderate intensity of the phosphorescence lines allow exposures to be obtained in one-half hour or less in many cases. Great difficulty with intensity was experienced, however, in the case of the C_6H_6 - $C_6H_4D_2$ mixed crystal. This was anticipated since here the small energy denominator leads to extremely rapid triplet excitation migration and triplet-triplet annihilation. Low phosphorescence quantum efficiencies result. Cooling the helium bath below the λ temperature, which does not shift the emission, was necessary in this instance for the attainment of adequate phosphorescence intensity. It is not known as yet whether the major cause of the greater than 10-fold increase in intensity is due to reduced Boltzmann populations and relaxation times or simply to more efficient cooling by the superfluid helium.

Table V-1 lists the measured shifts and the vibrational assignments of the phosphorescence lines, while Table V-2 lists the most prominent lines grouped according to the vibrational progression to which they belong. The strongest lines can be measured to within $\pm 0.2 \text{ cm}^{-1}$, but the weaker lines have a larger margin of error. Only those lines observed in all three host crystals are included in Table V-1. Many other weak lines (>200) in the very rich phosphorescence spectrum of C_6H_6 in C_6D_6 were not sufficiently strong in the

Table V-1.

Observed shifts of C_6H_6 phosphorescence in isotopic hosts.*

$\nu(\text{vac}) C_6H_6$ in C_6D_6 (cm^{-1})	$\delta(C_6D_6)-$ $\delta(C_6H_3D_3)$ (cm^{-1})	$\delta(C_6D_6)-$ $\delta(C_6H_4D_2)$ (cm^{-1})	Rel. Int.	Assignment (0,0)- (cm^{-1})
28 653.0	+3.9	+8.0	vw	985
28 483.5	3.8	6.9	m	1178
28 074.1	3.4	6.2	s	1595
28 055.5	3.7	6.7	w	606+992
27 663.7	3.3	6.3	vw	985+992
27 494.3	4.0	7.1	s	1178+992
27 090.0	3.4	5.7	vs	1595+992
27 063.5	3.2	6.1	m	606+2·992
26 505.6	3.8	6.6	m	1178+2·992
26 106.3	3.3	5.8	s	1595+2·992
26 074.0	3.7	5.9	w	606+3·992
25 732.1	4.5	6.2	vw	1595+2·1178
25 518.2	3.9	8.3	vw	1178+3·992
25 328.0	4.5	5.0	m	1178+2·1595
25 308.0	4.4	5.4	vw	1178+1595+606+992
25 124.0	3.0	5.8	w	1595+3·992
25 086.5	2.9	5.7	vw	606+4·992
24 925.8	4.9	6.3	vw	2·1595+606+992
24 900.5	4.4	6.6	vw	3·1595

* δ is the spectral shift referred to the line positions of C_6H_6 for infinite energy denominator ΔE . Since the shift is to lower energy with decreasing deuterium substitution, δ is always a negative number and is more negative the less the deuteration. The assignment involves electronic ground-state vibrations of species a_{1g} (992 cm^{-1}), e_{2g} ($606, 1178, \text{ and } 1595\text{ cm}^{-1}$), and b_{2g} (985 cm^{-1}). Note that in the crystal this b_{2g} frequency is 1004 cm^{-1} .

Table V-2.

Observed shifts of the strongest lines
of C_6H_6 phosphorescence grouped
according to vibrational type.

Vibrations (cm^{-1})	n	$\delta(C_6D_6)-$ $\delta(C_6H_3D_3)$ (cm^{-1})	$\delta(C_6D_6)-$ $\delta(C_6H_4D_2)$ (cm^{-1})
606+n·992 (C-C mode)*	1	+3.7	+6.7
	2	3.2	6.1
	3	3.7	5.9
	4	2.9	5.7
1178+n·992 (C-H mode)	0	3.8	6.9
	1	4.0	7.1
	2	3.8	6.6
	3	3.9	8.3
1595+n·992 (C-C mode)	0	3.4	6.2
	1	3.4	5.7
	2	3.3	5.8
	3	3.0	5.8

* In Fermi resonance with $1595+(n-1)\cdot 992$.

other two hosts to measure. Examination of the data shows several features: 1) the direction of the shift is as expected, the host associated with the smaller energy denominator giving the larger red shift; 2) the red shift in the spectrum of C_6H_6 in $C_6H_3D_3$ relative to that in C_6D_6 is approximately 3.5 cm^{-1} , whereas the shift in the spectrum of C_6H_6 in $C_6H_4D_2$ relative to that in C_6D_6 is approximately 6.0 cm^{-1} ; and 3) the shifts tend to group themselves according to vibrational types although the differences between different types is small. Note that only relative shifts can be measured in these experiments since there are quasiresonance shifts in all three hosts.

The strongest progressions observed are based upon two different C-C modes and one C-H mode in the ground electronic state. Vibrational quasiresonance effects are expected to depend upon the normal coordinates as well as the vibrational energy denominators, yet the shifts in the three strong progressions are of similar magnitudes, that in the C-H progression being roughly 15% greater than those in the two C-C progressions. It seems unlikely, therefore, in view of the low sensitivity of the shifts to vibrational characteristics, that vibrational perturbations alone can be responsible for the shifts. It therefore seems that the greatest part of the observed shifts is purely electronic in origin. The minimum electronic contributions to the relative shifts are taken to be $3.0 \pm 0.5\text{ cm}^{-1}$ and $5.5 \pm 0.5\text{ cm}^{-1}$,

respectively, for the red shift in the spectrum of C_6H_6 in $C_6H_3D_3$ relative to that in C_6D_6 and the shift in the spectrum of C_6H_6 in $C_6H_4D_2$ relative to that in C_6D_6 , with vibrational contributions amounting to about $0.5-1.0\text{ cm}^{-1}$. That the largest vibrational perturbation should be associated with the C-H progression is expected, since the greatest variation in vibrational energy denominator with isotopic substitution occurs for the C-H modes. The small size of the vibrational quasiresonance shifts is consistent with the small resonance (correlation field) splittings found in the infrared spectrum of crystalline benzene (80, 81).

The relatively large size of the electronic interaction is further indicated by the difficulty in obtaining phosphorescence from C_6H_6 in $C_6H_4D_2$ and the complete absence of detectable phosphorescence emission from C_6H_6 dissolved in a C_6H_5D host crystal at 1.8°K . In the latter case the energy denominator is only 33 cm^{-1} and the C_6H_6 trap states are so thoroughly mixed with the triplet exciton states of the host that excitation migration and triplet-triplet annihilation rates approach those of the pure crystal. The phosphorescence spectrum is therefore strongly quenched just as it is

(80) S. Zwerdling and R. S. Halford, J. Chem. Phys., 23, 2221 (1955); W. Vedder and D. F. Hornig, Advan. Spectry., 2, 231-235 (1961).

(81) Note that ungerade vibrations are studied in the infrared while gerade vibrations arise in the electronic spectrum.

in the pure crystal (82).

Additional quantitative evidence supporting the interpretation given here can be obtained from an examination of the 2650 Å singlet-singlet absorption and emission (fluorescence) spectra of these mixed crystals (83). The fluorescence spectrum, of course, involves the same ground-state vibrational levels as the phosphorescence spectrum. Both the fluorescence spectrum and the (0,0) band in absorption show shifts which are about twice those for the singlet-triplet emission by virtue of the stronger exciton interactions in the lowest excited singlet state. However, the important point which I want to make here is that, like the phosphorescence spectrum, the shifts do not vary by more than about 0.5-1.0 cm⁻¹ among the various vibrational lines of the fluorescence spectrum. Furthermore, the (0,0) band in both the fluorescence and absorption spectra, which for the first singlet-singlet transition is made allowed by crystal perturbations, shows virtually the same shift as do all the vibronic components of the fluorescence. Thus, the conclusion is that both in the singlet-singlet and the singlet-triplet spectra the major contribution to the quasiresonance shift is electronic rather than vibrational in nature.

(82) See the last part of Sect. IV.

(83) More detailed information is given in Sect. VI, where the quasiresonance shift will be used to give a new interpretation to the exciton splitting in absorption.

4. Analysis of the Data. An analysis of these data in terms of the triplet exciton interaction in crystalline benzene requires a knowledge of the relative magnitudes of the matrix elements with respect to all other molecules in the crystal. The principal contribution to the triplet excitation transfer matrix elements is probably due to intermolecular exchange integrals (84). Exchange integrals fall off rapidly with distance and are fairly sensitive to the intermolecular orientation of the benzene π orbitals, the greatest interaction occurring when the π orbitals are pointed directly toward one another. Keeping these facts in mind, an examination of the crystal structure (85) suggests that the three-dimensional interaction can be approximated by a two-dimensional one where each benzene primarily interacts with but four nearest neighbors (or more accurately, four groups of three translationally inequivalent nearest neighbors each). Providing the energy denominator ΔE is much larger than the matrix element, a perturbation calculation can be used. The energy shift then becomes

$$\delta = 4\beta^2 / \Delta E, \quad (22)$$

where β represents the nearest-neighbor pair interaction

(84) R. E. Merrifield, J. Chem. Phys., 23, 402 (1955).

(85) E. G. Cox, Rev. Mod. Phys., 30, 159 (1958). A more detailed discussion of the relationship between exciton interactions and crystal structure is given in Sect. VI.

matrix element, and the factor 4 arises from the fact that the four most strongly interacting neighbors are equivalent. For the real crystal structure the interpretation of β has to be modified as outlined in Sect. VI, but it is seen there that the pair interaction description is not a bad one.

Equation 22 has been shown to hold within about 10% accuracy for $\beta \leq \Delta E/2$, the "correct" shift (δ) being obtained through computer calculations (86), with periodic boundary conditions, on finite isotropic two-dimensional crystals containing up to 41 molecules. Fig. V-2 compares these results for model crystals containing various numbers of molecules, both for $\beta = 10 \text{ cm}^{-1}$ (the approximate triplet interaction energy) and for $\beta = 20 \text{ cm}^{-1}$ (the approximate singlet interaction energy). Note that increasing the size of the two-dimensional model increases the magnitude of δ from a value less to a value slightly greater than that given by Eq. 22. This size effect is more pronounced the larger the value of β , and probably has to do with the fact that perturbation contributions of higher order than second are neglected in Eq. 22.

Computer calculations using periodic boundary conditions for a three-dimensional model containing one trap (87) and 107 host molecules have also been made. These results

(86) These were done on a Burroughs 220 computer. I would like to acknowledge the assistance of Joel Kwok in the programming of this problem.

(87) Molecule 41 in the nomenclature of Sect. VI.

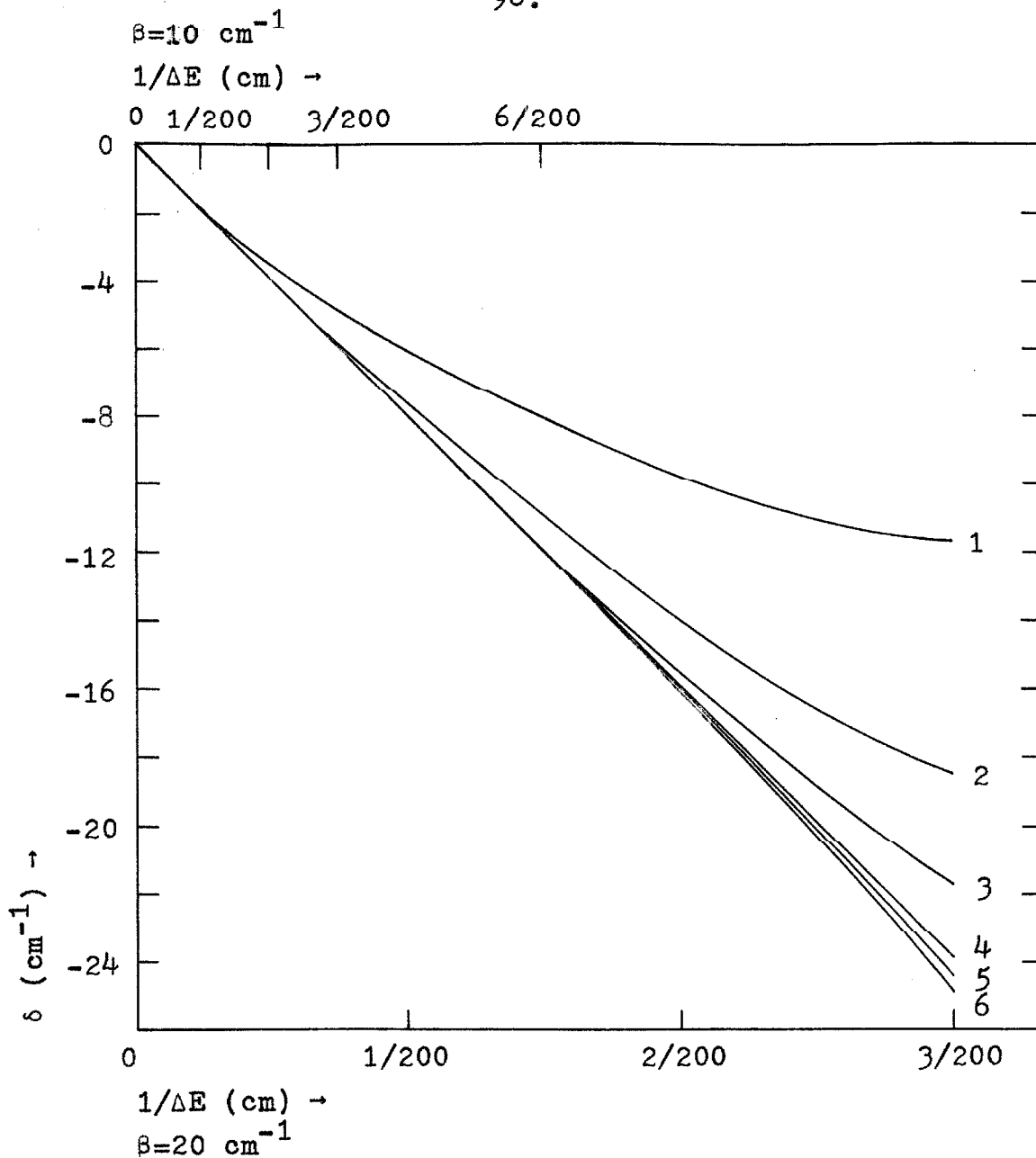


Fig. V-2. Quasiresonance shift (δ) for various sized isotropic two-dimensional crystals as a function of energy denominator ΔE . Top scale: $\beta = 10 \text{ cm}^{-1}$ (\sim triplet interaction energy). Bottom scale: $\beta = 20 \text{ cm}^{-1}$ (\sim singlet interaction energy). The curves are labelled for various cases as follows:

- | | |
|---|--------------------------|
| 1) 5 molecules, | 4) $4\beta^2/\Delta E$, |
| 2) $\begin{pmatrix} -\Delta E & 2\beta \\ 2\beta & 0 \end{pmatrix}$, | 5) 25 molecules, |
| 3) 13 molecules, | 6) 41 molecules. |

are shown in Fig. V-3 for both triplet and singlet interaction matrix elements along with the curve representing Eq. 22 and the experimental points. Because of the nature of the model chosen, this three-dimensional crystal corresponds roughly to a two-dimensional model with 9 molecules. Thus it would appear that here also Eq. 22 is a very good approximation to the actual quasisonance shift. The direction of the observed error, i.e., the actual shift is less than the predicted shift, would also seem to be indicated by these calculations.

By equating the theoretical relative shift $\delta(C_6D_6) - \delta(C_6H_3D_3)$ deduced from Eq. 22 to the experimentally observed relative shift ($3.0 \pm 0.5 \text{ cm}^{-1}$) we obtain $12 \pm 1 \text{ cm}^{-1}$ for the (0,0) interaction between two nearest-neighbor molecules in crystalline benzene, i.e., for β . Eq. 22, because of relationships between the energy denominators, further implies that

$$[\delta(C_6D_6) - \delta(C_6H_4D_2)] = 2[\delta(C_6D_6) - \delta(C_6H_3D_3)].$$

The experimental shifts of $5.5 \pm 0.5 \text{ cm}^{-1}$ and $3.0 \pm 0.5 \text{ cm}^{-1}$ are in agreement with this prediction indicating again that the simple perturbation result does give a reasonable approximation to δ at least within the experimental error. We should also note that the above value of $12 \pm 1 \text{ cm}^{-1}$ for β is in excellent agreement with the order of magnitude value of 9 cm^{-1} derived from the triplet excitation migration studies in

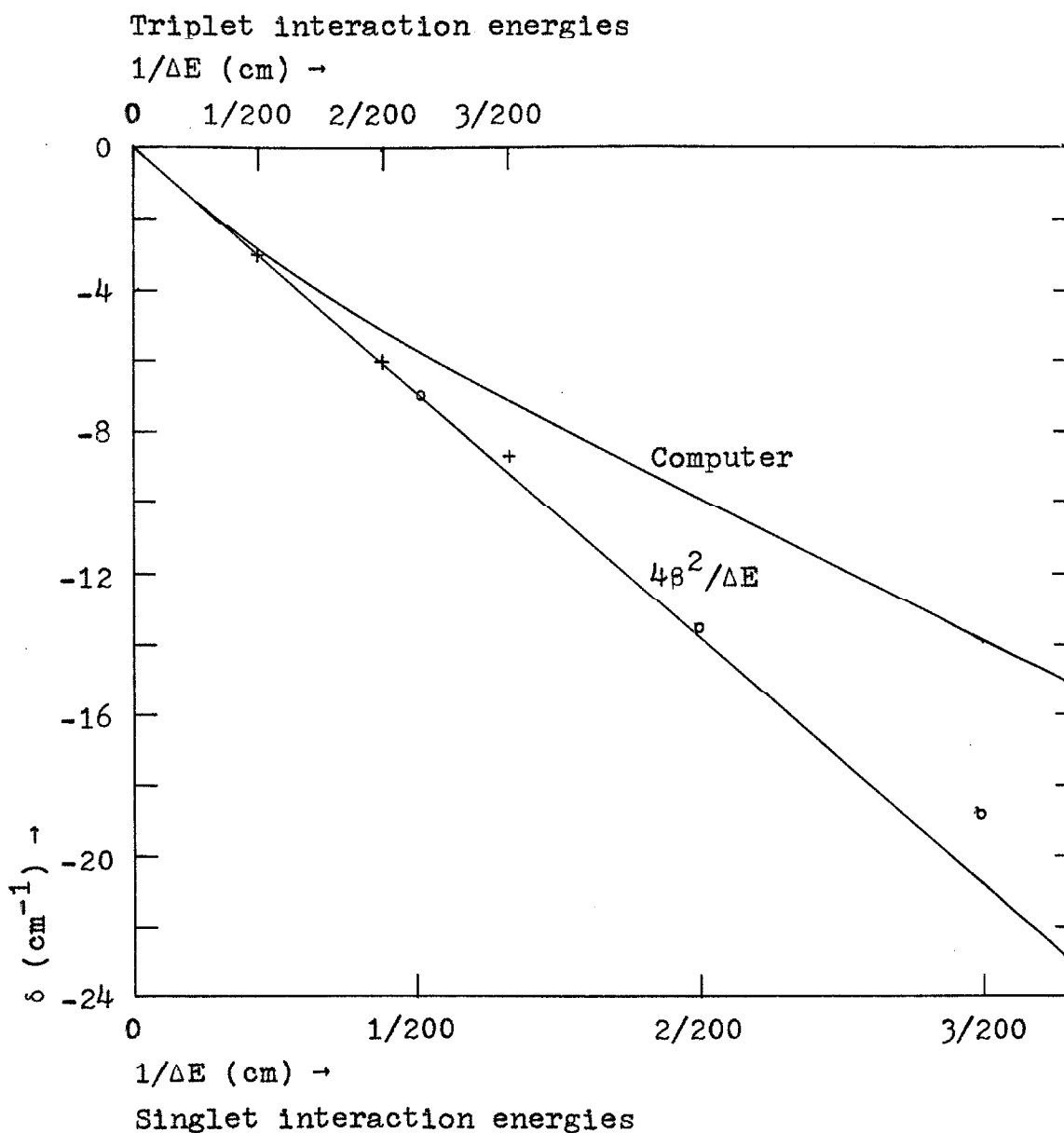


Fig. V-3. Quasiresonance shift for benzene as a function of energy denominator ΔE . Top scale: triplet interaction energies. Bottom scale: singlet interaction energies. The curve labelled "computer" is calculated for a model three-dimensional benzene crystal containing 107 host molecules and 1 guest molecule. + indicates experimental points for the triplet quasiresonance shift; o indicates experimental points for the singlet quasiresonance shift.

Sect. III.

The over-all electronic interaction is obtained by summing the interactions over all totally symmetric vibrations in the excited electronic state. Unfortunately no knowledge of the perturbation in other than the zeroth vibrational level can be gained from these experiments. It is expected, however, that the distribution of the interaction over the various totally symmetric levels is equivalent to the Franck-Condon distribution of intensity over these vibrational levels in absorption (88). This distribution can be roughly estimated from the singlet-singlet spectrum which places 25% of the intensity in the lowest member of the totally symmetric progression (89). Thus, the over-all electronic interaction is about four times that for the zeroth vibrational state, i.e., of the order of 48 cm^{-1} .

The large triplet resonance interaction is no doubt a general phenomenon for π -electron systems and is probably present in many other types of molecules. It corresponds to a transition time for excitation transfer between nearest neighbors of less than 10^{-12} sec. Therefore, barring quenching mechanisms, as many as 10^{12} such transitions can take

(88) W. T. Simpson and D. L. Peterson, J. Chem. Phys., 26, 588 (1957); D. S. McClure, Solid State Physics (Academic Press Inc., New York, 1959), Vol. 8, p 1.

(89) W. F. Radle and C. A. Beck, J. Chem. Phys., 8, 507 (1940); D. P. Craig, J. Chem. Soc., 1950, 2146.

place during the >1 -second lifetime of these triplet states! The consequences of these results in energy transfer problems are fairly obvious and have been discussed previously in Sections III and IV.

VI. THE EXCITON BAND STRUCTURE OF BENZENE

1. General Theory (90). One of the manifestations of the excitation transfer interaction is the splitting of a single gas phase electronic transition into several polarized components in the crystalline phase (91). It is the purpose of this section to investigate the nature of this factor group splitting as it relates to the crystal structure and to the experimentally observed β .

The crystal structure (92) of benzene, a diagram of which is shown schematically in Fig. VI-1, is orthorhombic with space group P_{bca} (D_{2h}^{15}). The factor group is isomorphic onto the point group D_{2h} , and the center of each molecule is at a center of inversion of the crystal. There are four molecules per unit cell centered at a corner and three face centers of the pseudo face-centered structure. The factor group splitting thus produces from the ${}^3B_{1u}$ molecular state

-
- (90) A portion of this work appears in G. C. Nieman and G. W. Robinson, J. Chem. Phys., 39, 1298 (1963). Note that Fig. 4 of this paper is incorrect as explained later.
- (91) A. Davydov, Zh. Eksperim. i Teor. Fiz., 18, 210 (1948); 21, 673 (1951). See also D. S. McClure, Solid State Physics (Academic Press Inc., New York, 1959), Vol. 8, 1; R. S. Knox, Theory of Excitons (Academic Press Inc., New York, 1963).
- (92) E. G. Cox, Rev. Mod. Phys., 30, 159 (1958); E. G. Cox, D. W. J. Cruickshank, and J. A. S. Smith, Proc. Roy. Soc. (London), A247, 1 (1958); G. E. Bacon, N. A. Curry and S. A. Wilson, Proc. Roy. Soc. (London), A279, 98 (1964).

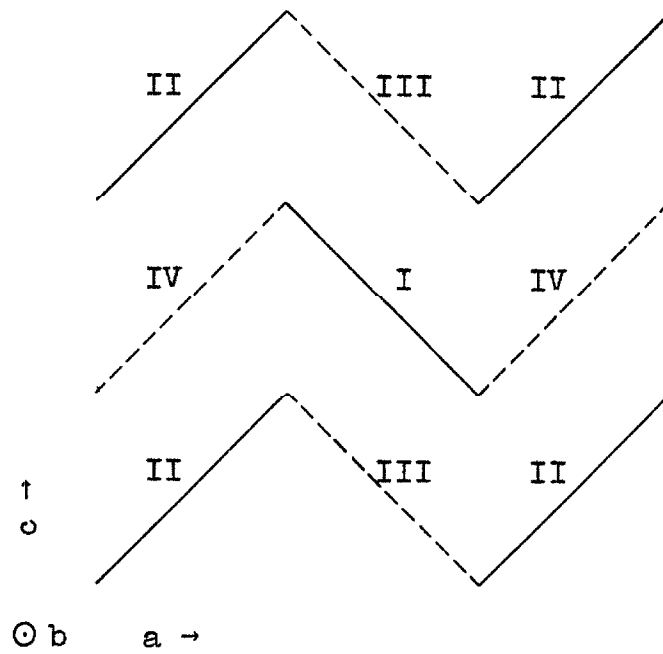


Fig. VI-1. Schematic diagram of benzene crystal. The lines represent benzene molecules viewed more or less edge on. b axis \perp to plane of paper; — in plane of paper; - - - $\frac{1}{2}b$.

four triplet levels in the pure benzene crystal, the levels transforming as A_{1u} , B_{1u} , B_{2u} , and B_{3u} under factor group operations (93, 94).

The symmetry of the crystal is sufficiently low that appropriate spin-orbit operators can be found which mix all four triplet levels with singlet levels of the type ${}^1B_{1u}$, ${}^1B_{2u}$, or ${}^1B_{3u}$. Thus, in a purely formal sense, symmetry-allowed but spin-forbidden transitions can occur between all four triplet levels and the totally symmetric ground state (${}^1A_{1g}$). In actual practice, however, the (0,0) band in the isotopic mixed crystal phosphorescence spectrum is extremely weak, just as it is in the unperturbed molecule. This experimental observation indicates that, contrary to the behavior of the 2650 Å singlet-singlet spectrum of crystalline benzene, the singlet-triplet transition has little or no crystal-induced part. It arises, as in the unperturbed molecule (95), primarily from a very small electric dipole contribution induced by a combination of spin-orbit interactions and nontotally symmetric vibrational motions of the molecule.

-
- (93) Singlet levels having the same transformation properties are produced from the ${}^1B_{2u}$ molecular state.
- (94) D. Fox and O. Schnepp, J. Chem. Phys., 23, 767 (1955). It should be noted that the Fox and Schnepp site numbering I, II, III, and IV does not correspond to that given by Cox (92). In this discussion I shall use the numbering of Fox and Schnepp where the II and IV labels of Cox have been interchanged.
- (95) A. C. Albrecht, J. Chem. Phys., 38, 354 (1963).

Crystal fields mixing, for example, the molecular ${}^3B_{1u}$ state with, say, the ${}^3E_{1u}$ state, which itself formally can mix with the ${}^1E_{1u}$ state by spin-orbit interactions to give an allowed component to the transition dipole, are therefore not very effective in this case. Since crystal induced intensities are second order in nature, the observation on the mixed crystals is expected to apply also to the pure crystal. This means, unfortunately, that the triplet exciton band structure in the vicinity of the (0,0) transition in pure crystalline benzene is not easily attainable by either optical emission or absorption studies. The naphthalene crystal, whose isotopic mixed crystal phosphorescence spectrum possesses a (0,0) band, would present a more favorable case for absorption studies. Nevertheless, it seems necessary here to make clear the relationship between the nearest-neighbor triplet interaction matrix element called β and the exciton band structure in the pure benzene crystal. This is now done.

We proceed in the usual way by assuming a "tight binding approximation" (96). The zero-order function

$$\psi_{ma} = G \varphi_{ma}^* \prod_{s \neq ma} \varphi_s^0, \quad (23)$$

represents a localized excitation, where φ_{ma}^* is the excited state wavefunction of the molecule at the a^{th} site of the

(96) F. Bloch, Z. Physik, 52, 555 (9128); C. Kittel, Introduction to Solid State Physics (John Wiley & Sons, Inc., New York, 1956), 2nd ed., pp. 586-587.

m^{th} unit cell. ϕ_s^0 is the ground state wavefunction of the molecule located at s , where the index s designates both the unit cell and the molecular site within this cell. The product is over all molecules of the crystal except that located at ma . \mathcal{G} is the antisymmetrization operator.

So-called one-site exciton functions

$$\phi_a(\vec{k}) = N^{-\frac{1}{2}} \sum_m \exp(i\vec{k} \cdot \vec{r}_{ma}) \psi_{ma} \quad (24)$$

for each of the four sites, $a=I, II, III, IV$, of the unit cell are formed from the above set of zero-order wavefunctions ψ_{ma} (Eq. 23).

In the case where the reciprocal lattice vector \vec{k} is zero, the secular equations can be reduced when the crystal eigenfunctions are classified according to representations of the factor group. Levels near that for which $\vec{k}=\vec{0}$ are of primary importance in optical spectra because of the $\Delta k=0$ selection rule. It is well known that for the case of the benzene crystal the four factor group wavefunctions which can be constructed from the $\vec{k}=\vec{0}$ one-site functions have the following form:

$$\begin{aligned} \Psi_\alpha &= \frac{1}{2} [\phi_I(\vec{0}) + \phi_{II}(\vec{0}) + \phi_{III}(\vec{0}) + \phi_{IV}(\vec{0})], \\ \Psi_\beta &= \frac{1}{2} [\phi_I(\vec{0}) - \phi_{II}(\vec{0}) - \phi_{III}(\vec{0}) + \phi_{IV}(\vec{0})], \\ \Psi_\gamma &= \frac{1}{2} [\phi_I(\vec{0}) - \phi_{II}(\vec{0}) + \phi_{III}(\vec{0}) - \phi_{IV}(\vec{0})], \\ \Psi_\delta &= \frac{1}{2} [\phi_I(\vec{0}) + \phi_{II}(\vec{0}) - \phi_{III}(\vec{0}) - \phi_{IV}(\vec{0})]. \end{aligned} \quad (25)$$

These functions are constructed to be antisymmetric under exchange of electrons. For the ${}^3B_{1u}$ molecular state as basis, α , β , γ , and δ levels of the crystal transform respectively as ${}^3B_{2u}$, ${}^3B_{3u}$, ${}^3A_{1u}$, and ${}^3B_{1u}$ under symmetry operations associated with the factor group (97, 98). The one-site exciton functions $\phi_a(\vec{0})$ are mixed by interactions between translationally inequivalent molecules. For triplet excitons the interactions are caused primarily by electron exchange between molecules, all orders of the transition multipole vanishing identically in a first approximation (99).

It can be seen from Fig. VI-1 that each molecule is surrounded by three different sets of nearest-neighbor sites, each set containing four molecules. The molecules within each set are translationally equivalent to one another but translationally inequivalent to those molecules of a different set. Let us designate by $M_{I,II}$, $M_{I,III}$, and $M_{I,IV}$, respectively, the pair interaction matrix elements between type I sites and sites of types II, III, and IV. Because of symmetry, $M_{I,II}$, $M_{I,III}$, and $M_{I,IV}$, also represent (III, IV), (II, IV), and (II, III) interactions, respectively.

(97) For the ${}^1B_{2u}$ molecular state as basis, α , β , γ , and δ levels of the crystal transform respectively as ${}^1B_{3u}$, ${}^1B_{2u}$, ${}^1B_{1u}$, and ${}^1A_{1u}$ under symmetry operations associated with the factor group (98).

(98) D. Fox and O. Schnepp, J. Chem. Phys., 23, 767 (1955).

(99) D. L. Dexter, J. Chem. Phys., 21, 836 (1953); R. E. Merrifield, J. Chem. Phys., 23, 402 (1955).

Diagonalization of the 4×4 one-site exciton matrix for $\vec{k}=\vec{0}$ yields the factor group splitting terms,

$$\begin{aligned}
 E_{\alpha} &= 4(+M_{I,II} + M_{I,III} + M_{I,IV}), \\
 E_{\beta} &= 4(-M_{I,II} - M_{I,III} + M_{I,IV}), \\
 E_{\gamma} &= 4(-M_{I,II} + M_{I,III} - M_{I,IV}), \\
 E_{\delta} &= 4(+M_{I,II} - M_{I,III} - M_{I,IV}),
 \end{aligned}
 \tag{26}$$

where the energy zero refers to the energy of the band center, i.e., the free molecule energy plus terms which shift all the factor group components equally.

In the case of the triplet state, the experimental band shift term is not accurately known because of the lack of precise gas-phase data on the singlet-triplet transition energy of C_6H_6 . Using the approximate gas-phase (0,0) line position of $29\,510\text{ cm}^{-1}$ given by Evans (100), the shift appears to be positive in sign, unlike the first singlet where the band shift in the crystal is 218 cm^{-1} to lower energies (101). The magnitude of the band shift for the triplet is of the order of 150 cm^{-1} , the triplet band center in the C_6H_6 crystal occurring at $29\,661 \pm 2\text{ cm}^{-1}$. This value is obtained from the measured (0,0) band position of the C_6H_6 in

(100) D. F. Evans, J. Chem. Soc., 1957, 3885.

(101) See the discussion of the singlet state at the end of this section.

C_6D_6 phosphorescence spectrum corrected by $+3.5 \text{ cm}^{-1}$ for the quasiresonance shift in this host. Since other than resonance or quasiresonance interactions are primarily responsible for the band shift, we are not concerned with it further here.

In the perturbation limit the quasiresonance shift in the isotopic mixed crystal is simply equal to the square of the matrix elements of the interaction of the guest with the host, summed over all host molecules, and divided by the guest-host energy denominator. It should be noted that it is immaterial whether the guest resides in site I, II, III, or IV since each site is coupled to the rest of the crystal in an identical fashion. In addition to the $M_{I,II}$, $M_{I,III}$, and $M_{I,IV}$ coupling constants there are elements M_a , M_b , and M_c connecting each molecule to the translationally equivalent nearest neighbors along the a, b, and c crystal axes. If, as expected for intermolecular electron exchange, the lattice sums converge rapidly, then nearest-neighbor interactions are of primary importance and the quasiresonance shift is given by,

$$\delta = 4(M_{I,II}^2 + M_{I,III}^2 + M_{I,IV}^2 + \frac{1}{3}M_a^2 + \frac{1}{3}M_b^2 + \frac{1}{3}M_c^2) / \Delta E. \quad (27)$$

The factors $\frac{1}{3}$ arise from the fact that there are but two translationally equivalent nearest neighbors along any given crystal axis. The triplet exciton "pair-interaction" matrix element β , as defined by Eq. 22 of Sect. V, is then related

to the coupling constants through the expression,

$$\beta^2 = M_{I,II}^2 + M_{I,III}^2 + M_{I,IV}^2 + \frac{1}{2}(M_a^2 + M_b^2 + M_c^2). \quad (28)$$

Thus the largest intermolecular exchange coupling constants in crystalline benzene must be of the order of β , i.e., 12 cm^{-1} . The discussion in Sections III, IV, and V, where the matrix element β is treated as a pair interaction, is valid only insofar as one of the six matrix elements dominates the other five and then, of course, the reference is to the very special mutual molecular orientation which is found in the crystal. The crude estimates to be made below do seem to indicate that $M_{I,II}$ dominates the other elements to an extent great enough for β to be considered as arising primarily from pair interactions in the ac planes of crystalline benzene.

Calculation of the matrix elements $M_{I,II}$, $M_{I,III}$, $M_{I,IV}$, M_a , M_b , and M_c is a difficult task since reliable molecular wavefunctions for the intermolecular regions are not available, and the intermolecular exchange integrals are tedious to evaluate even if the wavefunctions were available. Rather than attempt a detailed calculation of these elements (102),

(102) Recently Stuart A. Rice at the University of Chicago has done some computer calculations of the exchange integrals for crystalline benzene using SCF wavefunctions. His unpublished results give a value for β of about one-half that given here, which at the present state of such theoretical calculations is very good agreement.

which even at best would require considerable guess-work, I prefer simply to choose for illustration's sake a set of values which have roughly the correct relative magnitudes and whose absolute magnitudes are consistent with the experimental "pair interaction" matrix element β . A "hypothetical" triplet exciton band structure for pure crystalline benzene may then be constructed from these parameters.

The rough estimates of the relative magnitudes of the matrix elements are obtained by first choosing eigenfunctions which have a realistic asymptotic behavior, by next calculating all two-center exchange integrals between carbon atoms on different molecules using the appropriate interatomic distances and orbital orientations, and finally by summing over all two-center interactions. For simplicity the contribution from multicenter integrals is neglected (103). Since one is ignorant in any case of the exact form of the benzene MO's at large distances from the nuclei, I further ignore for these relative estimates any variation of the LCAO coefficients around the ring. Fairly realistic AO's for the calculation can be obtained by fitting a self-consistent field (SCF) function for carbon in the range around

(103) S. Choi in a private discussion has pointed out that the multicenter integrals for intermolecular interactions may contribute as much as or more than the two-center integrals. It is hoped, however, that even though the absolute values of the coupling constants cannot be obtained by these simple estimates, the relative values are more reliable.

$R=4.0 \text{ \AA}$ to a single 2p-type Slater orbital, the appropriate Z_{eff} being about 2.0 at this distance (104). Exchange integrals from these "adjusted" Slater orbitals were then calculated by the method described by Rüdénberg (105) or found in the tables of Kotani et al. (106), and plotted logarithmically against distance. The plots, shown in Fig. VI-2, were used for obtaining the crude estimates of all two-center exchange integrals. While the exchange integrals between two carbon atoms are themselves positive, the triplet exciton interaction enters with a negative sign (107). Thus I take all the

-
- (104) E. Clementi, C. C. J. Roothaan, and M. Yoshimine, Physical Review, 127, 1618 (1962).
- (105) K. Rudenberg, J. Chem. Phys., 19, 1459 (1951).
- (106) M. Kotani, E. Ishiguro, and K. Hijikata, J. Phys. Soc. (Japan), 2, 553 (1954); 8, 463 (1953).
- (107) R. E. Merrifield, J. Chem. Phys., 23, 402 (1955). Merrifield's calculation while inclusive of exchange omits other kinds of intermolecular overlap effects. Some of these interaction terms are analogous to that given by Eq. (6) of Sternlicht, Nieman, and Robinson. These are of the same sign as the exchange integrals. Others, however, correspond to interactions between electrons and screened nuclei and therefore have a different sign than the exchange terms. See R. A. Buckingham and A. Dalgarno, Proc. Roy. Soc. (London), A213, 327 (1952) where a detailed calculation is carried out for a similar problem. If of sufficient magnitude, the latter kind of integrals could modify and even change the sign of some of the coupling constants. In fact, because of the crudity of the estimates here, I really do not know whether the important coupling constants have positive or negative signs. I feel, however, that they should be negative since the mutual orientation of the π orbitals in aromatic crystals is not optimum for intermolecular overlap integrals but still allows fairly large exchange integrals. I acknowledge H. M. McConnell for assistance on this point.

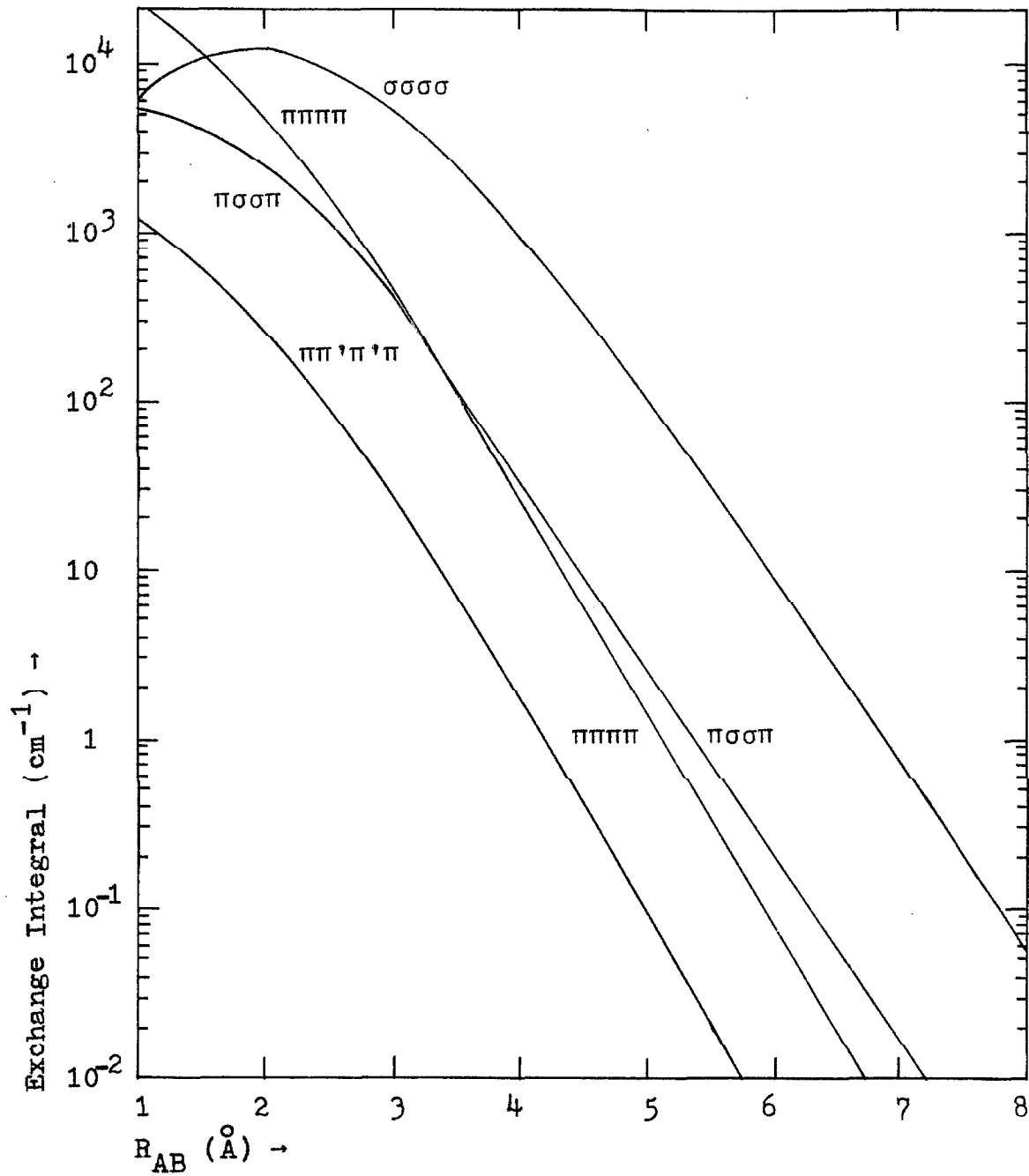


Fig. VI-2. Exchange integrals for 2 carbon atoms R_{AB} apart with $Z_{\text{eff}}=2.0$.

$$\sigma\sigma\sigma\sigma = e^2 \langle 2p_{zA}^*(1) 2p_{zB}^*(2) | r_{12}^{-1} | 2p_{zB}(1) 2p_{zA}(2) \rangle,$$

$$\pi\sigma\sigma\pi = e^2 \langle 2p_{xA}(1) 2p_{zB}(2) | r_{12}^{-1} | 2p_{zB}(1) 2p_{xA}(2) \rangle,$$

$$\pi\pi\pi\pi = e^2 \langle 2p_{xA}(1) 2p_{xB}(2) | r_{12}^{-1} | 2p_{xB}(1) 2p_{xA}(2) \rangle,$$

$$\pi\pi'\pi'\pi = e^2 \langle 2p_{xA}(1) 2p_{yB}(2) | r_{12}^{-1} | 2p_{yB}(1) 2p_{xA}(2) \rangle.$$

coupling constants to be negative.

The results of the above estimates show that the ratios of the matrix elements are very roughly given by,

$$M_{I,II}:M_{I,III}:M_{I,IV}:M_a:M_c=20:12:8:1:3.$$

The constant M_b is very small and it is taken to be zero.

Using these ratios together with Eq. 28 and the experimental value of 12 cm^{-1} for β yields $M_{I,II}=-10 \text{ cm}^{-1}$, $M_{I,III}=-6 \text{ cm}^{-1}$, $M_{I,IV}=-4 \text{ cm}^{-1}$, $M_a=-0.5 \text{ cm}^{-1}$, $M_b=0.0 \text{ cm}^{-1}$, and $M_c=-1.5 \text{ cm}^{-1}$.

In the pure crystal, the elements connecting translationally equivalent molecules do not contribute to the factor group splitting. They do, however, contribute a term $2(M_a+M_b+M_c)$ to the band shift at $\vec{k}=\vec{0}$. The factor group splitting depends upon $M_{I,II}$, $M_{I,III}$, and $M_{I,IV}$ in the manner described by Eqs. 26. The use of these equations gives for the "hypothetical" splitting terms: $E_\alpha=-80 \text{ cm}^{-1}$; $E_\beta=+48 \text{ cm}^{-1}$; $E_\gamma=+32 \text{ cm}^{-1}$; and $E_\delta=0 \text{ cm}^{-1}$. The zero value for E_δ is purely coincidental. The triplet factor group splittings are expected to be of comparable magnitude in other aromatic crystals. Thus, if the proper experimental conditions of long path length, very low temperature, and sharp-lined spectra can be obtained, there should be little difficulty in observing the factor group splitting directly in absorption. In the naphthalene crystal, for example, where there are two molecules per unit cell, the two triplet factor group components will in all probability show a

splitting of $10\text{-}100\text{ cm}^{-1}$ (108).

2. Computer Calculations. The factor group splitting for $\vec{k}=\vec{0}$ is fairly straightforward to calculate. However for $\vec{k}\neq\vec{0}$, it is not nearly as easy to visualize just what is happening. In order to obtain a better understanding of the entire exciton band structure in pure benzene and in isotopic mixed crystals of benzene, a computer program (109) was written so that the energy level distribution could be calculated as a function of the reciprocal lattice vector \vec{k} . This model calculation treated a finite three-dimensional benzene crystal containing 108 molecules. Cyclic boundary conditions were applied. Phonon-exciton interactions and interactions between excitons and molecular vibrational degrees of freedom were neglected. Numerical values for the six nearest-neighbor coupling constants were taken to be the "hypothetical" values obtained above, nonnearest-neighbor coupling being ignored.

As is often the case, instead of immediately simplifying the problem, the results of these calculations were rather difficult to correctly interpret. Because of this confusion I was led astray for about a year until a recent

(108) Some calculations by J. L. Katz, J. Jortner, S. Choi, and S. A. Rice, J. Chem. Phys., 39, 1897 (1963) of the triplet exciton splitting agree with this prediction.

(109) For the IBM 7090 computer. I would like to acknowledge the assistance of Al Dubin in writing this program.

reinvestigation of this problem pointed out the fallacies in my earlier interpretation of the results (110).

There are three main steps involved in this type of calculation: 1) setting up the secular determinant appropriate to the particular crystal structure involved; 2) diagonalization of this determinant, determining both the eigenvalues (energies) and eigenvectors; and 3) interpretation of these eigenvectors in terms of the ordinary reciprocal lattice vector (\vec{k}) notation.

The basic problem in setting up the secular determinant has to do with the correlation of a matrix row (m) and column (n) with a particular lattice site (a, b, c) in the model crystal. A particular column (n) of the secular determinant represents a zero-order state (Eq. 23) of the system with triplet (singlet) excitation localized on the molecule at lattice site (a, b, c). To set up the problem it is necessary to establish a one-to-one correspondence between columns (rows) and lattice sites. This we shall now do.

The model benzene crystal chosen contained 108 molecules, and we shall number the columns (rows) of the secular determinant consecutively, 1, 2, 3,108. It is convenient to simplify the problem by first considering only translationally equivalent molecular sites. Since benzene

(110) For this reason Fig. 4 of G. C. Nieman and G. W. Robinson, J. Chem. Phys., 39, 1298 (1963) is incorrect in its interpretation of the magnitude of k .

has four molecules per unit cell we first need to consider only 27 of the original 108 molecules. This reduces the 108x108 interaction matrix to 16 27x27 submatrices. Let the first 27 columns (rows) correlate with the translationally equivalent sites of type I. It is now apparent that the three-dimensional model is really only a 3x3x3 lattice of unit cells and thus is a rather small model (111).

We begin the numbering (correlation) scheme by choosing one of the three crystallographic axes, the c-axis in this case, and number each lattice site consecutively in this direction. Thus neighboring lattice sites (a,b,c) and (a',b',c) are numbered n and n+1 or n and n-1 depending upon the choice of positive and negative directions. This same rule applies both within the crystal and at the boundaries. Thus this rule defines the periodic boundary conditions in the direction of the c-axis. Incidentally, the numbers n are modulo 27, i.e., $27+n=n$.

Looking at our 3x3x3 model we see that this first rule of numbering works fine until we try to assign number 4 to a lattice site. To do this we need a new rule to relate lattice sites in directions other than parallel to the c-axis. Again choose a crystallographic axis, say the a-axis, and number consecutive sites in this direction by numbers differing by 3. Therefore neighboring lattice sites (a,b,c)

(111) But the largest the machine could handle.

and (a, b', c') are numbered n and $n+3$ or n and $n-3$ depending upon the choice of positive and negative directions. Once again this same scheme is used to determine the periodic boundary conditions in the direction of the a -axis. To help clarify these rules Fig. VI-3 shows the lattice numbering for our model up to the present with circles around the virtual boundary sites.

At lattice site 10 we once again must choose a new axis, the b -axis, for our numbering scheme. In a manner similar to that used before, neighboring lattice sites (a, b, c) and (a', b, c') are numbered n and $n+9$ or n and $n-9$. This rule also applies at the boundaries and allows the completion of the assignment of the first 27 columns (rows) of our matrix.

We now insert matrix elements into our matrix at the appropriate locations. That is, a matrix element (M_c) representing interaction between translationally equivalent molecules parallel to the c -axis is put into the matrix locations $(n, n+1)$ and $(n, n-1)$, etc. This gives a symmetric 27×27 matrix (D) of the form shown in Fig. VI-4, where a simplifying nomenclature has been used. This matrix represents a three-dimensional, one molecule per unit cell crystal with nearest-neighbor interactions only.

We now must return and include the translationally inequivalent molecules. This is done by simply labeling the site II molecule in the same unit cell as the site I molecule n by the number $n+27$. Thus molecule n and molecule

	1	3	5	7	9	11	13	15	17	19	21	23	25	27
	2	4	6	8	10	12	14	16	18	20	22	24	26	
1		γ	α			β				β			α	γ
2	γ		γ	α			β				β			α
3		γ		γ	α			β				β		α
4	α		γ		γ	α			β			β		
5		α		γ		γ	α			β			β	
6			α		γ		γ	α			β			β
7				α		γ		γ	α			β		β
8					α		γ		γ	α			β	
9						α		γ		γ	α			β
10	β						α		γ		γ	α		
11		β						α		γ		γ	α	
12			β						α		γ		γ	α
13				β						α		γ		γ
14					β						α		γ	
15						β						α		γ
16							β						α	
17								β						α
18									β					
19	β									α		γ		γ
20		β									α		γ	
21			β									α		γ
22				β									α	
23					β									α
24						β								
25	α						β							
26		α						β						
27	γ	α							β					

Fig. VI-4. D matrix. This matrix relates translationally equivalent molecules and represents a three-dimensional, one-molecule per unit cell exciton problem. Here the substitutions $\alpha=M_a$, $\beta=M_b$, and $\gamma=M_c$ are made.

$n+27$ are in the same unit cell, but are related geometrically the same as site I and site II molecules. Similarly the site III and site IV molecules in the same unit cell as site I molecule n are numbered respectively $n+54$ and $n+81$.

Now comes the big problem; that of locating the appropriate coupling constants connecting these translationally inequivalent sites. Let us consider only sites I and II, the other sites being treated in a similar fashion. Each molecule of type I is surrounded by four molecules of type II (See Fig. VI-1), one in the same unit cell and three in neighboring unit cells. Thus in column (row) n of our matrix there must be four matrix elements $M_{I,II}$. One of these, representing interactions within one unit cell, will be in row (column) $n+27$. The location of the other $M_{I,II}$ matrix elements is best found by looking at a model lattice built and labeled according to the above numbering recipe. There are four possible choices of the numbering scheme for the four nearest translationally inequivalent neighbors depending upon the choice of the positive directions of the crystallographic and unit cell axes. This ambiguity, however, is unimportant since there are four 27×27 submatrices consisting of $M_{I,II}$ matrix elements only. The numbering, and thus the location of matrix elements, in any individual submatrix is a reflection of the choice of positive axes, but the same four submatrices, B , B' , B^t , B'^t , appear irregardless of this choice. Note that B^t is the transpose of B . Because

of the cyclic numbering of the translationally equivalent molecules one needs to determine only the number labels of the four translationally inequivalent nearest neighbors of one particular molecule. The neighbors of any other molecule are found from these neighbors by applying the various recursion relations given above. Thus the matrix elements are located parallel to the diagonal of the matrix as shown in Fig. VI-5. Fig. VI-5 shows the $M_{I,II}$ matrix B in the numbering system used for these calculations.

Fig. VI-6 shows how the appropriate 27x27 submatrices are assembled into the full matrix to be diagonalized. Fig. VI-7 shows the appropriate column $14+\eta\cdot 27$ ($\eta=0,1,2,3$) of the twelve off-diagonal submatrices, all of which look somewhat similar to the matrix B of Fig. VI-5. From this column and the recursion relations above the complete 108x108 matrix can be constructed.

We now turn to the easy part of the problem. Having thus set up the matrix appropriate to the benzene crystal one must diagonalize this matrix, i.e., solve the corresponding secular determinant. This was done by means of a two-part program written in Fortran (Ver 3) for the IBM 7090 computer. The use of two separate programs was necessitated by storage limitations. The first part of the program constructed the matrix to be solved using the appropriate recursion relations and inserted matrix elements into the designated locations. By letting the computer construct the

	1	3	5	7	9	11	13	15	17	19	21	23	25	27														
	2	4	6	8	10	12	14	16	18	20	22	24	26															
1	B B		B B																									
2		B B		B B																								
3			B B		B B																							
4				B B		B B																						
5					B B		B B																					
6						B B		B B																				
7							B B		B B																			
8								B B		B B																		
9									B B		B B																	
10										B B		B B																
11											B B		B B															
12												B B		B B														
13													B B		B B													
14														B B		B B												
15															B B		B B											
16																B B		B B										
17																	B B		B B									
18																		B B		B B								
19																			B B		B B							
20																				B B		B B						
21																					B B		B B					
22																						B B		B B				
23																							B B		B B			
24	B																							B B		B		
25		B B																								B B		
26			B B																								B B	
27	B			B B																								B

Fig. VI-5. B matrix. This is one of the off-diagonal 27x27 submatrices. Here the substitution $B=M_{I,II}$ is made.

$$\begin{array}{c}
 \text{I} \\
 \text{II} \\
 \text{III} \\
 \text{IV}
 \end{array}
 \begin{array}{c}
 \text{I} \\
 \text{II} \\
 \text{III} \\
 \text{IV}
 \end{array}
 \left(\begin{array}{cccc}
 0 & 27 & 28 & 108 \\
 D & B & A & C \\
 B^\dagger & D & C' & A' \\
 A^\dagger & C'^\dagger & D & B' \\
 C^\dagger & A'^\dagger & B'^\dagger & D
 \end{array} \right)$$

Fig. VI-6. Complete 108x108 matrix for the calculation of the benzene factor group structure. Submatrix D is shown in Fig. VI-4. Submatrices A, B, and C resemble the B matrix of Fig. VI-5 and are constructed, respectively, of $M_{I,II}$, $M_{I,III}$ and $M_{I,IV}$ matrix elements according to Fig. VI-7 and the text.

Row	A	A'	A ^t	A', ^t	B	B'	B ^t	B', ^t	C	C'	C ^t	C', ^t
1												
2									C			
3												
4	A											
5	A	A							C	C		
6		A										
7												
8										C		
9												
10					B							
11					B	B			C			C
12						B						
13	A			A	B		B					
14	A	A	A	A	B	B	B	B	C	C	C	C
15		A	A			B	B					
16								B				
17							B	B		C	C	
18							B					
19												
20												C
21												
22				A								
23			A	A						C	C	
24			A									
25												
26										C		
27												

Fig. VI-7. The appropriate column $14+\eta \cdot 27$ ($\eta=0,1,2,3$) of the 12 off-diagonal submatrices of Fig. VI-6. The row is $x+\eta' \cdot 27$ as appropriate. Again the matrix elements A, B, and C are, respectively, $M_{I,II}$, $M_{I,III}$, and $M_{I,IV}$. The complete submatrices resemble the B matrix of Fig. VI-5 in that all matrix elements parallel the main diagonal.

matrix each of the 1000-odd individual matrix elements does not have to be specified by the programmer. Besides the great savings in time, this also allows one to easily change the magnitude of the coupling between any specified pair of molecules. The second part of the program used a subroutine called MLEW (Share 1375) which diagonalized the matrix giving both the eigenvalues and the corresponding normalized and orthogonalized eigenvectors. The individual components (108 of them) of each eigenvector are in the same order as the original states 1, 2, 3, ..., 108 and thus the square of each component represents the probability density of finding the excitation at that particular molecular site in the lattice.

The remaining problem is to interpret these results. It is easy to identify the $\vec{k}=\vec{0}$ energies since the corresponding eigenvectors have identical components except possibly for the sign, i.e., $1/(108)^{\frac{1}{2}}=0.0962$. Also these levels are nondegenerate whereas all other energies are doubly degenerate, corresponding to the $\pm\vec{k}$ degeneracy due to the center of inversion in the benzene crystal structure. For a given eigenvector if one plots the components as a function of site number, i.e., consecutively, one obtains a sinusoidal curve whose frequency is related to the wavevector \vec{k} of this function. There are discontinuities in this curve between sites 27-28, 54-55, 81-82, and 108-1. Because of the manner in which the matrix was constructed the first 27 components represent a one-site exciton function (ϕ_I) on site I, the

components 28 through 54 represent a one-site exciton function (ψ_{II}) on site II molecules, etc. As one would expect the frequency for each of these 27-unit sections of one function is the same. The easiest way of determining this frequency is to count the number of zeros of the function, i.e., the number of sign changes in the first 27 components. This will be an even number from 0 to 26.

At the boundaries between one-site functions (27-28, 54-55, and 81-82) there occur two things: 1) the same series of coefficients as before continues with a possible change of sign and 2) a shift by a constant number of sites. Thus, for example, the coefficient number 28 is always \pm the coefficient number 26, the coefficient number 55 is always \pm the coefficient number 52, and the coefficient number 82 is always \pm the coefficient number 81. These changes in sign of the coefficients identify the symmetry of the function just as in Eqs. 25, i.e., identify the function as ψ_{α} , ψ_{β} , ψ_{γ} , or ψ_{δ} . The number shifts are related to a phase shift in \vec{k} on changing from one one-site function to another and are respectively from site I to sites II, III, and IV, $2=(1+3)/2$, $5=(1+9)/2$, and $6=(3+9)/2$. Because of the numbering system used for the model, the unit of length (the difference in identification number) is different in the three directions, being 1, 3, and 9 in the directions \vec{c} , \vec{a} , and \vec{b} respectively. Thus the phase shifts in going from site I to site II, III, and IV molecules are respectively $\exp[i\vec{k}\cdot(\vec{c}+\vec{a})/2]$,

$\exp[i\vec{k}\cdot(\vec{c}+\vec{b})/2]$, and $\exp[i\vec{k}\cdot(\vec{a}+\vec{b})/2]$. Note that the vectors $(\vec{c}+\vec{a})/2$, $(\vec{c}+\vec{b})/2$, and $(\vec{a}+\vec{b})/2$ are just the vectors connecting lattice sites I and II, I and III, and I and IV, respectively. It follows that the correct symmetry adapted wavefunctions of the tight binding Hamiltonian are as a function of wave vector \vec{k} ,

$$\begin{aligned} \psi_{\alpha} &= \frac{1}{2} \left[\phi_I(\vec{k}) + e^{i\vec{k}\cdot\frac{\vec{c}+\vec{a}}{2}} \phi_{II}(\vec{k}) + e^{i\vec{k}\cdot\frac{\vec{c}+\vec{b}}{2}} \phi_{III}(\vec{k}) + e^{i\vec{k}\cdot\frac{\vec{a}+\vec{b}}{2}} \phi_{IV}(\vec{k}) \right], \\ \psi_{\beta} &= \frac{1}{2} \left[\phi_I(\vec{k}) - e^{i\vec{k}\cdot\frac{\vec{c}+\vec{a}}{2}} \phi_{II}(\vec{k}) - e^{i\vec{k}\cdot\frac{\vec{c}+\vec{b}}{2}} \phi_{III}(\vec{k}) + e^{i\vec{k}\cdot\frac{\vec{a}+\vec{b}}{2}} \phi_{IV}(\vec{k}) \right], \\ \psi_{\gamma} &= \frac{1}{2} \left[\phi_I(\vec{k}) - e^{i\vec{k}\cdot\frac{\vec{c}+\vec{a}}{2}} \phi_{II}(\vec{k}) + e^{i\vec{k}\cdot\frac{\vec{c}+\vec{b}}{2}} \phi_{III}(\vec{k}) - e^{i\vec{k}\cdot\frac{\vec{a}+\vec{b}}{2}} \phi_{IV}(\vec{k}) \right], \\ \psi_{\delta} &= \frac{1}{2} \left[\phi_I(\vec{k}) + e^{i\vec{k}\cdot\frac{\vec{c}+\vec{a}}{2}} \phi_{II}(\vec{k}) - e^{i\vec{k}\cdot\frac{\vec{c}+\vec{b}}{2}} \phi_{III}(\vec{k}) - e^{i\vec{k}\cdot\frac{\vec{a}+\vec{b}}{2}} \phi_{IV}(\vec{k}) \right]. \end{aligned} \tag{29}$$

The one-site exciton functions $\phi_a(\vec{k})$ are given by Eq. 24. Note that these equations reduce to Eqs. 25 for the optically important case where $\vec{k}=\vec{0}$.

We next inquire further into the \vec{k} dependence of the energy. We shall consider here only the first 27 components of the eigenvectors, since all of the others are directly related to these. Also we shall limit the momentum vector \vec{k} to the first Brillouin zone, i.e., $-\pi/a < k_a < \pi/a$, $-\pi/b < k_b < \pi/b$, and $-\pi/c < k_c < \pi/c$, where k_i is the projection of \vec{k} on the i -axis and a , b , and c are the magnitudes (lengths) of the respective lattice vectors. It was originally assumed that as the number of zeros of the eigenfunction went from 0 to 27

the magnitude of the wave vector, $|\vec{k}|$, went from 0 to π/r . However, this is not strictly true.

What is needed is to properly interpret the square of the eigenfunction coefficient as a probability density distribution in three dimensions. It was only very recently concluded that this relationship between number of zeros, i.e., frequency, and wavevector \vec{k} is quite complicated. This relationship was unraveled by setting various of the coupling constants to zero and then comparing the resultant energies with the case when this coupling constant was non-zero.

First let us consider the effect on the energy and factor group splitting due to the interactions between translationally equivalent molecules. From simple one-dimensional exciton calculations one would expect a cosine-like energy dependence upon \vec{k} . If we consider the number-of-zeros variable as an angle which goes linearly from 0 to π as the number of zeros goes from 0 to 27, the following gives this energy contribution to each of the energies E_α , E_β , E_γ , and E_δ :

$$E_{tr} = 2(M_c \cos\theta + M_a \cos 3\theta + M_b \cos 9\theta). \quad (30)$$

The factor 2 comes from the fact that there are two translationally equivalent nearest-neighbors for each site. It should be emphasized that each of the four factor group energies is affected separately and equally, and thus the

factor group splitting is unaffected by the interactions among translationally equivalent sites. Note that the factors 1, 3, and 9 appear. Again, this results from the differences in the units of length in the three principal directions. Since the factors 1, 3, and 9 are related to \vec{r} vectors \vec{c} , \vec{a} , and \vec{b} , respectively, the more conventional energy contribution due to interactions among translationally equivalent nearest-neighbor molecules is:

$$E_{tr} = 2[M_a \cos(k_a a) + M_b \cos(k_b b) + M_c \cos(k_c c)]. \quad (31)$$

As expected we have a simple cosine term.

Turning now to the factor group splitting caused by the interactions among translationally inequivalent molecules, we expect a cosine-like dependence, perhaps involving half-angles because of the phase factors introduced into the wavefunctions, Eqs. 29. Again by setting some matrix elements equal to zero one can deduce the effect of each type of matrix element separately and arrive at an energy expression, which is given here for E_α ,

$$E_\alpha = +2M_{I,II}(\cos 1\theta + \cos 2\theta) + 2M_{I,III}(\cos 4\theta + \cos 5\theta) + 2M_{I,IV}(\cos 3\theta + \cos 6\theta). \quad (32)$$

Here again θ is linearly related to the number of zeros of the eigenfunction. For the energy functions E_β , E_γ , and E_δ the signs in front of the coupling constants M_{Ia} are changed in accordance with Eqs. 26 where $\vec{k}=\vec{0}$. Note that $1=(3-1)/2$,

$2=(3+1)/2$, $4=(9-1)/2$, $5=(9+1)/2$, $3=(9-3)/2$, and $6=(9+3)/2$.

Now making the same correlation between 1, 3, and 9 and \vec{c} , \vec{a} , and \vec{b} as before, we arrive at the following dependence of energy upon \vec{k} due to interactions among the translationally inequivalent molecules:

$$\begin{aligned}
 E \begin{pmatrix} \alpha \\ \beta \\ \gamma \\ \delta \end{pmatrix} &= \begin{pmatrix} + \\ - \\ - \\ + \end{pmatrix} 2M_{I,II} \left[\cos \frac{k_a a - k_c c}{2} + \cos \frac{k_a a + k_c c}{2} \right] \\
 &\quad \begin{pmatrix} + \\ - \\ + \\ - \end{pmatrix} 2M_{I,III} \left[\cos \frac{k_b b - k_c c}{2} + \cos \frac{k_b b + k_c c}{2} \right] \\
 &\quad \begin{pmatrix} + \\ + \\ - \\ - \end{pmatrix} 2M_{I,IV} \left[\cos \frac{k_b b - k_a a}{2} + \cos \frac{k_b b + k_a a}{2} \right].
 \end{aligned} \tag{33}$$

Note that Eqs. 33 reduce to Eqs. 26 when $\vec{k}=\vec{0}$. These energy relationships were first given in another form by Eq. (11) in the paper by Fox and Schnepf (112). However I find it reassuring to be able to reproduce their result by an entirely different means. Fig. VI-8 shows a plot of the \vec{k} dependence of the factor group splitting along three crystallographic directions: a) parallel the c-axis ($k_a=k_b=0$, $k_c \neq 0$); b) parallel the face-diagonal vector $\vec{a}+\vec{c}$ ($k_b=0$, $k_a=k_c \neq 0$); and c) parallel the body-diagonal vector $\vec{a}+\vec{b}+\vec{c}$ ($k_a=k_b=k_c \neq 0$). In Fig. VI-8 the "hypothetical" coupling constants derived above were used, and the effect of the

(112) D. Fox and O. Schnepf, J. Chem. Phys., 23, 767 (1955).

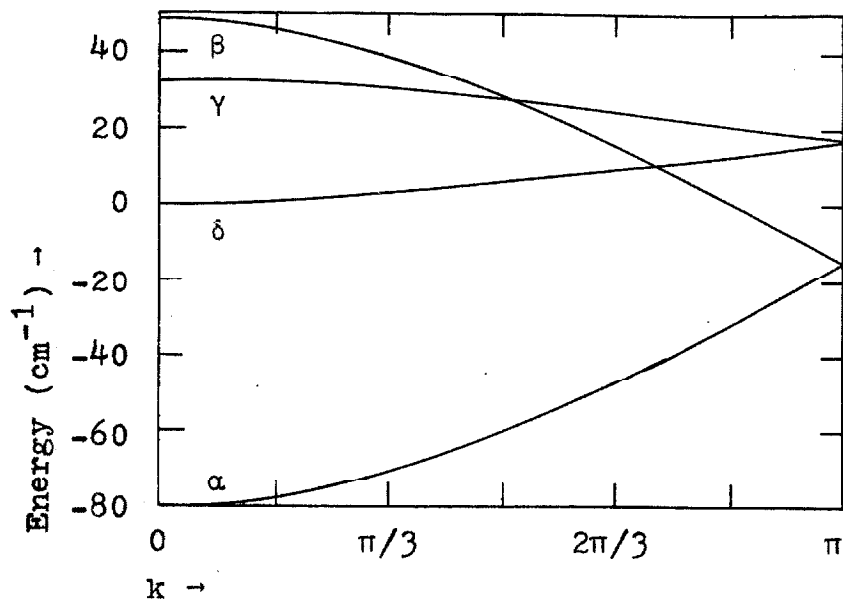


Fig. VI-8a. Exciton band structure for benzene.*
 $k = k_c$ $k_a = k_b = 0$

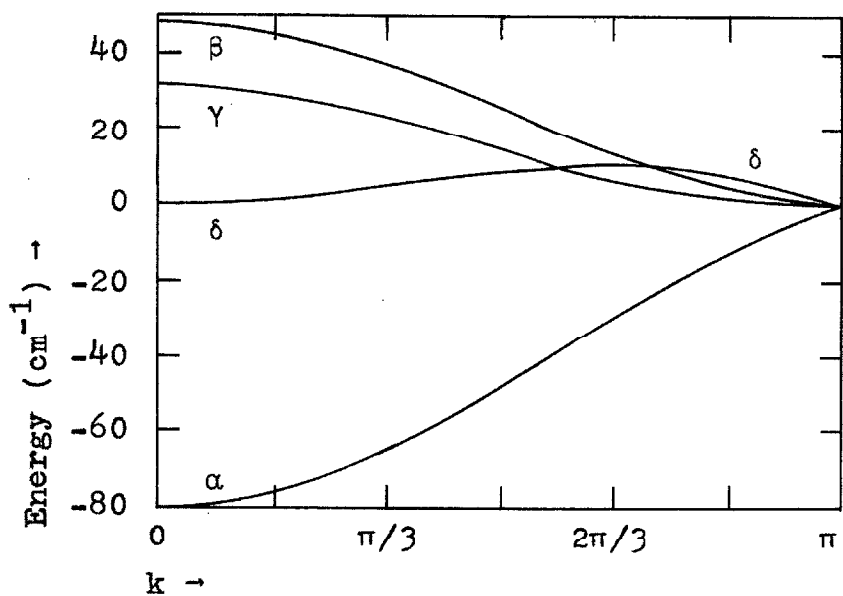


Fig. VI-8b. Exciton band structure for benzene.*
 $k = k_c = k_a$ $k_b = 0$

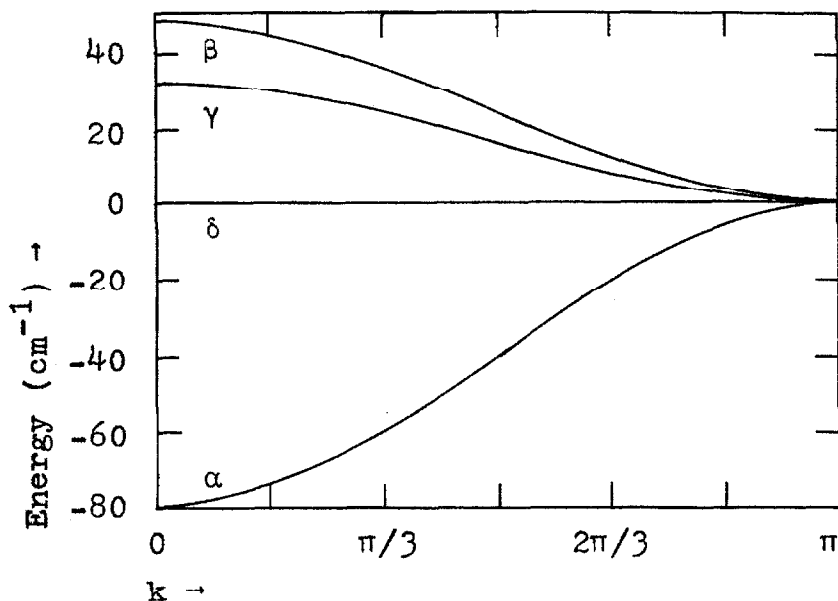


Fig. VI-8c. Exciton band structure for benzene.*

$$k=k_c \quad c=k_a \quad a=k_b$$

* This is a "hypothetical" triplet exciton band structure derived from computer calculations on a three-dimensional benzene crystal containing 108 molecules. The "hypothetical" coupling constants $M_{I,II}=-10 \text{ cm}^{-1}$, $M_{I,III}=-6 \text{ cm}^{-1}$, and $M_{I,IV}=-4 \text{ cm}^{-1}$ were used for these calculations. A given curve connects a set of energy states whose eigenfunctions transform alike under factor group operations. For the triplet band structure the levels α , β , γ , and δ transform, respectively, as B_{2u} , B_{3u} , A_{1u} , and B_{1u} .

interactions among translationally equivalent molecules has been neglected since it just adds a small cosine curve to each of the above curves. It should be mentioned that all of the computer calculated energies were for the case when $k_a = k_b = k_c$, but I believe that this result is an artifact of the manner in which the computer must handle the true three-dimensional problem.

It is interesting to note that this type of calculation applied to the isotopically mixed crystal (e.g., 107 hosts plus one guest at molecular site 41) shows the triplet "trap state" to be 99% "localized" for the 200 cm^{-1} trap, 96% "localized" for the 100 cm^{-1} trap, and 92% "localized" for the 67 cm^{-1} trap. For the 33 cm^{-1} trap the significance of the "trap state" is lost since there is a great deal of mixing with triplet exciton states of the host crystal. It is therefore not surprising that phosphorescence from the C_6H_6 - $\text{C}_6\text{H}_5\text{D}$ mixed crystal is missing. As a matter of fact the missing phosphorescence for the 33 cm^{-1} trap but not for the 67 cm^{-1} trap is completely consistent with the suggested magnitude of the coupling constants, but is inconsistent with much smaller or much larger values. I feel that these qualitative observations along with the measured quasiresonance shifts go far in making the argument for 10-100 cm^{-1} triplet factor group splittings in aromatic crystals a convincing one. The question as to whether the magnitude of the interactions can be adequately explained on the basis of first-order exchange

coupling alone awaits better calculations of the intermolecular exchange integrals than were attempted here.

3. The Singlet Exciton Band. The method of variation of energy denominators has also been applied to the first singlet-singlet transition of mixed isotopic benzene crystals. Table VI-1 lists the observed relative quasiresonance shifts for the singlet fluorescence spectra. Note that the relative shifts are approximately double those found for the phosphorescence and again are nearly independent of the vibrational progression involved. In the same manner as before one arrives at the value of $\beta_S = 18 \pm 2 \text{ cm}^{-1}$, for the "pairwise" singlet exciton coupling constant.

The factor group splitting for the first singlet-singlet transition can be directly observed in absorption. These line positions along with the energy "zero" allow the calculation of the M_{Ia} coupling constants by means of Eqs. 26. Note that, unlike for the ${}^3B_{1u}$ molecular state, for the ${}^1B_{2u}$ molecular state as basis, α , β , γ , and δ levels of the crystal transform respectively as ${}^1B_{3u}$, ${}^1B_{2u}$, ${}^1B_{1u}$, and ${}^1A_{1u}$ under symmetry operations associated with the factor group. From these experimental coupling constants it is possible to calculate the value of the root mean square coupling constant β_S and to compare this value with that obtained from the quasiresonance-shift studies.

The singlet exciton band center of C_6H_6 was found to lie at $37\,872 \pm 2 \text{ cm}^{-1}$ as compared to the gas phase value of

Table VII-1.

Observed shifts of C_6H_6 fluorescence in isotopic hosts.*

$\nu(\text{vac}) C_6H_6$ in C_6D_6 (cm^{-1})	$\delta(C_6D_6)-$ $\delta(C_6H_3D_3)$ (cm^{-1})	$\delta(C_6D_6)-$ $\delta(C_6H_4D_2)$ (cm^{-1})	$\delta(C_6D_6)-$ $\delta(C_6H_5D)$ (cm^{-1})	Assignment (0,0)- (cm^{-1})
37 852.2	+6.8	+10.6	+25.2	0
37 246.2	6.8	10.6	18.9	606
36 862.6	6.0	10.8	22.7	992
36 269.7	7.2	11.0	22.5	1595
36 250.3	6.7	10.8	23.1	606+992
35 873.7	6.5	11.0	23.2	2·992
35 285.4	6.9	10.2	24.6	1595+992
35 258.9	6.8	10.8	22.6	606+2·992
34 301.8	7.2	10.5		1595+2·992
34 269.2	7.5	10.9		606+3·992

* δ is the spectral shift referred to the line positions of C_6H_6 for infinite energy denominator ΔE . Since the shift is to lower energy with decreasing deuterium substitution, δ is always a negative number and is more negative the less the deuteration. The assignment involves electronic ground-state vibrations of species a_{1g} (992 cm^{-1}) and e_{2g} (606 and 1595 cm^{-1}).

38 090 cm^{-1} (113). The band center was determined by correcting the observed position of the (0,0) absorption of C_6H_6 in C_6D_6 for the quasiresonance shift and for the shift in the $\vec{k}=\vec{0}$ component caused by interactions among translationally equivalent molecules. These corrections were +7 and $\sim+10 \text{ cm}^{-1}$, respectively. Included in the $\sim+10 \text{ cm}^{-1}$ correction is a contribution of $+2 \text{ cm}^{-1}$ arising from quasiresonance interactions between the zeroth vibrational level of the guest and excited totally symmetric vibrational levels of the host. The lowest lying of these is approximately 900 cm^{-1} above the zeroth level of the host. This increases the energy denominator of the perturbation problem by a factor of five while the numerator remains nearly constant. Thus such interactions may contribute an additional 20%-30% to the quasiresonance shift. This additional correction changes very little with different hosts and thus cancels in the experimentally measured relative shifts. However, it must be considered in determining the absolute shift.

Using the above band center frequency with the three experimental factor group line frequencies at 37 803.2, 37 841.8, and $37 847.1 \text{ cm}^{-1}$ from our own measurements of the absorption spectrum of pure crystalline C_6H_6 (at 4°K), one obtains $M_{\text{I,II}}=+11.7 \text{ cm}^{-1}$, $M_{\text{I,III}}=-12.4 \text{ cm}^{-1}$, and $M_{\text{I,IV}}=-6.9$

(113) F. M. Garforth, C. K. Ingold, and H. G. Poole, J. Chem. Soc., 1948, 513.

cm^{-1} for the coupling constants in this case. For this calculation the most recent polarization assignments of Broude (114) were accepted. This paper apparently reverts to the older idea (115) where only two factor group components with a- and c-axis polarizations were thought to occur. Criticisms of the validity of Davydov's approximations have already been given (116, 117). In some of Broude's earlier work (118) a- and c- as well as b-axis polarizations were cited. It should be noted however that the original a- and c-axis assignments given in the 1957 work have been interchanged in the 1962 paper. The coupling constants above are based upon somewhat reluctant acceptance of Broude's more recent a- and c-axis assignments in conjunction with the older b-axis assignment.

These polarization assignments lead to an identification of the factor group lines as B_{1u} , B_{3u} , and B_{2u} in order of increasing wavenumber. The A_{1u} component, which is not observed because of selection rules, would therefore lie at

-
- (114) V. L. Broude, Usp. Fiz. Nauk, 74, 577 (1961) [English Transl. Soviet Phys.--Usp., 4, 584 (1962)].
- (115) A. Davydov, Zh. Eksperim. i Teor. Fiz., 18, 210 (1948); 21, 673 (1951).
- (116) D. Fox and O. Schnepp, J. Chem. Phys., 23, 767 (1955).
- (117) H. Winston, J. Chem. Phys., 19, 156 (1951).
- (118) V. L. Broude, V. S. Medvedev, and A. F. Prikhot'ko, Opt. i Spektroskopiya, 2, 317 (1957); Chem. Abstr., 51, 11065d (1957).

37 966 cm^{-1} (calc.). An interchange of the above a- and c- assignments would lead to identification of the factor group components as B_{3u} , B_{1u} , and B_{2u} in order of increasing frequency, while the coupling constants become $M_{I,II}=+6.9 \text{ cm}^{-1}$, $M_{I,III}=-12.4 \text{ cm}^{-1}$, and $M_{I,IV}=-11.7 \text{ cm}^{-1}$. It is noted that a change in the polarization assignments does not affect the magnitudes of the three coupling constants nor does it affect the magnitude of β_S . It at most changes the signs of the coupling constants and their identification with a particular M_{Ia} . It is also noted that this new analysis of the factor group terms does not agree with the old one (116), nor do the coupling constants derived above agree with those calculated solely upon the basis of transition octopoles (119).

Using the above coupling constants and Eq. 28, one

(119) Fox and Schnepf (116) give $M_{I,II}=0 \text{ cm}^{-1}$, $M_{I,III}=-4.6 \text{ cm}^{-1}$, and $M_{I,IV}=+2.8 \text{ cm}^{-1}$; but this calculation neglects exchange interactions, higher-pole Coulomb interactions, as well as second-order contributions to the splitting. In addition, a number of other approximations were made in order to partially simplify the tedious evaluation of matrix elements. While second-order terms probably amount to no more than a couple of cm^{-1} , the results presented above for the triplet state show that exchange interactions cannot be neglected. There is at present no good way of evaluating the other approximations used by Fox and Schnepf. It would not be surprising, however, if their simple octopole-octopole theory alone was found to give an inadequate representation of the ${}^1B_{2u}$ exciton band structure in crystalline benzene. See the discussion near the end of Sect. (d) in McClure's (120) article.

(120) D. S. McClure, Solid State Physics (Academic Press Inc., New York, 1959), Vol. 8, pp. 13-16.

calculates $\delta_S = 18.4 \text{ cm}^{-1}$, a value which within the uncertainty of the band center position is in very good agreement with that independently calculated ($18 \pm 2 \text{ cm}^{-1}$) from quasi-resonance shifts. This agreement further confirms the validity of the method of variation of energy denominators.

Finally it should be remarked that this analysis also is in disagreement with that given of the structure near $37\,800 \text{ cm}^{-1}$ in the recent long paper of Broude (114). I feel that the most obvious difficulty with Broude's analysis lies in his location of the (0,0) band center in the crystal. The value of $37\,872 \text{ cm}^{-1}$ based upon isotopic studies and reported above should not be far wrong providing there are no large effects due to vibrational overlap integrals (78). Yet in Sect. 9 of Broude's paper a method is described by which the value of $37\,835 \text{ cm}^{-1}$ is obtained for the band center. In essence his value is obtained by subtracting the 520 cm^{-1} (e_{2g} excited state vibration) vibrational frequency from the position of the average of the two "observed components" of the $(0,0) + 520 \text{ cm}^{-1}$ transition in pure C_6H_6 . This method of locating the band center is valid only if there are no terms which shift the $(0,0) + 520 \text{ cm}^{-1}$ transition relative to the (0,0) transition in C_6H_6 and then only if a correct analysis of the factor group components in this part of the transition has been made. The validity of Broude's method is therefore questionable.

My results show that the absorption spectrum of C_6H_6 in

any given deuterated benzene host is shifted by approximately the same amount for the four transitions: (0,0); (0,0)+520 cm⁻¹; (0,0)+925 cm⁻¹; and (0,0)+520 cm⁻¹+925 cm⁻¹. At first sight this is quite disturbing since the resonance interaction for states involving nontotally symmetric vibrations is expected to be quite small. For example, the (0,0)+520 cm⁻¹ transition in the pure crystal appears to contain two components split by only 6 cm⁻¹. This fact, which puzzled Broude, is caused by (121) the vanishing of vibrational overlap integrals in the first-order interaction between resonance states. For example, matrix elements of the type

$$\langle \varphi'_A(e_{2g}) | \varphi^0_A(a_{1g}) \rangle \langle \varphi^0_B(a_{1g}) | \varphi'_B(e_{2g}) \rangle \langle \psi'_A \psi^0_B | V_{AB} | \psi^0_A \psi'_B \rangle$$

are zero, the first two factors vanishing because of symmetry. Here the φ 's are vibrational wavefunctions, the ψ 's electronic wavefunctions, superscripts (') and (0) indicate excited and ground electronic states, respectively, and A and B indicate the two interacting molecules. However, quasiresonance interactions of the type

$$\langle \varphi'_A(e_{2g}) | \varphi^0_A(e_{2g}) \rangle \langle \varphi'_B(a_{1g}) | \varphi^0_B(a_{1g}) \rangle \langle \psi'_A \psi^0_B | V_{AB} | \psi^0_A \psi'_B \rangle$$

are nonzero and are in fact of the same order of magnitude as the resonance interactions. Because of the difference in energy of the e_{2g} vibrations in the ground and ${}^1B_{2u}$ electron-

(121) D. P. Craig and S. H. Walmsley, Mol. Phys., 4, 113 (1961).

ic state (606 and 520 cm^{-1} , respectively) this is not a resonance interaction and does not contribute to the splitting of the vibrationally excited levels of pure C_6H_6 . However, it does contribute to a shift in position of the (0,0)+520 cm^{-1} transition in isotopic mixed crystals and even in pure C_6H_6 where the energy denominator is 86 cm^{-1} . Thus while the splitting of the nontotally symmetric vibronic levels is small the quasiresonance shifts are of the same magnitude as those for totally symmetric levels. These shifts must be taken into account when determining the true factor group band center in nontotally symmetric levels. Such effects were completely neglected by Broude. Thus, in spite of Broude's implication of the definitiveness of the work covered in his long paper, I cannot accept any part of his analysis of the factor group components in either the totally symmetric or nontotally symmetric vibronic levels in the ${}^1\text{B}_{2u}$ state of crystalline benzene.

Even though many features of the singlet-singlet spectrum of crystalline benzene seem to be neatly tied together by the preliminary isotopic mixed crystal work here, still more definitive polarization experiments are needed before one has very much confidence in the over-all interpretation of this spectrum.

VII. NONHEXAGONAL BENZENE IN THE TRIPLET STATE

1. Introduction. This section is somewhat unrelated to the previous sections in that it is not concerned with triplet exciton effects. It does, however, concern the lowest triplet state of benzene and is an outgrowth of the analysis of the phosphorescence spectra taken originally for the various exciton studies.

Some recent experiments by de Groot and van der Waals (122) have indicated that benzene in its lowest triplet state (${}^3B_{1u}$) does not possess hexagonal symmetry (D_{6h}). This is in contrast to the hexagonal configuration in the ground state (${}^1A_{1g}$) and first excited singlet state (${}^1B_{2u}$). Specifically, their magnetic resonance spectrum indicated no three-fold (or greater) symmetry axis. This result had been anticipated earlier by Lewis and Kasha (123) and by Redlich and Holt (124) who suggested a quinoid structure with the parallel spins in the para position. Liehr (125) has also suggested that there is an indirect Jahn-Teller instability

-
- (122) M. S. de Groot and J. H. van der Waals, Mol. Phys., 6, 545 (1963).
- (123) G. N. Lewis and M. Kasha, J. Am. Chem. Soc., 66, 2100 (1944).
- (124) O. Redlich and E. K. Holt, J. Am. Chem. Soc., 67, 1228 (1945).
- (125) A. D. Liehr, Z. Naturf. A, 16, 641 (1961); Advanc. Chem. Phys., 5, 241 (1963).

for B_{1u} electronic states of benzene due to mixing with the nearby E_{1u} state.

Because of the difficulties in obtaining spin resonance spectra of triplet states in rigid glasses there is possibly some question concerning de Groot and van der Waals's interpretation of their spectra. I hope in this section to present convincing optical evidence that benzene in its lowest triplet state, indeed, is not a regular hexagon.

2. Experimental Evidence. When first analyzed the phosphorescence spectra of isotopic mixed crystals of benzene were puzzling in two respects: 1) the phosphorescence spectrum of C_6H_5D in C_6D_6 shows a doublet structure for all emission lines, i.e., for every one line in the C_6H_6 spectrum there are two lines in the C_6H_5D spectrum, and 2) the relative intensities of the components of these doublets are concentration dependent, the lower energy component being more intense the higher the concentration. At first, this was thought to be due to the splitting of the degenerate e_{2g} vibrations of C_6H_6 in the less symmetrical C_6H_5D . However, the observed frequencies do not correspond to those previously measured for these vibrations (126). It was also found that both components of the former e_{2g} vibration sometimes appear and that both are doublets. Thus this cannot

(126) D. H. Whiffen, Phil. Trans. Roy. Soc. (London), A248, 131 (1955).

be the correct explanation of this splitting.

Having become interested in this problem, a careful examination of the available phosphorescence spectra was undertaken. This revealed that the phosphorescence of 1,3,5- $C_6H_3D_3$ in C_6D_6 consists of single lines just as does that of C_6H_6 , and that the phosphorescence of 1,4- $C_6H_4D_2$ in C_6D_6 consists of doublets just as does that of C_6H_5D . It should be noted that the doublet splittings for C_6H_5D and 1,4- $C_6H_4D_2$ are respectively $7.0 \pm 0.5 \text{ cm}^{-1}$ and $13.0 \pm 1.0 \text{ cm}^{-1}$, and are independent of vibrational progression, even occurring in the (0,0) band.

Fig. VII-1 shows a portion of the phosphorescence spectra of C_6H_6 , C_6H_5D , 1,4- $C_6H_4D_2$, and 1,3,5- $C_6H_3D_3$, all in C_6D_6 at $4.2^\circ K$. The assignments of these lines are listed in Table VII-1.

3. Explanation of These Observations. These observations can be explained if the benzene molecule in the crystal has D_{2h} symmetry (127), i.e., is nonhexagonal, in either the ground state or the lowest triplet state. For the case of D_{2h} symmetry there are two nonequivalent forms of both C_6H_5D and 1,4- $C_6H_4D_2$, but only one form of both C_6H_6 and 1,3,5- $C_6H_3D_3$. Fig. VII-2 shows these possible configura-

(127) Specifically, these observations imply the lack of a three-fold axis perpendicular to the molecular plane, but the presence of a two-fold axis perpendicular to this plane. However, one cannot determine whether the molecule is still planar.

A PORTION OF THE PHOSPHORESCENCE SPECTRA OF VARIOUS ISOTOPIC BENZENES
 SHOWING THE SPLITTINGS DUE TO THE NONHEXAGONALITY OF
 BENZENE IN ITS LOWEST TRIPLET STATE

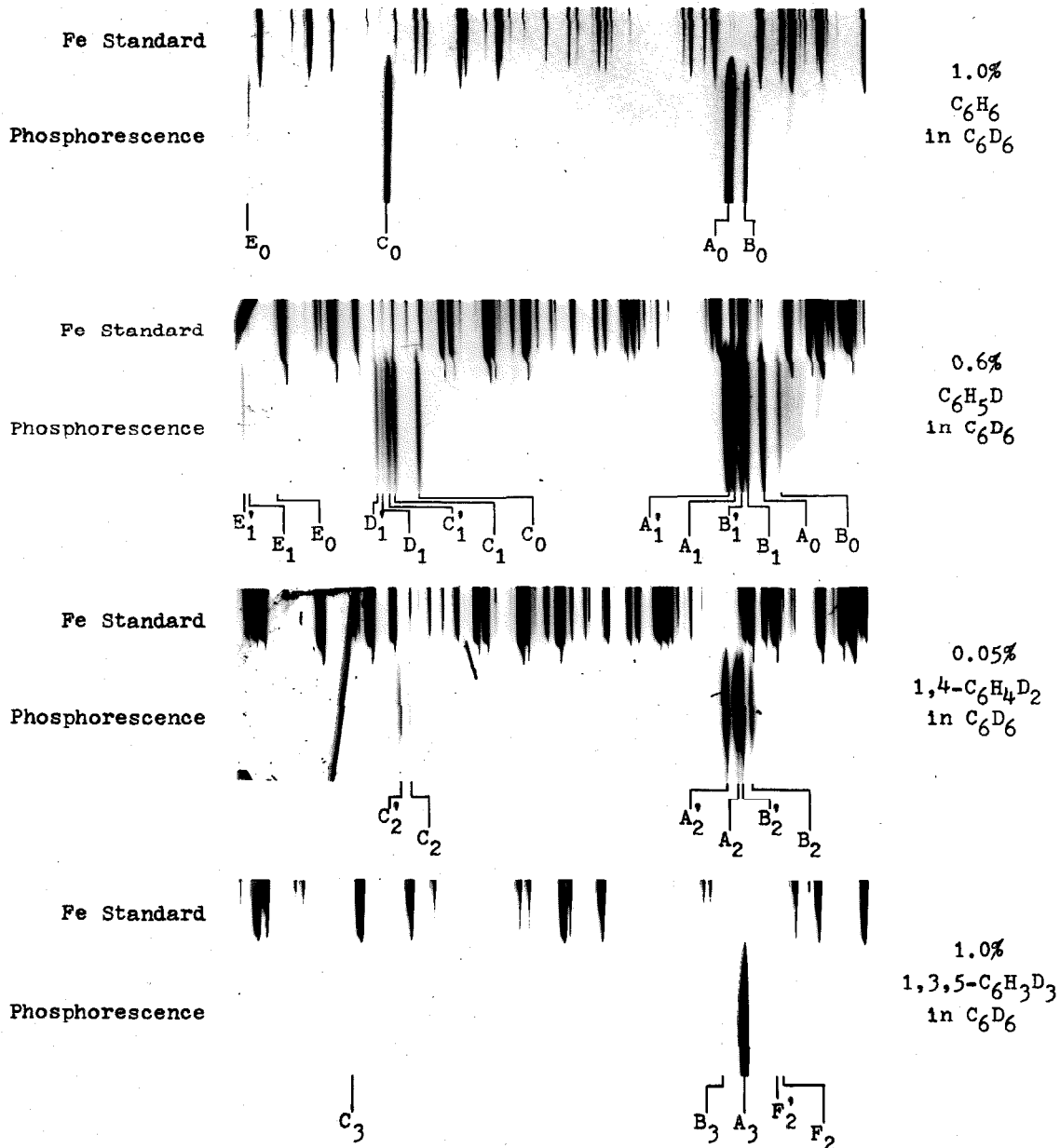


Fig. VII-1. Note the splitting of the phosphorescence lines of C_6H_5D and 1,4- $C_6H_4D_2$ and the lack of splitting of the lines of C_6H_6 and 1,3,5- $C_6H_3D_3$. See Table VII-1 concerning the assignment of these lines.

Table VII-1.

Assignment of the phosphorescence lines shown in Fig. VII-1.

Compound	Line*	Assignment (0,0)-(cm ⁻¹)
C ₆ H ₆	A ₀	1595** (e _{2g})
	B ₀	606+992** (e _{2g})
	C ₀	1178 (e _{2g})
	E ₀	985 (b _{2g})
C ₆ H ₅ D	A ₁	1574*** (b ₁)
	B ₁	1591*** (a ₁)
	C ₁	1175 (a ₁)
	D ₁	1158 (b ₁)
	E ₁	995 (b ₂)
1,4-C ₆ H ₄ D ₂	A ₂	1569**** (a _g)
	B ₂	1587**** (b _{1g})
	C ₂	1173 (a _g)
1,3,5-C ₆ H ₃ D ₃	A ₃	1573 (e')
	B ₃	593+956 (e')
	C ₃	1102 (e')
1,3-C ₆ H ₄ D ₂	F ₂	1583 (a ₁)

* Primed (') lines arise from the high energy form.
Unprimed lines arise from the low energy form.

** Fermi resonance between 1595 and 606+992.

*** Fermi resonance among 1574, 1591, and 602+980.

**** Fermi resonance among 1569, 1587, and 600+978.

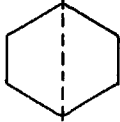
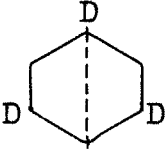
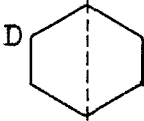
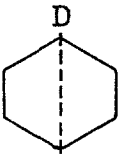
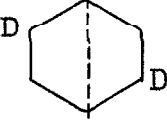
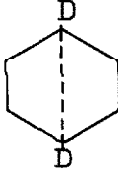
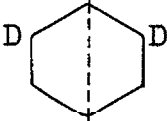
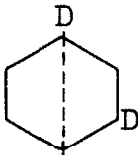
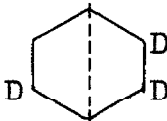
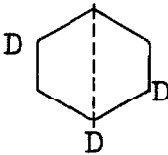
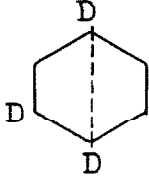
Compound	Form A	Form B	Form C	Statistical Probability A:B:(C)
C_6H_6				1
$1,3,5-C_6H_3D_3$				1
C_6H_5D				2:1
$1,4-C_6H_4D_2$				2:1
$1,3-C_6H_4D_2$				1:2
$1,2,4-C_6H_3D_3$				1:1:1

Fig. VII-2. Possible configurations of deuterated benzenes assuming D_{2h} symmetry.

tions of the deuterium atoms along with their statistical probabilities. For simplicity in drawing the figures an exaggerated conformation I of de Groot and van der Waals (122) has been assumed, the dotted axis being the short diagonal.

This D_{2h} symmetry may result from one of the following: 1) the distortion of the deuterated molecule by the crystal field in which it sits; 2) an unsymmetrical effect upon particular vibrational frequencies; or 3) benzene in the lowest triplet state has D_{2h} symmetry. Since the first effect is equivalent to the presence of different lattice sites, and there is no splitting in the C_6H_6 spectrum, one has to assume that the crystal field is able to differentiate between hydrogen and deuterium atoms. In view of the identical sizes and electronic structures of these isotopes this seems highly unlikely. Because of changes in vibrational frequencies upon deuteration it might be thought that the crystal field could in this way differentiate between hydrogen and deuterium atoms. However, this, too, seems very unlikely.

These first two effects occur in the ground state and its vibrations. Thus, the same effects, i.e., the same doublet structure, should appear in the fluorescence spectra since this transition involves the same ground state and its vibrations. In fact, the very same vibrations appear. Careful examination of the fluorescence spectrum for each isotopic benzene shows no doublet structure, all deuterated benzenes giving single-lined progressions.

Having thus conclusively proven that this is not a ground state phenomenon, the doublet structure must be an excited state phenomenon involving the lowest triplet state but not the first excited singlet state. Since, at low temperatures, all emission is from the zeroth vibrational level of the excited state, this effect involves this level of the triplet state. Therefore, one is forced to conclude that the benzene molecule is not a regular hexagon in its lowest triplet state.

The next question to ask is, "Why are the energies of the two forms, A and B, of C_6H_5D , for example, different?"



At first, one might think that there is a slight difference in the electronic energy of these two configurations, but, because of the close similarities of the hydrogen and the deuterium atoms, this is very unlikely.

Nevertheless, certain excited state vibrational frequencies of A will be different than those of B because of mass effects. Primarily these will be the "e" carbon-hydrogen modes which do not possess three-fold symmetry (128).

(128) E. B. Wilson, Jr., J. C. Decius, and P. C. Cross, Molecular Vibrations (McGraw-Hill Book Co., Inc., New York, 1955), pp. 240-272, 328.

These frequency differences are expected to be quite small and will not appear in the phosphorescence since they involve excited state vibrations. However, these differences will appear in the zero-point energy ($\sum_1 \frac{1}{2} h\nu_1$) and therefore in the energy of the zeroth vibrational level. For the case of C_6H_5D a total difference of only 14 cm^{-1} in vibrational frequencies would account for the observed 7 cm^{-1} splitting. This value is entirely reasonable in view of the $\sim 20\,800 \text{ cm}^{-1}$ zero-point energy.

If the benzene molecule indeed does have D_{2h} symmetry, one would expect that substitution of a para deuterium should about double the C_6H_5D splitting. The 13 cm^{-1} splitting of $1,4-C_6H_4D_2$ is in excellent agreement with this prediction.

One might now ask, "Which form, A or B, lies at the higher energy and what is the rate of intramolecular conversion between the two configurations?" The latter part of this question is rather easy to answer qualitatively. If the rate of conversion were fast compared to the phosphorescence lifetime ($\tau \sim 10 \text{ sec.}$), the intensity ratio of the two forms should be the same as the ratio of their statistically weighted Boltzmann factors. Experimentally, this is not observed. Rather, the intensity ratio is strongly concentration dependent, the lower energy form being more intense the higher the concentration. This implies that trap-to-trap excitation migration can favorably compete with the inter-

conversion process.

Table VII-2 lists the relative intensities of various pairs of lines for C_6H_5D . Individual numbers in this table are subject to rather large errors both in the measurement of intensities and due to the effects caused by the presence of impurity traps (129). However the total ratios and their general trends should be somewhat more reliable. Fig. VII-3 shows the concentration dependence of the ratio of the intensities of the upper to the lower energy forms. Note that the zero concentration limit of this ratio is approximately two, which is just what one expects for the statistical probability ratio of the two forms. This indicates that whenever a particular site is excited by radiation or by excitation transfer, there is a statistical probability of populating each form. A similar relationship holds for 1,4- $C_6H_4D_2$ where again the higher energy form appears to be twice as prevalent as the lower energy form at low concentrations.

These results imply that the "configuration lifetime" is considerably longer than the phosphorescence lifetime, i.e., >10 sec. (130). Some temperature studies at $3^{\circ}K$ and at $1.8^{\circ}K$ have been made, but it is impossible to say if

(129) See Sect. III.

(130) De Groot and van der Waals (122) obtain a value of $\sim 10^{-10}$ sec. at $20^{\circ}K$. It is not understood whether this discrepancy is a temperature or a crystal effect.

Table VII-2.

Ratio of the intensity of the high energy form
to the intensity of the low energy form
(I_A/I_B) for C_6H_5D .

Transition (0,0)-	Composition (in C_6D_6)							
	0.8% C_6H_5D	0.4% C_6H_5D 0.4% C_6H_6	0.2% C_6H_5D * 0.2% 1,3,5- $C_6H_3D_3$	0.2% C_6H_5D * 0.2% C_6H_6	0.1% C_6H_5D 0.01% C_6H_6	0.05% C_6H_5D 0.05% 1,3,5- $C_6H_3D_3$	0.04% C_6H_5D 0.04% C_6H_6	
1574	0.92	1.72	1.75	1.67	2.44	2.08	1.85	
1591	0.92	1.25	2.78	1.56	2.63		1.75	
1175+980	0.76		1.14	0.91	1.05			
1574+980	0.98	1.78	2.08	1.70	2.70	2.63	4.25	
1591+980	0.94	1.28	2.13	1.64	2.56	2.70	1.56	
1574+2·980	0.93		2.63		5.26	2.13		
1591+2·980	0.91	1.22	1.82		2.04			
Total	0.93	1.47	2.08	1.54	2.63	2.18	2.18	

* Data from the work of Steven Colson.

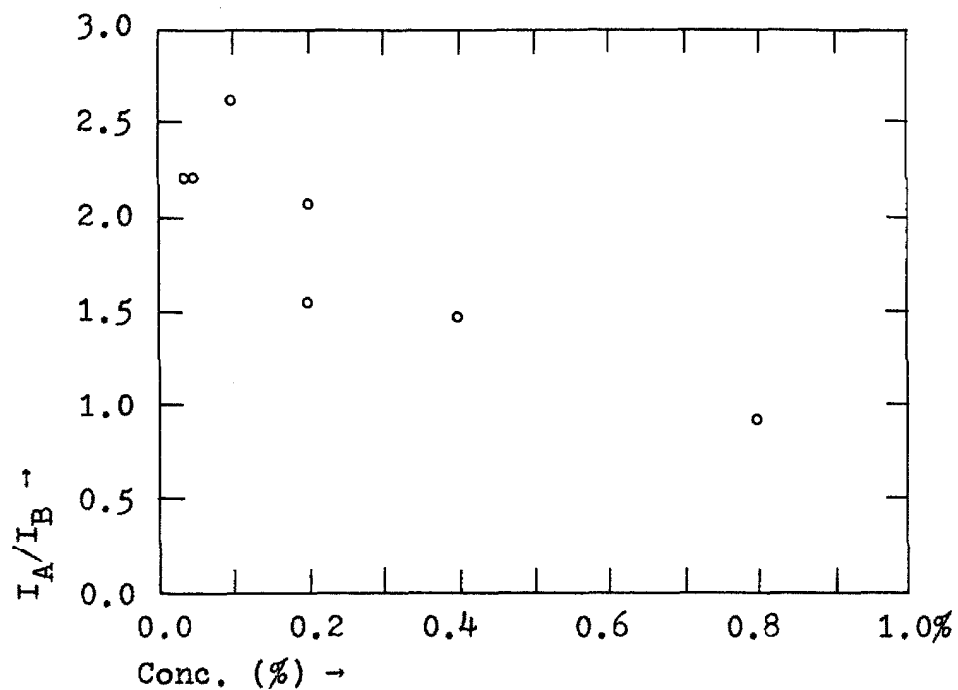


Fig. VII-3. Concentration dependence of the ratio of the intensity of the high energy form to the intensity of the low energy form (I_A/I_B) for C_6H_5D in C_6D_6 at $4.2^\circ K$. See Table VII-2. These numbers are too large because of impurity effects.

there are any effects other than a reduction in the rate of excitation migration. Studies at higher temperatures would be useful, but they are limited to temperatures below 15°K where all phosphorescence is quenched in these systems.

This 2-to-1 ratio further serves to identify the configurations of the high and low energy forms, i.e., the statistically favored form A is the high energy form, and B is the low energy form. This is reasonable if one assumes that the vibration principally responsible for the energy difference involves a high amplitude of motion along the dotted axis, i.e., the short diagonal. The approximately double splitting observed for $1,4\text{-C}_6\text{H}_4\text{D}_2$ is also consistent with this assumption. This vibration is probably the e_{2g} carbon-hydrogen mode at about 3045 cm^{-1} (131). The e_{2g} carbon-hydrogen bending mode at about 1175 cm^{-1} may also be involved.

The phosphorescence spectra of each of the forms are, as expected, nearly identical except for some slight differences in the intensities of some minor lines. It is observed that the very weak 606 cm^{-1} (e_{2g}) and $(0,0)+n\cdot 992\text{ cm}^{-1}$ (a_{1g}) transitions are relatively too weak in the low energy form, especially in $\text{C}_6\text{H}_5\text{D}$. This effect is not nearly as pronounced in $1,4\text{-C}_6\text{H}_4\text{D}_2$. In $\text{C}_6\text{H}_5\text{D}$ the 1178 cm^{-1} e_{2g} vibra-

(131) Ingold, et al. (132) pictures the normal coordinate motions of benzene rather well.

(132) C. R. Bailey, C. K. Ingold, H. G. Poole, and C. L. Wilson, J. Chem. Soc., 1946, 231.

tion of C_6H_6 splits into an a_1 component at 1175 cm^{-1} and a b_1 component at 1158 cm^{-1} , both of which are observed in the phosphorescence spectrum. In this case the relative intensity of the transition arising from the low energy form B appears to be too strong for the a_1 component and too weak for the b_1 component. The implications of these intensity differences are, as yet, not fully understood. Perhaps, they indicate something about the shape of the A and B forms, i.e., is the dotted axis elongated or shortened?

4. Other Experiments. There are several checks on this nonhexagonality of benzene. One, which we (133) pursued, involves the phosphorescence spectra of these isotopic benzenes in solid rare gas matrices. It was found that the spectra were sufficiently sharp in solid argon at 4.2°K that possible splittings could be observed. The somewhat disappointing results can be summarized as follows: 1) the line widths of C_6H_6 and C_6D_6 emissions are about 3 cm^{-1} ; 2) the line width of $1,3,5-C_6H_3D_3$ emission is about 5 cm^{-1} ; 3) the line width of C_6H_5D emission is about 7 cm^{-1} ; 4) the line width of $1,4-C_6H_4D_2$ emission is about 10 cm^{-1} ; 5) no distinct splittings are observed; and 6) all of the fluorescence line widths appear to be about 3 cm^{-1} , but these lines are very weak. It also should be noted that the vibrational

(133) I would like to acknowledge the help of Dino S. Tinti with these experiments. Also our many discussions concerning this problem have been most useful.

frequencies of benzene in solid argon appear to be very nearly those found in the gas phase, i.e., somewhat higher ($2-5 \text{ cm}^{-1}$) than those found in the crystal.

These results can be explained if: 1) the lowest triplet state of benzene is hexagonal in solid argon; 2) the interconversion rate between the two forms is much more rapid in argon than in the crystal; or 3) the difference in zero-point energies of the two forms is less than in the crystal. In view of the changes in vibrational frequencies upon going to argon, and the increased linewidths of $\text{C}_6\text{H}_5\text{D}$ and 1,4- $\text{C}_6\text{H}_4\text{D}_2$, this last explanation seems most reasonable.

In addition to the deuterated benzenes mentioned above there is some evidence of splitting in the phosphorescence spectrum of 1,3- $\text{C}_6\text{H}_4\text{D}_2$. This species occurs as an isotopic impurity in 1,3,5- $\text{C}_6\text{H}_3\text{D}_3$, and lying at lower energy, it appears in the phosphorescence of 1,3,5- $\text{C}_6\text{H}_3\text{D}_3$ in C_6D_6 . While the assignment of lines to this impurity is somewhat difficult, the $1583+n\cdot 970 \text{ cm}^{-1}$ progression can be tentatively assigned. The splitting appears to be about 8 cm^{-1} . It is hoped that we can test this assignment by using a solution of "pure" 1,3- $\text{C}_6\text{H}_4\text{D}_2$ in C_6D_6 . This compound is of interest since it should show a reversal of the previous statistical probabilities, i.e., the low energy form should be twice as probable as the high energy form (Fig. VII-2).

Another test of the proposed nonhexagonal benzene triplet involves the phosphorescence spectrum of 1,2,4- $\text{C}_6\text{H}_3\text{D}_3$

in C_6D_6 . This is the only isotopic species which exists in more than two forms. In this case there are three nonequivalent configurations of the deuterium atoms, all of equivalent statistical weights as shown in Fig. VII-2. Therefore, there should be a splitting of the phosphorescence lines into three components instead of two. Since the magnitude of the splitting appears to be a linear function of the number of deuterium atoms along the dotted axis, it seems reasonable that the lines of these triplets should be roughly equally spaced with an approximately 14 cm^{-1} over-all splitting.

In conclusion, it would seem that these phosphorescence measurements confirm that benzene in its lowest triplet state is nonhexagonal and that it most likely has D_{2h} symmetry.

APPENDIX

This appendix includes the analyses of the phosphorescence spectra of C_6H_6 and various deuterated benzenes. The spectra were all taken in C_6D_6 mixed crystals at 4.2° K. The line positions can be measured to ± 0.2 cm^{-1} for the strong lines and to ± 1.0 cm^{-1} for the very faintest lines. Because of errors in the location of the (0,0) transition the frequencies listed may have somewhat larger errors.

The frequencies listed in the assignments are the gas phase values given by Whiffen (134). These values in turn are mostly from the work of Ingold, et al. (135). See also Mair and Hornig (136). The frequencies in the solid are generally $1-5$ cm^{-1} less than those in the gas phase.

Only lines of rather definite assignment are listed. For the case of C_6H_6 over 200 phosphorescence lines have been measured. Most of those not listed appear to involve lattice modes. The spectra of the deuterated benzenes become almost a continuum of lines as one goes away from the (0,0) transition and no attempt has been made to assign these weak lines.

(134) D. H. Whiffen, Phil. Trans. Roy. Soc. (London), A248, 131 (1955).

(135) See the long series of papers by C. K. Ingold, et al., J. Chem. Soc. (London), 1936, 912-1210; J. Chem. Soc. (London), 1946, 222-333; and J. Chem. Soc. (London), 1948, 406-517.

(136) R. D. Mair and D. F. Hornig, J. Chem. Phys., 17, 1236 (1949).

A. Phosphorescence Spectrum of C_6H_6 in C_6D_6 .

$$(0,0)=29\ 657.1\ \text{cm}^{-1}$$

Frequency (0,0)- (cm^{-1})	Rel. Int.	Assignment (0,0)- (cm^{-1})	Symmetry
0.0	vvw	0	a_{1g}
606.2	vw	606	e_{2g}
703.7	w	703	b_{2g}
816.6	vvw	2.405	$e_{2g}(2 \cdot e_{2u})$
989.8	w	992	a_{1g}
1004.1	m	985	b_{2g}
1173.2	s	1178	e_{2g}
1243.8	vvw	1178+70	
1386.3	vvw		
1482.6	vvw	1480?	e_{1u}
1573.0	vw		
1583.5	vs	1595	e_{2g}
1601.6	s	606+992	e_{2g}
1653.6	m	1595+70	
1693.4	m	703+992	b_{2g}
1811.1	vw	3.606	e_{2g}
1859.2	vvw		
1979.1	w	2.992	a_{1g}
1993.4	m	985+992	b_{2g}
2163.3	s	1178+992	e_{2g}

Phosphorescence Spectrum of C_6H_6 in C_6D_6

Continued.

Frequency	Int.	Assignment	Symmetry
2234.0	w	1178+992+70	
2386.0	vw		
2464.6	vw	1480+992?	e_{1u}
2567.0	vvs	1595+992	e_{2g}
2581.7	vw		
2586.4	vw		
2593.5	s	606+2·992	e_{2g}
2637.4	m	1595+992+70	
2681.3	w	703+2·992	b_{2g}
2802.5	vw	1178+1595	a_{1g}, e_{2g}
2853.0	vw		
2859.3	vw	3·992	a_{1g}
2981.1	m	985+2·992	b_{2g}
3051.7	vw	3047	e_{2g}
3151.4	s	1178+2·992	e_{2g}
3222.7	vw	1178+2·992+70	
3356.5	w	1595+1178+606	e_{2g}
3376.5	vw	1178+2·606+992	e_{2g}
3433.9	vw		
3454.9	vw	1480+2·992?	e_{1u}
3550.4	s	1595+2·992	e_{2g}
3568.8	w		

Phosphorescence Spectrum of C_6H_6 in C_6D_6

Continued.

Frequency	Int.	Assignment	Symmetry
3583.2	m	606+3.992	e_{2g}
3621.5	w	1595+2.992+70	
3653.3	vw	703+3.992	b_{2g}
3759.0	w	606+2.1595	e_{2g}
3924.6	m	1595+2.1178	e_{2g}
3967.7	w	985+3.992	b_{2g}
4137.7	m	1178+3.992	e_{2g}
4162.3	vw	985+2.1595?	
4231.0	vvw	1178+3062	e_{2g}
4328.7	s	1178+2.1595	e_{2g}
4349.5	m	1178+1595+606+992	e_{2g}
4512.4	vw		
4533.1	s	1595+3.992	e_{2g}
4552.6	vw		
4570.5	m	606+4.992	e_{2g}
4627.8	vw	703+4.992	b_{2g}
4642.1	w	1595+3062	e_{2g}
4732.6	m	2.1595+606+992	e_{2g}
4757.5	m	3.1595	e_{2g}
4907.6	m	1595+2.1178+992	e_{2g}
4952.3	vvw	985+4.992	b_{2g}
5124.0	w	1178+4.992	e_{2g}

Phosphorescence Spectrum of C_6H_6 in C_6D_6

Continued.

Frequency	Int.	Assignment	Symmetry
5304.5	s	1178+2·1595+992	e_{2g}
5333.7	m	1178+1595+606+2·992	e_{2g}
5513.6	m	1595+4·992	e_{2g}
5555.7	vw	606+5·992	e_{2g}
5610.5	vw		
5625.1	w	1595+3062+992	e_{2g}
5706.7	w	2·1595+606+992	e_{2g}
5736.3	m	3·1595+992	e_{2g}
5766.5	vvw		
5888.7	vw	1595+2·1178+2·992	e_{2g}
6282.1	w	1178+2·1595+2·992	e_{2g}
6317.5	vw	1178+1595+606+3·992	e_{2g}
6714.5	vw	3·1595+2·992	e_{2g}
6750.4	vvw		
6875.2	vvw	1595+2·1178+3·992	e_{2g}
7065.8	vvw		
7258.4	vvw	1178+2·1595+3·992	e_{2g}

Lines involving X+1595 and X+606+992 are in Fermi resonance. The concentration of C_6H_6 is 1%. The totally symmetric (a_{1g}) frequency is 992 cm^{-1} and 70 cm^{-1} is a lattice mode.

B. Phosphorescence Spectrum of C_6H_5D in C_6D_6 .
 $(0,0)=29\ 692.9\ cm^{-1}$

Frequency ($0,0$)- (cm^{-1})	Rel. Int.	Assignment ($0,0$)- (cm^{-1})	Symmetry
0.0	vw	0	a_1
7.9	vvw	" +7.9	
602.2	vw	602	a_1, b_1
607.1	vvw	" +4.9	
704.1	vw	698	b_2
710.8	vvw	" +6.7	
792.6	vvw	779+7	b_2
857.9	vw	857	b_1
865.7	vvw	" +7.8	
937.8	vvw	922?	b_2
944.4	vvw	" +6.6	
980.6	vw	980	a_1
986.7	vvw	" +6.1	
998.0	w	995	b_2
1005.7	vw	" +7.7	
1077.5	vw	1075	b_1
1085.6	vvw	" +8.1	
1157.4	m	1158	b_1
1163.8	vw	" +6.4	

Phosphorescence Spectrum of C_6H_5D in C_6D_6

Continued.

Frequency	Int.	Assignment	Symmetry
1171.7	s	1175	a_1
1179.2	s	" +7.5	
1193.8	vw	2·602?	
1246.1	vw	1175+70	
1299.0	vw	1292?	b_1
1306.0	vw	" +7.0	
1320.8	vw	1320?	b_1
1326.6	vw	" +5.8	
1368.5	vw	308+980+7	b_2
1392.8	vw	405+980+7	a_2
1449.5	w	1449	b_1
1456.3	vw	" +6.8	
1495.1	vw	1479+7	a_1
1556.9	w		
1577.1	vvs	1574	b_1
1583.7	vs	" +6.6	
1593.5	vvs	1591	a_1
1600.0	vs	" +6.5	
1646.7	w	1574+70	
1661.8	w	1591+70	
1683.9	vw	698+980	b_2
1689.7	vw	" +5.8	

Phosphorescence Spectrum of C_6H_5D in C_6D_6

Continued.

Frequency	Int.	Assignment	Symmetry
1780.8	vw		
1787.2	vw	" +6.4	
1836.7	vw	857+980	b_1
1844.7	vw	" +8.0	
1916.6	vw	922+980?	b_2
1923.5	vw	" +6.9	
1958.5	vw	2·980	a_1
1965.3	vw	" +6.8	
1977.0	w	995+980	b_2
1984.5	vw	" +7.5	
2056.4	w	1075+980	b_1
2064.5	vw	" +8.1	
2136.3	s	1158+980	b_1
2143.6	m	" +7.3	
2151.5	vs	1175+980	a_1
2159.1	s	" +7.6	
2173.8	vw	2·602+980?	
2181.7	vw	" +7.9	
2220.4	vw	1175+980+70	
2276.0	vw	1292+980?	
2283.2	vw	" +7.2	

Phosphorescence Spectrum of C_6H_5D in C_6D_6

Continued.

Frequency	Int.	Assignment	Symmetry
2300.7	VW	1320+980?	b_1
2306.1	VVW	" +5.4	
2350.0	VVW	308+2·980+7?	b_2
2426.5	VW	1449+980	b_1
2433.9	VVW	" +7.4	
2520.3	VVW		
2527.6	VW	" +7.3	
2551.8	VVS	1574+980	b_1
2558.8	VS	" +7.0	
2573.4	VVS	1591+980	a_1
2580.7	VS	" +7.3	
2817.3	VW	857+2·980	b_1
2894.1	VW	922+2·980?	b_2
2900.6	VVW	" +6.5	
2954.6	W	995+2·980	b_2
2961.7	VW	" +7.1	
2978.9	VVW		
2986.0	VVW	" +7.1	
3033.4	VW	1075+2·980	b_1
3042.5	VVW	" +9.1	
3114.6	VW	1158+2·980	b_1
3122.0	VVW	" +7.4	

167.

Phosphorescence Spectrum of C_6H_5D in C_6D_6

Continued.

Frequency	Int.	Assignment	Symmetry
3129.2	w	1175+2·980	a_1
3136.4	vw	" +7.2	
3140.2	vw		
3525.0	s	1574+2·980	b_1
3513.7	s	" +6.7	
3551.4	s	1591+2·980	a_1
3558.2	s	" +6.8	
4074.9	w	1158+3·980	b_1
4114.2	w	1175+3·980	a_1
4196.8	w		
4215.1	w		
4340.8	w	1175+2·1591	a_1
4416.8	m		
4495.9	m	1574+3·980	b_1
4502.9	w	" +7.0	
4528.1	w	1591+3·980+7	a_1
4628.0	w		
4628.8	m		
4692.8	w	2·1591+1574	
4730.3	m	3·1591	
5087.2	m		
5112.1	m		

Phosphorescence Spectrum of C_6H_5D in C_6D_6

Continued.

Frequency	Int.	Assignment	Symmetry
5697.0	w	2·1591+1574+980	
5724.3	w	3·1591+980	

The concentration of C_6H_5D is 0.6%. The totally symmetric (a_1) frequency is 5980 cm^{-1} and 70 cm^{-1} is a lattice mode. The (0,0) assignment is for the high energy form. Lines assigned " $+7\text{ cm}^{-1}$ " are the low energy form equivalent of the previous line. The lines assigned as 1574 and 1591 cm^{-1} are actually Fermi resonance component of 1574 , 1591 , $602+980$, and $602+980$ (a_1 and b_1 symmetries).

C. Phosphorescence Spectrum of 1,4-C₆H₄D₂ in C₆D₆.

$$(0,0)=29\,719.8\text{ cm}^{-1}$$

Frequency (0,0)- (cm ⁻¹)	Rel. Int.	Assignment (0,0)- (cm ⁻¹)	Symmetry
0.0	w	0	a _g
12.4	vw	" +12.4	
592.0	vvw	597	b _{1g}
598.4	vvw	601	a _g
606.4	vvw	597+14.4	b _{1g}
613.6	vvw	601+15.2	a _g
641.8	w	634	b _{3g}
655.6	vw	" +13.8	
742.4	vvw	736	b _{3g}
755.3	vvw	" +12.9	
780.6	vvw	367+405?	b _{1g}
793.1	vvw	" +12.5	
807.9	vvw	2·405	a _g
821.3	vvw	" +13.4	
906.9	s	909	b _{1g}
921.4	m	" +14.5	
971.1	m	967	b _{3g}
981.7	w	" +10.6	
1171.8	vs	1173	a _g
1184.4	s	" +12.6	

170.

Phosphorescence Spectrum of 1,4-C₆H₄D₂ in C₆D₆

Continued.

Frequency	Int.	Assignment	Symmetry
1227.8	vw	814+405	b _{3g}
1241.6	vw	" +13.8	
1298.6	vw	1309?	b _{1g}
1312.1	vw	" +13.5	
1321.0	vw		
1431.3	vw		
1491.2	vw		
1516.5	vw		
1547.8	vw		
1566.3	vvs	1569	a _g
1578.6	vvs	" +12.3	
1585.0	vvs	1587	b _{1g}
1595.9	vvs	" +10.9	
1712.8	vw	736+978	b _{3g}
1723.5	vw	" +10.7	
1768.8	vw		
1880.2	w	909+978	b _{1g}
1896.7	w	" +16.5	
1941.6	vw	2·978	a _g
1955.8	vw	" +14.2	
2111.6	w		
2127.2	vw	" +15.6	

171.

Phosphorescence Spectrum of 1,4-C₆H₄D₂ in C₆D₆

Continued.

Frequency	Int.	Assignment	Symmetry
2145.3	s	1173+978	a _g
2158.9	m	" +13.6	
2225.9	vw	1173+978+70?	
2273.4	vw	1309+978	b _{1g}
2286.8	vw	" +13.4	
2294.8	vw		
2446.9	vw		
2470.1	vw		
2475.8	vw		
2508.8	vw		
2520.2	vw	" +11.4	
2533.0	vvs	1569+978	a _g
2546.6	vvs	" +13.6	
2557.3	vvs	1587+978	b _{1g}
2571.6	vvs	" +14.3	
2871.1	w	909+2·978	b _{1g}
2918.3	vw	3·978	a _g
3131.2	w	1173+2·978	a _g
3500.2	s	1569+2·978	a _g
3513.4	m	" + 13.2	
3533.9	s	1587+2·978	b _{1g}
3545.3	m	" + 11.4	

Phosphorescence Spectrum of 1,4-C₆H₄D₂ in C₆D₆

Continued.

Frequency	Int.	Assignment	Symmetry
4042.0	w		
4094.9	w	1173+3·978	a _g
4328.1	w	2·1587+1173	a _g
4481.6	w	1569+3·978+13	a _g
4500.5	w	1587+3·978	b _{1g}
4516.0	w	" +15.5	
4629.5	w		
4685.0	w	2·1569+1587	
4713.4	w	3·1569	
4755.8	w		

The concentration of 1,4-C₆H₄D₂ is 0.05%. The totally symmetric (a_g) frequency is 978 cm⁻¹. The (0,0) assignment is for the high energy form. Lines assigned " +13 cm⁻¹ are the low energy form equivalent of the previous line. The lines assigned as 1569 and 1587 cm⁻¹ are actually Fermi resonance components of 1569, 1587, 601+978, and 596+978 (a_g and b_{1g} symmetries).

D. Phosphorescence Spectrum of 1,3,5-C₆H₃D₃ in C₆D₆.

$$(0,0)=29\,754.4\text{ cm}^{-1}$$

Frequency (0,0)- (cm ⁻¹)	Rel. Int.	Assignment (0,0)- (cm ⁻¹)	Symmetry
595.0	vw	593	e'
833.6	vw	834	e'
929.6	vw	915	a ₂ ''
956.9	vw	956	a ₁ '
1101.8	w	1102	e'
1317.8	vw	373+956?	e''
1412.6	vw	1408	e'
1430.0	vw	595+834	e', a ₁ '
1546.4	w	593+956	e'
1571.9	vs	1573	e'
1789.2	vw	834+956	e'
1837.7	vw		
1883.2	vw	915+956	a ₂ ''
1908.1	vw	2·956	a ₁ '
1932.0	vw		
2032.3	vw		
2038.5	vw	1102+915?	e''
2058.8	w	1102+956	e'
2106.3	vw		
2244.5	vw		

Phosphorescence Spectrum of 1,3,5-C₆H₃D₃ in C₆D₆

Continued.

Frequency	Int.	Assignment	Symmetry
2365.5	vw	1408+956	e'
2383.5	vw		
2414.2	vvw		
2498.2	s	593+2·956	e'
2526.0	vvs	1573+956	e'
2977.7	vw	1573+1408?	e', a ₁ '
3007.2	vw	1102+2·956	e'
3447.5	m	593+3·956	e'
3477.6	vs	1573+2·956	e'
3974.4	vw	1102+3·956?	e'
4220.3	vw		
4396.9	vw	593+4·956	e'
4428.8	m	1573+3·956	e'
4618.9	vw		
4681.3	vw	2·1573+593+956	e'
4686.0	vw		
4708.3	m	3·1573	e'
4927.2	vw	1102+4·956?	e'

The concentration of 1,3,5-C₆H₃D₃ is 1%. The totally symmetric (a₁') frequency is 956 cm⁻¹.

E. Intensity distribution for benzene phosphorescence.

C ₆ H ₆ Line* (0,0)-	Relative Intensity			
	C ₆ H ₆	C ₆ H ₅ D	1,4- C ₆ H ₄ D ₂	1,3,5- C ₆ H ₃ D ₃
1178 cm ⁻¹	0.060	0.028	0.038	0.008
1595	0.240	0.222	0.213	0.386
606+992	0.017	0.160	0.159	0.027
1178+992	0.110	0.038	0.046	0.008
1595+992	0.315	0.248	0.213	0.410
606+2·992	0.050	0.167	0.167	0.049
1178+2·992	0.055	0.020	0.026	0.004
1595+2·992	0.125	0.076	0.082	0.095
606+3·992	0.028	0.058	0.066	0.020

* These nine lines in C₆H₆ and the corresponding lines in the other deuterated benzenes account for at least 80-90% of the total phosphorescence intensity in the mixed crystal. For the cases of C₆H₅D and 1,4-C₆H₄D₂ the sum of the intensities of the split components is tabulated. The deuterated benzenes have somewhat less intensity in these lines than C₆H₆, but this loss of intensity amounts to 10% at most. The figures tabulated are ±10%.

F. Fermi Resonance Splittings
of the $1595+n\cdot 992$ and $606+(n+1)\cdot 992$ Lines.*

n	C_6H_6	C_6H_5D	$1,4-$ $C_6H_4D_2$	$1,3,5-$ $C_6H_3D_3$
Phosphorescence Splittings (cm^{-1})				
0	18.1	16.4	18.7	26.2
		16.3'	17.3'	
1	26.5	21.6	24.3	28.2
		22.6'	25.0'	
2	32.8	26.4		30.1
		26.5'	31.9'	
3	37.4			31.9
		25.2'	34.3'	
4	42.1			
Fluorescence Splittings (cm^{-1})				
0	18.6	16.7	19.7	26.4
1	26.4	23.0	28.0	28.4
2	32.9		30.2	28.9
3	37.4			

* And the corresponding lines in the various deuterated benzenes. The splittings marked (') are for the low energy form. The gas phase values for increasing n are 20, 26, 31, 37, and 39 cm^{-1} .

G. Assignment of the 1004 cm^{-1} Line.

This frequency forms the basis for the fourth strongest progression in the C_6H_6 phosphorescence spectrum, yet its assignment is quite uncertain. It has been tentatively assigned as the 985 cm^{-1} b_{2g} frequency. Mair and Hornig (136) assign a value of 995 cm^{-1} to this vibration, but still the agreement of the frequencies is much worse than for any other line and also this is a C-H mode. The C-C mode of the same symmetry (703 cm^{-1}) is much weaker. This assignment is made on the basis of the required symmetry (137) and by comparison of the various deuterated species. The other two possible assignments are 1010 cm^{-1} (b_{1u}) and 606+405 ($e_{2g} \times e_{2u} = a_{1u}, a_{2u}, e_{2u}$) neither of which seems reasonable. The table below compares the different assignments for the various deuterated benzenes with the observed frequencies.

Compound	Observed Frequency	b_{2g}	b_{1u}	$e_{2g} \times e_{2u} =$
C_6H_6	1004 cm^{-1}	985 cm^{-1} (995)	1010 cm^{-1}	606+405=1011 cm^{-1}
$\text{C}_6\text{H}_5\text{D}$	998	995	1007	602+380= 982
1,4- $\text{C}_6\text{H}_4\text{D}_2$	971	967	992	598+367= 965
1,3,5- $\text{C}_6\text{H}_3\text{D}_3$	930	915	1004	593+373= 966

(137) A. C. Albrecht, J. Chem. Phys., 38, 354 (1963).

H. Frequency Correlations
for the Various Isotopically Substituted Benzenes.

C_6H_6	C_6D_6	1,3,5- $C_6H_3D_3$	1,4- $C_6H_4D_2$	C_6H_5D
a_{1g} 992 cm^{-1} 3062	943 cm^{-1} 2293	a_1 956 cm^{-1} 3053	a_g 978 cm^{-1} 3055	a_1 980 cm^{-1} 3060
a_{2g} 1326	1037	a_2' 1230	b_{1g} 1309	b_1 1292
b_{2g} 705	601	a_2'' 691	b_{3g} 634	b_2 698
985	827	915	967	995
e_{2g} 606	577	e' 593	b_{1g} 597	b_1 602
			a_g 601	a_1 602
1178	867	1102	b_{1g} 909	b_1 1158
			a_g 1173	a_1 1176
1595	1552	1573	b_{1g} 1587	b_1 1574
			a_g 1569	a_1 1591
3047	2265	2292	b_{1g} 3042	b_1 3044
			a_g 2280	a_1 3055
e_{1g} 849	662	e'' 710	b_{2g} 850	a_2 850
			b_{3g} 736	b_2 779
a_{2u} 671	497	a_2'' 533	b_{1u} 597	b_2 608
b_{1u} 1010	963	a_1' 1004	b_{2u} 992	a_1 1007
3062	2290	2282	3040	3066
b_{2u} 1110	825	a_2' 916	b_{3u} 1106	b_1 1075
1648	1571	1600	1613	1620
e_{2u} 405	352	e'' 373	a_u 405	a_2 405
			b_{1u} 367	b_2 380
970	793	947	a_u 970	a_2 970
			b_{1u} 876	b_2 922
e_{1u} 1033	811	e' 834	b_{2u} 1033	a_1 1031
			b_{3u} 814	b_1 857
1480	1332	1408	b_{2u} 1469	a_1 1479
			b_{3u} 1413	b_1 1449
3080	2283	3082	b_{2u} 2275	a_1 2269
			b_{3u} 3079	b_1 3077

179.

PROPOSITIONS

PROPOSITION I

By comparing the (0,0) band of the experimental $C_6H_6-C_6H_5D$ absorption spectrum with the computer calculated spectrum one can determine the true nature of the factor group splitting of the first singlet-singlet transition in crystalline benzene and also the true symmetry assignment of the first excited singlet state of the benzene molecule.

In Sect. VI of this thesis a new interpretation of the singlet absorption spectrum of crystalline benzene is presented. The purpose of this proposition is to present an experimental means of verifying this interpretation.

The absorption spectrum of the first excited singlet state of crystalline benzene shows the features of a forbidden electronic transition made allowed by mixing with allowed transitions through nontotally symmetric vibrations and through crystal perturbations. At $4.2^\circ K$ the (0,0) transition, which is made allowed through crystal field mixing, consists of a band approximately 140 cm^{-1} wide (1). For

-
- (1) Several studies (2, 3, 4) of this transition have been made since A. Kronenberger, Z. Physik, 63, 497 (1930).
 - (2) D. Fox and O. Schnepp, J. Chem. Phys., 23, 767 (1955).
 - (3) A. Zmerli, J. Chim. Phys., 56, 387 (1959).
 - (4) V. L. Broude, Usp. Fiz. Nauk, 74, 577 (1961) [English Transl. Soviet Phys.--Usp., 4, 584 (1962)].

C_6H_6 , starting at the lowest frequency, there is a line at $37\ 803.2\ cm^{-1}$ followed by two closely spaced lines at $37\ 841.8\ cm^{-1}$ and $37\ 847.1\ cm^{-1}$ ($\pm 0.5\ cm^{-1}$). These are commonly believed to be the factor group components and have been given the polarizations a, c, and b, respectively, by Broude (4, 5). At higher energies lies a diffuse band approximately $75\ cm^{-1}$ wide which contains several embedded lines. This structure is commonly believed to be due solely to lattice vibrational modes. The embedded lines seem to lie $\sim 70\ cm^{-1}$ above each of the factor group components and $70\ cm^{-1}$ is known to be a prominent lattice frequency of crystalline benzene (6).

This interpretation of the (0,0) band in terms of Frenkel exciton levels and lattice vibrations has recently been questioned by P. Pesteil (7) and others of the French workers. Pesteil believes that the entire band structure is due to a Wannier type exciton, i.e., a quasihydrogenic exciton, but this view does not seem to me to be supported by the available experimental evidence. First, the agreement between the positions of his calculated lines and the true

(5) Note that this assignment is different from that of V. L. Broude, V. S. Medvedev, and A. F. Prikhot'ko, Opt. i Spektroskopiya, 2, 317 (1957); Chem. Abstr., 51, 11065d (1957). See also the end of Sect. VI of the thesis.

(6) A. Fröhling, J. Chem. Phys., 18, 1119 (1950); Ann. Phys. Paris, 6, 401 (1951).

(7) P. Pesteil, J. Chim. Phys., 58, 661 (1961).

lines is very poor and many lines are missing. Second, the exciton interactions in aromatic crystals (8) are not nearly large enough to bring about the Wannier exciton limit. Third, if the Wannier exciton limit were applicable, the rate of excitation migration in such crystals would be very much larger than that which is observed. Fourth, aromatic crystals in this case would be very much better photoconductors than they are since the high energy limit of the Wannier exciton band is the ionization potential. Finally, contrary to the statement of Benarroche (9), the fluorescence (and phosphorescence) spectra of pure C_6H_6 and of isotopic mixed crystals show no structure to higher energies than the main components of each vibrational progression. However, to lower energies in each band lattice vibrational structure, similar to that observed in absorption, appears in the fluorescence and phosphorescence spectra, i.e., the "mirror image" relationship of absorption and emission holds.

The earlier calculation of the factor group splitting for benzene by Fox and Schnepf (2) was performed in order to test the symmetry assignment of the lowest excited singlet state of benzene, i.e., is it a $^1B_{1u}$ or a $^1B_{2u}$ state? Their calculation is incomplete in several respects: 1) they consider only octopole-octopole interactions; 2) they neglect

(8) See the main body of the thesis.

(9) M. M. Benarroche, Compt. Rend., 257, 1249 (1963).

exchange interactions; 3) they assume that the observed difference in line positions ($\sim 40 \text{ cm}^{-1}$) is the total splitting; and 4) they do not take into account the fact that the observed splitting in the (0,0) transition is only about one-fourth (10) the total electronic interaction which they calculate. Contrary to the conclusion of Fox and Schnepf, it would seem that their calculations more nearly support the thesis that the symmetry of the lowest excited singlet state of benzene is ${}^1B_{1u}$ rather than the usually accepted ${}^1B_{2u}$. Thus their calculated values are too large by a factor of four and the experimental splitting with which they compare their results is small by a factor of about three due to a lack of knowledge concerning the energy zero (11).

The first experiment which needs to be performed is a check on the polarization assignments of the (three) factor group components in solid C_6H_6 . The experiment which I should like to propose as a test of the interpretation presented in the thesis is outlined below. This experiment would also provide a test of the symmetry assignment of the lowest excited singlet state of benzene.

It has been noted in our work that the absorption

(10) This is due to Franck-Condon vibrational factors. See D. S. McClure, Solid State Physics (Academic Press Inc., New York, 1959), Vol. 8, pp. 21, 27-30.

(11) For the ${}^1B_{1u}$ electronic molecular state the calculated (2) splittings are about 15 times those for the ${}^1B_{2u}$ state.

5.

spectra of various deuterated benzenes show a fourth component in the factor group splitting. This extra component lies between the two widely separated components. This extra line appears to arise from the absorption due to the 1-2% isotopic impurity containing one less deuterium than the solvent.

The simplest case involves the C_6H_6 impurity in C_6H_5D . Because of the small energy denominator ($\sim 33 \text{ cm}^{-1}$) the C_6H_6 states are mixed with those of C_6H_5D and the observed line positions in the factor group structure should be highly dependent upon the concentration of isotopic impurity in a predictable manner. For each of the various models this behavior could be predicted by the use of a slightly modified version of the computer program which was outlined in Sect. VI of the thesis.

For the pure crystal the diagonal elements of the matrix representing the crystal can be assumed to be zero, this being the energy zero to which everything is referred. For the isotopic mixed crystal diagonal elements ($\Delta E = -33 \text{ cm}^{-1}$) need to be introduced in proportion to the concentration of isotopic impurity. Since for any model all of the matrix elements are known experimentally from the factor group splitting in pure C_6H_6 , and the assumed symmetry of the first singlet state of benzene, the spectrum can be calculated for the C_6H_6 in C_6H_5D mixed crystal as a function of C_6H_6 concentration. The optically allowed levels near $\vec{k}=\vec{0}$ can be found

from the computer calculations by looking for the symmetric eigenfunctions to which they correspond. It is also possible to solve exactly for these optical levels in the pure crystal as in Sect. VI and simply to follow them as one increases the impurity concentration.

Comparison of the calculated and observed absorption spectra as a function of C_6H_6 concentration provides not only a check on the postulated energy zero from which the factor group splitting is calculated and the model for the calculation, but also a check on the symmetry assignment of the lowest excited singlet state of benzene. A preliminary experiment of this kind has been performed using 5% C_6H_6 in C_6H_5D at $4.2^\circ K$. Here it was noted that the line positions of the two longest wavelength components changed by several cm^{-1} from their positions in a crystal containing 1% C_6H_6 in C_6H_5D , which is an easily measurable change for these sharp lines.

PROPOSITION II

The temperature dependence of anthracene fluorescence excited by red light is explained in terms of different concentrations of different impurities.

This proposition suggests an explanation for some unusual results obtained by Lipsett (1). Recently much interest has been stirred by the observation of red-light-excited blue fluorescence of anthracene crystals. Both triplet-triplet annihilation (2) and two quantum absorption (3) have been proposed to explain the production of excited singlet states. Lipsett has measured the temperature dependence of this anthracene fluorescence excited by red light from a xenon lamp and a monochromator. Fig. 1 taken from Lipsett's work, shows the temperature dependence of the total fluorescence, no time differentiation being made. The normal UV-excited fluorescence shows a monotonic increase as one lowers the temperature.

I believe that Lipsett's results can be explained on the basis of the presence of three different impurities having different concentrations. It is very reasonable to

-
- (1) S. Singh and F. R. Lipsett, to be published.
 - (2) R. G. Kepler, J. C. Caris, P. Avakian, and E. Abramson, Phys. Rev. Letters, 10, 400 (1963).
 - (3) W. L. Peticolas, J. P. Goldsborough, and K. E. Rieckhoff, Phys. Rev. Letters, 10, 43 (1963).

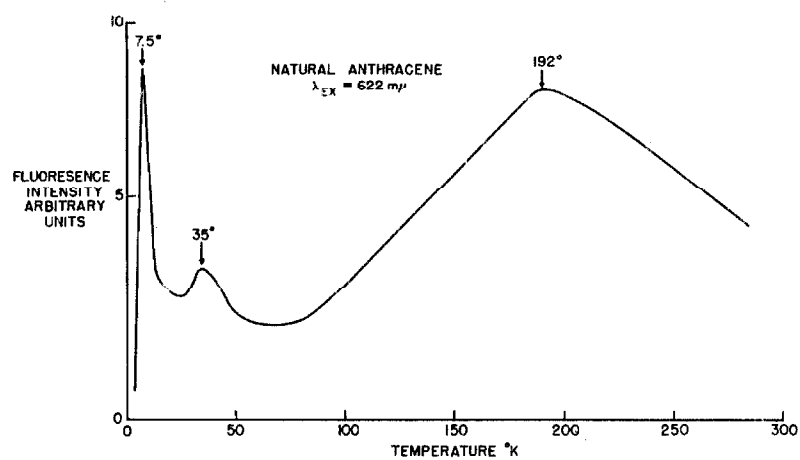


Fig. 1 Effect of temperature on the fluorescence of anthracene excited by red light from a xenon lamp and monochromater.

From the work of S. Singh and F. R. Lipsett,
to be published.

assume that the shallowest impurity traps are present in the highest concentration since such molecules should most closely resemble the host and thus be the most difficult to remove during purification. It is also assumed, at least at low temperatures, that the rate of impurity trapping is greater than the rate of triplet-triplet annihilation.

For simplicity let us consider the case of two impurity species A and B having trap depths 100 and 1000 cm^{-1} , respectively, and concentrations 10^{-4} and 10^{-5} molar, respectively. Now, what happens as one lowers the temperature during a red-light-excited fluorescence experiment? The quantum efficiency of fluorescence from the excited singlet state increases. Also, but at a lower rate, the rate of triplet-triplet annihilation decreases because of the decreased rate of triplet excitation migration. This accounts for the negative slope of the high temperature portion of the curve shown in Fig. 1.

In our impure crystal, after a certain temperature ($\sim 200^\circ\text{K}$) has been reached, the deep trap B begins to trap triplet excitations. This trapping soon greatly decreases the rate of triplet-triplet annihilation so that a positive slope results in Fig. 1. This first change in slope is also predicted if one has two rather different temperature dependencies for the rates of triplet-triplet annihilation and of fluorescence from excited singlet states.

The real problem comes when one tries to explain the

second change in slope, this time from positive to negative. As one lowers the temperature still further the rate of excitation migration drops and soon ($\sim 50^{\circ}\text{K}$) the excitations are being trapped by the shallow traps A and never reach the rather few deep traps B. Since the concentration of A is much greater than that of B, long-range, trap-to-trap triplet-triplet annihilation (4) can once more increase the rate of production of excited singlet states. Thus, since the excitations are now closer together, the trapping by the more prevalent, shallower traps may increase the chances of triplet-triplet annihilation compared to the case when the trapping is by very far apart and very deep traps.

If this explanation is correct the temperature dependence of the fluorescent lifetime should show some of the same anomalies as Fig. 1.

(4) H. Sternlicht, G. C. Nieman, and G. W. Robinson, J. Chem. Phys., 38, 1326 (1963).

PROPOSITION III

It is proposed to search for the second triplet state of benzene by means of the phosphorescence action spectrum of isotopic mixed crystals.

There is much theoretical interest in the location of the second triplet state of benzene (1, 2). This state is particularly important since its true location will provide a test of the semiempirical theories (3) which predict the location of triplet states by using singlet state wavefunctions and integrals. If found, it will also provide the basis for a semiempirical Pariser-Parr calculation based upon true triplet state wavefunctions and integrals.

Most of the theoretical calculations locate the second triplet state of benzene below the first excited singlet state, and thus it should be optically observable. However, because of the low oscillator strength of this singlet-triplet transition, it has not yet been detected. Optimum conditions for the observation of this state involve low temperatures (liquid helium), long path lengths, and extremely pure crystals. Some studies by Mrs. Coyne (4) were plagued

(1) D. R. Kearns, J. Chem. Phys., 36, 1608 (1962).

(2) J. R. Platt, J. Mol. Spectry., 2, 288 (1962).

(3) See H. E. Simmons, J. Chem. Phys., 40, 3554 (1964).

(4) L. Coyne, unpublished results. The impurity was phenol.

by the presence of minute amounts of impurities which completely masked any possible second triplet absorption. In using absorption techniques one is troubled also by the problem of trying to detect a small difference (the amount of light absorbed) in two large quantities (the incident and transmitted light intensities).

These problems can be circumvented if one uses an action spectrum technique, i.e., if one looks at an effect resulting from the excitation of a few states instead of directly at their excitation. Such a technique has been used by Avakian *et al.* (5) to record the first triplet absorption spectrum of anthracene. In this case the observed effect was the delayed fluorescence produced by triplet-triplet annihilation. The experiment involved scanning the absorption region with a monochromator and a xenon lamp while monitoring the fluorescence region with a photomultiplier.

Delayed fluorescence could also be used in the case of benzene, but the quantum yield for its production is quite low and one has much greater light filtering problems. It is proposed here that the phosphorescence from the first triplet state be used as an internal monitor on the second triplet state absorption. To eliminate phosphorescence quenching, it would be necessary to use a mixed crystal such

(5) P. Avakian, E. Abramson, R. G. Kepler, and J. C. Caris, J. Chem. Phys., 39, 1127 (1963).

as 1% C_6H_6 in C_6D_6 . In this case the C_6D_6 absorption would be monitored by observing the phosphorescence of C_6H_6 , any triplet excitation in this host being quickly transferred to the C_6H_6 traps.

By using this approach one not only eliminates having to make direct absorption measurements, but also greatly reduces the impurity problem. Thus, by carefully looking at only the very sharp C_6H_6 phosphorescence, one would not see any emission resulting from impurity absorption. The probability of excitation transfer from the singlet state of an impurity to the triplet state of C_6H_6 is very small and, because of the high energy of the first triplet state of benzene, most every likely impurities' triplet state would lie at lower energies. Also much thinner crystals (a few mm) could be used.

This same technique might also be applied to the problem of observing the first triplet absorption, and its exciton splitting, in benzene crystals.

PROPOSITION IV

As a means of studying the Raman spectra of gases, and as a means of extending the frequency range of gas lasers, it is proposed that molecular gases be added to the ordinary gas laser.

One of the disadvantages of lasers for optical studies is their limited frequency range. This can be extended somewhat by the stimulated Raman effect (1) in which a liquid, such as benzene, is placed within the resonant cavity of a ruby laser. The laser is also a convenient source for Raman studies because it is an intense source of monochromatic light.

It is proposed that these two experiments be combined in a gas laser. Thus one could add a gas whose Raman spectrum was desired to the rare gas (He, Ne, A) used in the laser. In this way the intensity of the Raman lines could be increased because they themselves might begin to show laser amplification. This would also provide additional frequencies of coherent light for other studies.

Because the population inversion of a cw gas laser is created by a gas discharge, there is a high probability of

(1) E. Gisela, R. W. Hellwarth, F. J. McClung, S. E. Schwarz, D. Weiner, and E. J. Woodbury, Phys. Rev. Letters, 9, 455 (1962).

dissociation of the added gas (2). Thus it would be best to pulse the gas laser, i.e., not operate it continuously.

- (2) C. K. N. Patel, R. A. McFarlane, and W. L. Faust, Phys. Rev., 133, A1244 (1964).

PROPOSITION V

It is proposed to study the polarized red light induced photocurrents in anthracene as a means of identifying charge carrier trapping sites. It is also proposed to study the photoconductivity of mixed aromatic crystals as a means of clarifying the mechanism of charge carrier generation.

Much research today, especially in industrial research laboratories, is concerned with the phenomenon of photoconductivity in organic crystals, such as anthracene. While much work is being done on this problem it is still little understood. Much of what is observed seems to be extrinsic, arising from effects due to the surface, impurities, and the electrodes (1).

Recent experiments by Schneider (2) have shown that ruby laser light can induce photocurrents in crystalline anthracene. While the direct generation of charge carriers is possible since the first excited singlet state is populated by such light (3), these results are best explained in terms

-
- (1) S. Z. Weisz, R. C. Jarnagin, M. Silver, M. Simhony, and J. Balberg, J. Chem. Phys., 40, 3365 (1964).
 - (2) K. Hasegawa and W. G. Schneider, J. Chem. Phys., 40, 2533 (1964).
 - (3) R. G. Kepler, J. C. Caris, P. Avakian, and E. Abramson, Phys. Rev. Letters, 10, 400 (1963).

of the detrapping of trapped charge carriers. The nature of the trapping centers is unclear, but Schneider believes them to be chemical impurities.

Silver, et al. (1) have also studied charge carrier trapping in anthracene and conclude that there are two basic charge carrier trapping mechanisms, one short-lived ($\sim 10^2$ μ -sec.) and one long-lived ($\sim 10^4$ μ sec.). Silver believes this trapping to be due to physical defects primarily.

By using polarized laser light one might hope to be able to differentiate between defect and impurity trapping. If one makes the reasonable assumptions that the detrapping is due to direct trap absorption, and that chemical impurities lie in substitutional sites, there should be a dependence of the detrapping upon the polarization of the incident light for the case of impurity trapping. Lattice defects, however, should occur randomly and detrapping from such traps should be unaffected by the polarization of the light.

One of the most basic unsolved problems relating to photoconductivity in molecular crystals concerns the mechanism of photoproduction of charge carriers in the bulk of the crystal. One proposed scheme involves exciton-exciton interactions for the photoproduction of carriers in the bulk (4).

(4) S. Choi and S. A. Rice, J. Chem. Phys., 38, 366 (1963); M. Silver, D. Olness, M. Swicord, and R. C. Jarnagin, Phys. Rev. Letters, 10, 12 (1963); and R. G. Kepler and R. E. Merrifield, J. Chem. Phys., 40, 1173 (1964).

In this connection there is a rather hot debate as to the relative roles of the singlet and the triplet states (5).

I should like to propose an experiment to shed some additional light on this last question. From my investigations of isotopic mixed crystals of benzene it was noted that the singlet state was essentially nonmigrating, while because of its long lifetime, the triplet state could easily migrate from trap to trap. Thus it would seem reasonable that the effects due to singlet excitons and those due to triplet excitons could be separated by studying the intrinsic photoconductivity of mixed crystals. It would be necessary to use rather shallow traps (say $\sim 200 \text{ cm}^{-1}$) in a rather high concentration (say 10%) so that the charge carriers would not be trapped to any large extent. Isotopic mixed crystals would be especially useful since the isotopic traps might be less efficient charge carrier traps.

In such experiments singlet excitons should be slowed to such an extent that they decay radiatively before they can interact to produce charge carriers, while the triplet excitons because of their long radiative lifetimes would be present in a large enough concentration to interact. The degree of trapping of charge carriers might be indicated by studying the time decay of the photocurrent. These experi-

(5) M. Kleinerman and S. P. McGlynn, J. Chem. Phys., 37, 1369 (1962); B. Rosenberg, J. Chem. Phys., 37, 1371 (1962); and D. Kearns, J. Chem. Phys., 39, 2697 (1963).

ments would best be done at low temperatures to accentuate the exciton trapping. This might make the experiments especially difficult because of the small photocurrents produced in the bulk.

A sharp drop in the photocurrent of the mixed crystal compared to that of the pure crystal would indicate a possible role is played by the singlet exciton. A small drop (say an order of magnitude) would indicate a possible role is played by the triplet exciton. In interpreting the effects observed in these experiments using various concentrations of traps would be useful, i.e., the lower concentrations affect triplet excitation migration less than singlet excitation migration. The role of traps in trapping charge carriers must be remembered in interpreting the results, along with the role of other possible mechanisms of charge carrier generation, such as single exciton generation (6).

(6) D. R. Kearns, J. Chem. Phys., 40, 1452 (1964); R. G. Kepler and R. E. Merrifield, J. Chem. Phys., 40, 1173 (1964).